2020

Studies On The Anatomy Of Teleosts

Katherine Elliott Bemis
William & Mary - Virginia Institute of Marine Science, keb242@cornell.edu

Studies on the Anatomy of Teleosts

A Dissertation

Presented to

The Faculty of the School of Marine Science

The College of William & Mary

In Partial Fulfillment

of the Requirements for the Degree of

Doctor of Philosophy

---

by

Katherine Elliott Bemis

January 2020

APPROVAL PAGE

This dissertation is submitted in partial fulfillment of

the requirements for the degree of

Doctor of Philosophy

Katherine Elliott Bemis

Approved by the Committee, December 2019

Eric J. Hilton, Ph.D.
Committee Chair / Advisor

Wolfgang Vogelbein, Ph.D.

Bruce B. Collette, Ph.D.
Smithsonian Institution
Washington, DC, USA

Nalani Schnell, Ph.D.
Muséum national d'Histoire naturelle,
Concarneau, France

Michael Vecchione, Ph.D.
NOAA National Systematics Laboratory
Washington, DC, USA

Dedicated to my parents, Betty Anne McGuire and William Elliott Bemis

ACKNOWLEDGEMENTS

I thank my dissertation committee, Eric J. Hilton, Bruce B. Collette, Nalani Schnell, Mike Vecchione, and Wolf Vogelbein and my parents, Betty Anne McGuire and William E. Bemis. I am grateful to the communities at VIMS, Northeast Fisheries Science Center, Smithsonian Institution, and Florida Museum of Natural History that have supported me during my dissertation.

Please see individual chapters for further acknowledgments.

ABSTRACT

The Longnose Lancetfish, *Alepisaurus ferox*, is a pelagic marine fish that has a heterodont dentition, including large fangs on both the upper and lower jaws. Their diet is well documented and includes salps, hyperiid amphipods, pelagic polychaete worms, mesopelagic fishes, and cephalopods. However, the function of the heterodont dentition, the structure of the teeth, and replacement mode is largely unknown. We studied a series of *A. ferox* to describe their dentition and tooth replacement. All teeth are replaced extraosseously. Palatine and dentary fangs develop horizontally in the oral epithelium on the lingual surface of dentigerous bones. Developing fangs rotate into place and attach to the bone through a pedicel that forms at the base of each tooth on the lingual side of the dentigerous bone. We compare extraosseous horizontal tooth replacement and rotation of large fangs in *A. ferox* to examples of other teleosts rotation of fangs.

Atlantic Cutlassfish, *Trichiurus lepturus*, have large, barbed premaxillary and dentary fangs and sharp, dagger-shaped teeth in their oral jaws. We used dry skeletons, histology, SEM, and micro-CT scanning to study *T. lepturus* to describe its dentition and tooth replacement. We identified and described three modes of intraosseous tooth replacement in *T. lepturus* depending on the location of the tooth in the jaw. Such distinct modes of tooth replacement in a teleostean species are unknown. We compared modes of replacement in *T. lepturus* to 20 species of scombroids to explore the phylogenetic distribution of these three replacement modes. Our study highlights the complexity and variability of intraosseous tooth replacement and that developmentally different tooth replacement processes can yield remarkably similar dentitions.

We review literature on the comparative anatomy of Ocean Sunfishes (Molidae) and presents new findings based on our studies. We document similarities and differences among the three living genera, *Ranzania, Masturus*, and *Mola* using an organ system approach to examine: general body form and external anatomy; skeleton; integument; brain and sense organs; digestive organs; heart and circulation; respiratory system; excretory system; and endocrine organs. Molids have many anatomical specializations such as the formation of the clavus from dorsal- and anal-fin elements, enlarged gills with unusual skeletal supports, a heart with thick walls and more valves than other teleosts, ontogenetic loss of the swimbladder, enlarged kidneys and a well-developed urinary bladder, reduced otoliths, and a spinal cord contained completely within the braincase. Tagging studies on locomotion and diving behavior demonstrate that molids move efficiently over horizontal and vertical distances in the water column, and this new information helps to interpret the many unusual features of molid anatomy.

AUTHORS NOTE

The chapters of my dissertation were written formatted as manuscripts for publication. Thus, the formatting of each chapter follows the guidelines of the journal or book to which the manuscript was or will be submitted. At the time of writing, citations for individual chapters are as follows:

CHAPTER 1: Bemis, K.E. and E.J. Hilton. Tooth morphology, development, and replacement in the Longnose Lancetfish, *Alepisaurus ferox* (Teleostei: Aulopiformes: Alepisauridae). In prep for Copeia.

CHAPTER 2: Bemis, K. E., S. M. Burke, C. A. St. John, E. J. Hilton, and W. E. Bemis. 2019. Tooth development and replacement in the Atlantic Cutlassfish, *Trichiurus lepturus*, with comparisons to other Scombroidei. Journal of Morphology 280:78–94. DOI: 10.1002/jmor.20919.

CHAPTER 3: Bemis, K.E., J.C. Tyler, E.J. Hilton, and W.E. Bemis. Comparative Anatomy and Ontogeny of Ocean Sunfishes (Tetraodontiformes: Molidae). Review material for this chapter accepted to *Evolution, Biology, and Conservation of the Ocean Sunfishes*, CRC Press; new material will be published separately.

Studies on the Anatomy of Teleosts

CHAPTER 1. Tooth morphology, development, and replacement in the Longnose Lancetfish, *Alepisaurus ferox* (Teleostei: Aulopiformes: Alepisauridae)

Katherine E. Bemis

Department of Fisheries Science, Virginia Institute of Marine Science, William & Mary

P.O. Box 1346, Gloucester Point, Virginia, 23062; kebemis@vims.edu

Corresponding author

Eric J. Hilton

Department of Fisheries Science, Virginia Institute of Marine Science, William & Mary

P.O. Box 1346, Gloucester Point, Virginia, 23062; ehilton@vims.edu

Running head: Tooth replacement in *Alepisaurus ferox*

Keywords: extraosseous, CT-scanning, histology

Formatted for Copeia

ABSTRACT

The Longnose Lancetfish, *Alepisaurus ferox*, is a pelagic marine fish that has a heterodont dentition, including large fangs on both the upper and lower jaws. Their diet is well documented and includes salps, hyperiid amphipods, pelagic polychaete worms, mesopelagic fishes, and cephalopods. However, the function of the heterodont dentition is unclear, and the structure of the teeth and their replacement mode is largely unknown. We used dry skeletons, histology, and microcomputed tomography (micro-CT) scanning to study a series of specimens of *A. ferox* from the western North Atlantic and North Pacific oceans to describe their dentition and tooth replacement. The smallest teeth in the oral jaws are conical teeth and occur in a gradient in size along the length of the premaxilla. The palatine and dentary both bear elongate, laterally compressed fangs and a series of sharp triangular, slightly recurved teeth. The dentary also has anterior symphysial teeth, symphysial fangs, and a series of small, laterally compressed teeth. Despite differences in sizes and types of teeth, all are replaced extraosseously. Palatine and dentary fangs develop horizontally in the oral epithelium on the lingual surface of dentigerous bones. Developing fangs rotate into place and become functional teeth, attaching to the bone through a pedicel that forms at the base of each tooth on the lingual side of the dentigerous bone. We compare extraosseous horizontal tooth replacement and rotation of large fangs in *A. ferox* to examples of other teleosts that have intraosseous horizontal tooth replacement and rotation of fangs.

INTRODUCTION

Teleostean fishes continuously replace teeth throughout life (e.g., Huysseune and Witten, 2006). Extraosseous and intraosseous tooth replacement patterns are the extremes of a continuum used to characterize tooth replacement (Trapani, 2001, Conway et al., 2015). Most species of teleosts with large fangs probably feed during the time that they are developing new teeth. Whether a tooth develops extraosseously or intraosseously impacts the tissues that protect the tooth during its development, and the tissues that teeth move through as well as those involved in the tooth's eruption and attachment to dentigerous bones. Large fangs have evolved more than 25 times in teleosts (Olsen and Davis, submitted), and are particularly interesting because of the potentially different ways to protect and accommodate their development because, in comparison to small teeth, large fangs are less easily protected by bone or soft tissues.

In a study of a teleost with large fangs, *Trichiurus lepturus*, we described how intraosseous replacement occurs, with emphasis on how large premaxillary fangs develop horizontally along the long axis of the bone, erupt, rotate into place, and attach to the bone (Bemis et al., 2019: 91–92). We suggested two possible explanations, not mutually exclusive, for horizontal fang development: (1) better protection of large fangs as they develop within the bones; (2) constrained space for fangs to develop vertically within the bone. Here, we describe dentition and tooth development of the Longnose Lancetfish, *Alepisaurus ferox* (Aulopiformes: Alepisauridae), which provides an interesting comparison to *T. lepturus* because its fangs develop extraosseously in the soft tissue before they contact the dentigerous bone and rotate into a vertical position. *Alepisaurus ferox* is also interesting because of its strongly heterodont dentition that includes small

teeth on the premaxilla, series of stout triangular teeth in both the palatine and dentary, and enlarged large fangs that form two distinct series on both the palatine and dentary.

Alepisaurus ferox is circumglobally distributed in the mesopelagic and orients vertically in the water column (Fig. 1A). The diet includes salps, hyperiid amphipods, pelagic polychaete worms, cephalopods, and teleosts from epipelagic to mesopelagic habitats and sizes ranging from larvae to large *A. ferox* (Matthews et al., 1977, Choy et al., 2013, Keller et al., 2016, Portner et al., 2017). Despite extensive study of their diet, facilitated by limited digestion in the stomach that allows for detailed prey identification (Portner et al., 2017, Wassersug and Johnson, 1976), we know little about feeding behavior or functional morphology of the dentition in *A. ferox*. One purpose of this study is to improve understanding about the dentition and replacement and how it may relate to this exceptionally broad diet.

MATERIALS AND METHODS

Collection abbreviations follow Sabaj (2019). We based identifications of *Alepisaurus* on Gibbs and Wilimovsky (1966) and Thompson (2002), and distinguished *A. ferox* from the only other species of *Alepisaurus*, *A. brevirostris,* based on snout length and dorsal fin ray counts.

Specimens.— Twelve *Alepisaurus ferox* were collected from the pelagic longline fishery off Hawaii by fisheries observers from NOAA Pacific Islands Fisheries Science Center. These fish were sent to us frozen (Fig. 1B); we dissected them, prepared skeletons following methods of Bemis et al. (2004) and made tooth counts. An additional series of

78 specimens collected in the Gulf of Mexico that were fixed in formalin and subsequently transferred to EtOH was gifted to us by the DEEPEND project. All 90 specimens from are deposited at the Nunnally Ichthyology Collection, Virginia Institute of Marine Science (VIMS). We also studied six specimens from the western North Atlantic Ocean that were already accessioned in collections, including specimens from USNM and YPM.

Clearing and staining.— Three juvenile *Alepisaurus ferox* (VIMS 42167, VIMS 42160, VIMS 42161) were cleared and stained using alizarin and KOH maceration based on methods of Taylor (1967).

Micro-computed tomography.— We scanned one specimen with micro-CT. We used a Xradia Versa XRM-500 nano-CT scanner in the Biotechnology Resource Center Multiscale Imaging Facility at Cornell University to prepare data sets for. Reconstructions prepared from these data sets have a resolution of 5–10 μm voxels. We made 2D orthogonal MPR (multiplanar reformatting) and 3D volume reconstructions using OsiriX™ (version 5.8.5, 64-bit edition) DICOM imaging software (Rosset et al., 2004) on Apple Macintosh computers running OSX 10.8.5. To view internal anatomy of teeth and bones, we digitally dissected reconstructions within OsiriX™.

Histology.—We decalcified portions of two formalin-fixed specimens using Ethylenediaminetetraacetic acid (EDTA), washed and dehydrated them for paraffin

embedding, cut sections at 6 μm, and stained them with hematoxylin and eosin (H&E) at the Cornell Veterinary College Diagnostic Laboratory.

Photography.—We used a Canon 7D digital camera to record color macrophotographs. We photographed histological sections using an Olympus SZX12 microscope equipped with an Olympus DP70 digital camera. Using Adobe Photoshop CS6, we adjusted images for color balance and contrast, and prepared plates and line drawings in Adobe Illustrator CS6.

Counts and measurements.— During dissection, we counted the number of each of the three types of teeth on the palatine and the five types of teeth on dentary, scoring each tooth in a two category system as either developing or attached to the bone (= functional). If a tooth was still surrounded by soft tissue and not yet in contact with the bone, then it was scored as developing. Once its ligamentous pedicel began to form and ossify, a tooth was scored as attached. We made the following measurements in the oral jaws: (1) functional palatal tooth row length, from the anterior tip of the palatine to the last attached tooth, i.e., developing triangular teeth posterior to the last attached triangular tooth were not included in this measurement; (2) functional dentary tooth row length, from the anterior tip of the dentary to the end of the of attached functional teeth, i.e., developing triangular teeth posterior to the last attached triangular tooth were not included in this measurement; (3) position of mid-palatal fang, from anterior tip of palatine to first attached mid-palatal fang; and (4) position of mid-dentary fang, from anterior tip of dentary to first attached mid-dentary fang.

RESULTS

Alepisaurus ferox have oral teeth on the premaxillae, palatines, and dentaries (Fig. 1C, 2). As are all bones in the skeleton of *A. ferox*, these dentigerous bones are thin and weakly ossified. Some teeth in our specimens are jagged, broken off near their base, and may have been damaged during capture. All teeth are in a single series along the dentigerous bones (Fig. 2) except where small teeth overlap with mid-dentary fangs. Teeth at all stages, not just those that are still developing, are hollow.

Premaxillary teeth.— There is graded series of 62–141 teeth, the number of which increases during ontogeny. The premaxillary teeth barely protrude through the oral epithelium and are conical in shape, unlike most teeth in the palatine and dentary, which are laterally compressed. The anteriormost 5-10 teeth are longer and more recurved; teeth become straighter and shorter along the length of the jaw. The posteriormost 10-15 teeth are variably curved anterio-medially. We did not study development or replacement of premaxillary teeth.

Palatine teeth.— On each side of the skull, there is typically one attached anterior palatal fang, followed by a diastema with no teeth, and then a series of 1 or 2 attached mid-palatal fangs (Fig. 2). The anterior palatal fangs are typically longer than the mid-palatal fangs. The mid-palatal fangs are in the approximate middle of the functional row of palatine teeth (55% ± 10% of length of functional palatal tooth row, n =10, 405-1155 mm SL). All palatal fangs are laterally compressed and have cutting keels on both the anterior and posterior edges; there are no barbs or serrations on the fangs. Posterior to the mid-palatal fangs is a series of short, palatal triangular teeth, which are wide at their bases and

laterally compressed. The triangular teeth are close together and slightly recurved (Fig. 2).

Dentary teeth.— The dentary has five types of teeth. The paired symphysial teeth are located at the very tip of the jaw, and are recurved, conical, and lack cutting edges (Fig. 2). Posterior to the symphysial teeth are the paired symphysial fangs, which bear small keels on both edges. Posterior to the symphysial fangs is a series of 4-8 attached, small, keeled teeth that are about half the height of the symphysial fangs (Fig. 2). Small teeth can also occur on the labial side of attached mid-dentary fangs.

Posterior or lingual to the small teeth are laterally compressed mid-dentary fangs (Fig. 2). The mid-dentary fangs are longer than the symphysial fangs and are positioned in the middle of the functional row of dentary teeth (42% ± 5% of length of functional palatal tooth row, n =10, 405-1155 mm SL). Mid-dentary fangs resemble palatal fangs except that they are typically slightly shorter and less recurved.

Posterior to the mid-dentary fangs is a series of triangular dentary teeth that are similar in size and shape to palatal triangular teeth (Fig. 2). Typically, the series of triangular teeth is longer in the dentary than on the palatine. These teeth attach to the lingual side of the jaw at approximately 60° angle, posteriorly directed (Fig. 3). In dorsal view, both the mid-dentary fangs and the dentary triangular teeth attach at an angle relative to the long axis of the dentary deflecting posterio-medially.

Development of new teeth.— As the jaws elongate during growth, larger teeth develop to fill the space. During jaw elongation, the diastema separating the anterior and mid-palatal fangs increases in length. In the dentary, the lengths of the regions of small teeth and

triangular teeth increase, which is how the mid-dentary fangs maintain a position near the middle of the functional row of dentary teeth throughout ontogeny.

No teeth develop on the labial surface of the palatine; the symphysial teeth are the only teeth that develop on the labial surface of the dentary. Only one attached symphysial tooth and one attached symphysial fang occur on each dentary at any given time (e.g., Fig. 2). These teeth are replaced in their same positions in the jaw without any posterior shift in their location with each wave of replacement. Replacement symphysial fangs develop on the lingual side of the dentary. The developing symphysial fangs are medial to the adjacent developing small teeth and are also covered by a thicker layer of soft tissue. They develop completely horizontal to the jaw.

Small teeth develop on the lingual side of the dentary, between approximately every other attached small tooth. These teeth do not develop horizontally, but are posteriorly directed at about a 45° angle; they are almost completely covered by oral epithelium during early development. Developing small teeth extend posterior to the region of attached small teeth, and form on the labial side of attached mid-dentary fangs. New small teeth develop at the previous locations of mid-dentary fangs.

Anterior palatal fangs, mid-palatal fangs, and mid-dentary fangs develop in a similar manner. All fangs begin development as small tooth germs on the lingual side of the palatine or dentary in a small individual pocket of oral epithelium within a larger fold, located near the eventual attachment sites (Fig. 4). Typically for fangs, several (1-4) posteriorly directed teeth develop in a series lying horizontally (Fig. 4B). The developing mid-palatal and mid-dentary fangs form in series with the anteriormost fang being the largest; it will be the first in the series to rotate and attach to the jaw (Fig. 4B). The

anteriormost developing tooth associated with the anterior palatal fangs is not is not always the most developed, i.e., it is not necessarily the next in the series to attach.

No fangs covered completely by oral epithelium had any observable wear or damage to them. When fangs approach their final size, they begin to tear through and erupt from the oral epithelium (Fig. 5A). A ligamentous connection between a tooth and the dentigerous bone develops before the tooth erupts out of the soft tissue and rotates into position (Fig. 6). The ligament does not mineralize until the tooth has rotated into its final position. There appear to be differences in the anterior and posterior of the collagen base as it mineralizes (Fig. 7) which may contribute to the rotation during replacement.

In both the palatine and dentary, developing triangular teeth only occur posterior to the posteriormost functional triangular tooth. There is a series of 4-8 developing triangular teeth posterior to the last attached tooth in successive stages of development. Triangular teeth develop pointing posteriorly at about a 45° angle (versus completely horizontal).

Attachment of teeth. **—** All teeth are firmly attached to the palatine and dentary by the ossified ligamentous pedicel. This pedicel is on the lingual side of the dentigerous bones except for the symphysial tooth in the dentary, which is located on the labial side. This ligamentous connection between a tooth and the dentigerous bone is likely responsible for rotating the fangs into place. The collagen fibers of the developing pedicel are white, and until they mineralize, a tooth can be manually depressed by a probe (Fig. 6). Once the tooth is upright and the ring of collagen ossifies, the tooth is firmly attached to the bone and can no longer be depressed. The collagenous attachment is not visible in the CT

reconstructions shown in Figures 5B and C, which show the area of the same specimen in Figure 5A because the ligament has not yet ossified.

The ossified ring of the pedicel left on the dentigerous bone indicates where teeth were previously attached and indicates that the attachment to the dentigerous bones was strong. After the functional tooth is lost, an ossified ring of the pedicel remains through the development and attachment of several subsequent teeth. For example, in the specimen in Figure 8, there are at least five previous attachment sites from mid-dentary fangs located anterior to the currently attached mid-dentary fang. The sizes of the ossified pedicel increase from anterior to posterior, indicating that newer mid-dentary fangs are larger than were earlier mid-dentary fangs. When new small teeth attach to the bone, the small teeth remodel the old pedicels of mid-dentary fangs and attach on top of them (Fig. 8).

DISCUSSION

We identified different types of teeth in different regions of the oral jaws of *Alepisaurus ferox*. In the palatine these are: 1) anterior fangs; 2) mid-palatal fangs; and 3) triangular teeth. In the dentary, these are: 1) symphysial teeth; 2) symphysial fang; 3) small teeth; 4) mid-dentary fangs; and 5) triangular teeth. Only a single type of tooth was found on the premaxilla. Because of this regionalization of tooth shapes, we can identify patterns in the types of teeth that are developing and where they will attach. Throughout ontogeny, different types of teeth are in the same relative positions in a jaw. For example, regardless of standard length, the mid-palatal fang or fangs are always in the middle of the series of functional palatine teeth, and the mid-dentary fang or fangs are always in the middle of the series of functional dentary teeth. Our preliminary data suggest that juvenile

Alepisaurus sp. have fewer teeth than larger specimens (Fig. 9), however, current taxonomic keys have overlap in key characters for juvenile *Alepisaurus* (e.g., Gibbs and Wilimovsky 1966 and Thompson 2002). Tooth counts for more individuals and of a broader size range with confirmed identifications are necessary to understand if the teeth in the jaw only increase in size (our data support this currently) or if they also increase in the number of the teeth (our current tooth data show this for premaxillary teeth only). In either case, in some circumstances, an older tooth is succeeded by a tooth of a different type. For example, the anteriormost incoming mid-dentary fang replaces the anteriormost triangular dentary tooth (Fig. 9). This results in maintenance of tooth regions in proportional position along the jaw as the fish grows. The mechanism(s) for maintaining this proportional regionalization is unknown, but the fact that the relative position of a type of tooth such as the mid-dentary fang remains constant during the ontogeny of the fish may relate to the genetic control of both shape and position of teeth along the jaw (Fraser et al. 2013). However, controls on patterning, tooth shape, and tooth development and how they are integrated in time and space is unknown for any teleost species.

Although there are many tooth types, all teeth in the jaws of *Alepisaurus ferox* are replaced extraosseously. Intraosseous horizontal tooth development and subsequent rotation occurs in at least three lineages of teleosts, in both freshwater (e.g., *Hydrolycus*, see Trapani, 2001 and *Hydrocynus,* see Gagiano et al., 1996), and marine taxa (e.g., *Trichiurus lepturus*, Bemis et al., 2019). Hubbs et al. (1953) recognized that the horizontal “depressible teeth” in a related aulopiform *Anotopterus pharao* were replacement teeth, but did not describe the pattern of replacement; this is the only aulopiform for which horizontal teeth have been noted in the literature, although

horizontal development also occurs in related *Omosudis lowii* (VIMS 42162) and likely in other related aulopiforms with fangs. *Alepisaurus ferox*, however, is the first teleost for which extraosseous tooth replacement and rotation of developing fangs has been described.

Unlike *Trichiurus lepturus,* which replaces only its large premaxillary fangs horizontally, *Alepisaurus ferox* horizontally replaces large fangs in both the palatine and dentary; small teeth and triangular teeth develop at approximately 45° angles. In *T. lepturus,* bone remodeling of the region around the developing tooth likely contributes to establishing its final vertical position, but we did not examine this region histologically to confirm this (Bemis et al. 2019). In comparison, our CT scans and histology show that the fangs of *A. ferox* rotate into place before the ligamentous collar mineralizes to form the attachment to the dentigerous bone. Now that we understand the mechanism for rotation in *A. ferox*, it would be useful to restudy rotation and attachment in *T. lepturus*.

MATERIALS EXAMINED

We studied specimens preserved in alcohol (A), decalcified-and stained sections (DSS), dried osteological preparations (SD) and cleared and stained materials (c&s). All specimens examined are single specimen lots unless otherwise indicated. Standard lengths (SL) or fork lengths (FL) are listed, if available.

Alepisaurus ferox:

USNM 119817, 1015 mm SL; USNM 201274; USNM 201277; USNM 444213; USNM 409556, 565 mm SL.

VIMS 40040, skeleton, 1395 mm FL; VIMS 40939, skeleton, 485 mm SL; VIMS 40940, skeleton, 475 mm SL; VIMS 42068, skeleton, 740 mm SL; VIMS 42069; VIMS 42070, 121 mm SL; VIMS 42071, skeleton, 141 mm SL; VIMS 42072, 640 mm SL; VIMS 42073, 640 mm SL; VIMS 42074 605 mm SL; VIMS 42075, 535 mm SL; VIMS 42076, 785 mm SL; VIMS 42077, 505 mm SL; VIMS 42084, 1155 mm SL; VIMS 42116; VIMS 42119; VIMS 42115; VIMS 42118; VIMS 42117; VIMS 42103, 8; VIMS 42166, 1, c&s; VIMS 42167, 1; VIMS 42104, 8; VIMS 42160, 1, c&s; VIMS 42161, 1, c&s; VIMS 42114, 1, skeleton; VIMS 42099, 2; VIMS 42108, 8; VIMS 42102, 4; VIMS 42163, 1; VIMS 42164, 1; VIMS 42110, 8; VIMS 42113, 10

YPM ICH 25379, skeleton.

Omosudis lowii

VIMS 42162, c&s; VIMS 42111, 6; VIMS 42112, 3; VIMS 42113, 10.

ACKNOWLEDGMENTS

New specimens of *Alepisaurus ferox* and comparative materials were collected and made available by NOAA fisheries observers and P. Woodworth-Jefcoats at the Pacific Islands Fisheries Science Center; A. Cook, N. Pruzinsky, and T. Sutton, Nova Southeastern University; D. McElroy, Northeast Fisheries Science Center, and Charles Cotton, Deep-C Consortium. We thank the following collections for loans of material used in this study: S. Huber, Nunnally Ichthyological Collection, VIMS; K. Murphy, D. Pitassy, and S. Raredon, Smithsonian Institution; G. Watkins-Colwell, Yale Peabody Museum. We

thank W. E. Bemis, Cornell University, B. B. Collette, Smithsonian Institution, M. Vecchione, NOAA National Systematics Laboratory, and T. Sutton and D. Kerstetter, Nova Southeastern University for discussing dentition and diet of *A. ferox* with us. T. Porri, Cornell University Multiscale Imaging Facility, CT scanned the specimen. This project was supported by an NSF Graduate Research Fellowship and VIMS Office of Academic Studies.

LITERATURE CITED

Bemis, W. E., E. J. Hilton, B. Brown, R. Arrindell, A. M. Richmond, C. D. Little, L. Grande, P. L. Forey, and G. J. Nelson. 2004. Methods for preparing dry, partially articulated skeletons of osteichthyans, with notes on making Ridewood dissections of the cranial skeleton. Copeia 2004:603–609.

Bemis, K. E., S. M. Burke, C. A. St. John, E. J. Hilton, and W. E. Bemis. 2019. Tooth development and replacement in the Atlantic Cutlassfish, *Trichiurus lepturus*, with comparisons to other Scombroidei. Journal of Morphology 280:78–94. DOI: 10.1002/jmor.20919.

Choy, C. A., E. Portner, M. Iwane, and J. C. Drazen. 2013. Diets of five important predatory mesopelagic fishes of the central North Pacific. Marine Ecological Progress Series, 492: 169–184.

Conway, K. W., Bertrand, N. G., Browning, Z., Lancon, T. W., & F. J. Clubb, Jr. 2015. Heterodonty in the New World: An SEM investigation of oral dentition in the clingfishes of the subfamily Gobiesocinae (Teleostei: Gobiesocidae). Copeia, 103(4), 973–998.

Gibbs, R. H. Jr., and N. J. Wilimovsky. 1966. Family Alepisauridae. In Fishes of the Western North Atlantic. Part Five: Orders Iniomi and Lyomeri. Memoir I. Sears Foundation for Marine Research. pp. 482–497.

Hubbs, C. L., G. W. Mead, and N. J. Wilimovsky. 1953. The widespread, probably antitropical distribution and the relationship of the bathypelagic Iniomous fish *Anotopterus pharao*. Bulletin of the Scripps Institution of Oceanography 6(5): 173-198.

Huysseune, A., and P. E. Witten. 2006. Developmental mechanisms underlying tooth patterning in continuously replacing osteichthyan dentitions. Journal of Experimental Zoology, 306B, 204–215. https://doi.org/10.1002/jez.b.21091

Keller, H. R., A. C. Hirons, and D. W. Kerstetter. 2016. Combined stomach content and $\delta^{13}C$/ $\delta^{15}N$ analyses of Oilfish, Escolar, Snake Mackerel and Lancetfish in the western North Atlantic. Marine Ecology 37: 727–736.

Matthews, F. D., D. M. Damkaer, L. W. Knapp, and B. B. Collette. 1977. Food of western North Atlantic tunas (*Thunnus*) and lancetfishes (*Alepisaurus*). NOAA Technical Report NMFS SSRF-706: 1–19.

Olsen, E. E., and M. P. Davis. Submitted. The Evolution of Fangs across Ray-finned Fishes (Actinopterygii).

Portner, E.J., J. J. Polovina, and C. A. Choy. 2017. Patterns in micronekton diversity across the North Pacific Subtropical Gyre observed from the diet of Longnose Lancetfish (*Alepisaurus ferox*). Deep Sea Research Part I 125: 40–51.

Taylor, W.R. 1967. An enzyme method of clearing and staining small vertebrates. Proceedings of the United States National Museum 122 (3596) 17 pages.

Thompson, B. A. 2003. Alepisauridae, Lancetfishes. Family Hemiramphidae. In K. E. Carpenter, ed. The Living Marine Resources of the Western Central Atlantic. Volume 2, Bony Fishes. Rome: Food and Agriculture Organization of the United Nations. FAO Species Identification Guide for Fishery Purposes. American Society of Ichthyologists and Herpetologists Special Publication 5. pp. 940.

Trapani, J. 2001. Position of developing replacement teeth in teleosts. Copeia, 2001(1), 35–51. https://doi.org/10.1643/0045-8511(2001)001[0035:PODRTI]2.0.CO;2

Wassersug, R. J. and R. K. Johnson. 1976. A remarkable pyloric caecum in the evermannellid genus *Coccorella* with notes on gut structure and function in alepisauroid fishes (Pisces, Myctophiformes). Journal of Zoology 179: 273–289.

FIGURE CAPTIONS

Figure 1. Longnose Lancetfish, *Alepisaurus ferox*. **A.** *Alepisaurus* cf. *ferox* orienting vertically in the water column. Image from NOAA Ship *Okeanos Explorer*. **B.** Lateral view of fresh specimen VIMS 42070, 121 mm SL. **C.** Lateral view of head to show teeth in relation to soft tissue (right side of specimen is shown; image has been reversed so that anterior faces left).

Figure 2. Skull showing heterodont dentition of *Alepisaurus ferox* and terminology for teeth. There are three tooth bearing bones in the skull: the premaxilla, palatine, and dentary. Premaxillary teeth are small, conical, and in a graded series of sizes from largest and most recurved anteriorly, to small posterior. Fangs are attached in two regions of the palatine separated by a toothless diastema. A series of triangular palatal teeth is posterior to the mid-palatal fangs. Small symphysial teeth are located on the labial side of the dentary; these are the only teeth in the oral jaws that form and attach on the labial surface of the bone. Symphysial fangs are located immediately posterior to the symphysial teeth, and these are followed by a series of small conical teeth with anterior and posterior keels. The remaining teeth of the dentary are the mid-dentary fangs, followed closely by a series of triangular dentary teeth. VIMS 35801.

Figure 3. Triangular dentary teeth of *Alepisaurus ferox* to highlight attachment to the lingual surface of the bone by ossified pedicels. **A.** Labial view of three attached teeth. **B.** Lingual view of the same teeth to show that the attachment us on lingual surface. Dashed line indicates extent of one of the three pedicels attaching teeth to the bone. YPM 25379, length unknown.

Figure 4. Developing mid-dentary fangs. **A.** Developing anterior and mid-palatal fangs lie horizontally in pockets of soft tissue. VIMS xxxx, xx mm SL. Right dentary, lingual view. **B.** A new mid-dentary fang begins to attach posterior to an attached mid-dentary fang. Posterior to it, a series of four mid-dentary fangs are developing horizontally. These mid-dentary fangs will eventually attach in locations that are currently occupied by triangular teeth. Right dentary, lingual view.

Figure 5. Transition between small teeth, mid-dentary fangs, and triangular teeth showing an attached mid-dentary fang and a second fang that newly rotated into place. **A.** Photograph of transition area in labial view. **B.** CT-scan of labial view of same specimen as in A. The position of the rotated mid-dentary fang was previously occupied by a triangular tooth that is eroding away. **C.** CT-scan of lingual view. Note that there is no mineralization of the pedicel at the base of the newly rotated fang.

Figure 6. An incoming mid-dentary fang attaches to the bone via its pedicel. The collagen fibers of the developing attachment are white, and until these fibers mineralize, teeth can still be depressed manually. VIMS 42068, 740 mm SL.

Figure 7. Histology of a developing fangs. **A.** Anterior attached and developing palatal fangs showing pedicel and developing pedicel before it contacts the bone. **B.** Developing symphysial fang.

Figure 8. Remnants of ossified pedicels (white arrows) mark earlier locations of at least five mid-dentary fangs. The sizes of these older pedicels increases along the

length of the jaw, indicating that with each new tooth, the mid-dentary fang size increases.

Figure 9. Attached and developing teeth in the dentary in a cleared and alizarin stained specimen of *Alepisaurus ferox*. Small teeth are colored in blue, mid-dentary fangs in gold, and triangular teeth in red. Developing small teeth are located between attached small teeth and posterior to the last attached tooth, including one small tooth that is developing posterior to the first attached mid-dentary fang (circled developing tooth). The pedicel of the attached mid-dentary fang is evident, as are three developing mid-dentary fangs located posterior to it. Five developing triangular teeth are located posterior to the six attached triangular teeth.

TABLES

Table 1. Measurements in the palatine.

Specimen number	Standard length	Length of functional palatine tooth row	Diastema length	Position of first mid-palatal fang
USNM 201274	405	47.5	10	27.4
Lancetfish-07	475	49.6	13.7	27.8
Lancetfish-06	485	50.67	16.7	29.9
Lancetfish-04	535	59.6	15.09	33.3
Lancetfish-03	605	58	11.3	18.9
Lancetfish-01	640	63.9	17	34.1
Lancetfish-02	640	58.4	Damaged	Damaged
Lancetfish-05	785	74.08	20.8	46.1
USNM 444212	875	81.8	17	35.4
USNM 119817	1015	99.1	31.1	61.2
VIMS 42084	1155	100.9	25.1	64.9

Table 2. Measurements in the dentary.

Specimen number	Standard length	Length of functional dentary tooth row	Position of first mid-dentary fang
USNM 201274	405	44.6	18.6
Lancetfish-07	475	51	22.5
Lancetfish-06	485	48.2	16.9
Lancetfish-04	535	56.7	23
Lancetfish-03	605	59	25.3
Lancetfish-01	640	54.3	19
Lancetfish-02	640	57.3	21
Lancetfish-05	785	74	31
USNM 444212	875	80.7	35.5
USNM 119817	1015	99	49.6
VIMS 42084	1155	103.8	46.6

CHAPTER 2. Tooth development and replacement in the Atlantic Cutlassfish, *Trichiurus lepturus*, with comparisons to other Scombroidei

Katherine E. Bemis

Department of Fisheries Science, Virginia Institute of Marine Science, College of William & Mary, P.O. Box 1346, Gloucester Point, Virginia, 23062; kebemis@vims.edu

Samantha M. Burke

Department of Ecology and Evolutionary Biology, Cornell University, Ithaca, New York 14853

Carl A. St. John

Department of Ecology and Evolutionary Biology, Cornell University, Ithaca, New York 14853

Eric J. Hilton

Department of Fisheries Science, Virginia Institute of Marine Science, College of William & Mary, P.O. Box 1346, Gloucester Point, Virginia, 23062

William E. Bemis

Department of Ecology and Evolutionary Biology and Cornell University Museum of Vertebrates, Cornell University, Ithaca, New York, 14853

Proposed running head: Tooth replacement in Atlantic Cutlassfish

Key words: alternate tooth replacement, bone remodeling, intraosseous tooth replacement, micro-CT scanning, Trichiuridae

Formatted for Journal of Morphology, published as:

Bemis, K. E., S. M. Burke, C. A. St. John, E. J. Hilton, and W. E. Bemis. 2019. Tooth development and replacement in the Atlantic Cutlassfish, *Trichiurus lepturus*, with comparisons to other Scombroidei. Journal of Morphology 280:78–94. DOI: 10.1002/jmor.20919.

RESEARCH HIGHLIGHTS.

Trichiurus lepturus has three modes of intraosseous tooth replacement depending on the locations of teeth. Large premaxillary fangs develop horizontally and rotate into place. Tooth replacement characters help to interpret scombroid evolution.

ABSTRACT. Atlantic Cutlassfish, *Trichiurus lepturus*, have large, barbed premaxillary and dentary fangs and sharp, dagger-shaped teeth in their oral jaws. Functional teeth firmly ankylose to the dentigerous bones. We used dry skeletons, histology, SEM, and micro-CT scanning to study 92 specimens of *T. lepturus* from the western North Atlantic to describe its dentition and tooth replacement. We identified three modes of intraosseous tooth replacement in *T. lepturus* depending on the location of the tooth in the jaw. Mode 1 relates to replacement of premaxillary fangs, in which new tooth germs enter the lingual surface of the premaxilla, develop horizontally, and rotate into position. We suggest that growth of large fangs in the premaxilla is accommodated by this horizontal development. Mode 2 occurs for dentary fangs: new tooth germs enter the labial surface of the dentary, develop vertically, and erupt into position. Mode 3 describes replacement of lateral teeth, in which new tooth germs enter a trench along the crest of the dentigerous bone, develop vertically, and erupt into position. Such distinct modes of tooth replacement in a teleostean species are unknown. We compared modes of replacement in *T. lepturus* to 20 species of scombroids to explore the phylogenetic distribution of these three replacement modes. Alternate tooth replacement (in which new teeth erupt between two functional teeth), ankylosis, and intraosseous tooth development are plesiomorphic to Bluefish + other Scombroidei. Our study highlights the complexity and variability of

intraosseous tooth replacement. Within tooth replacement systems, key variables include sites of formation of tooth germs, points of entry of tooth germs into dentigerous bones, coupling of tooth germ migration and bone erosion, whether teeth develop horizontally or immediately beneath the tooth to be replaced, and how tooth eruption and ankylosis occur. Developmentally different tooth replacement processes can yield remarkably similar dentitions.

INTRODUCTION.

Teleostean fishes continuously replace teeth throughout life (Bemis et al., 2005; Huysseune and Witten, 2006; Berkovitz and Shellis, 2017). Extraosseous and intraosseous tooth replacement are two main patterns used to characterize tooth replacement (Trapani, 2001), although these may be extremes of a continuum (Conway et al., 2015). In this paper, we focus on intraosseous tooth replacement in the oral jaws, which has evolved in at least three clades of teleosts (Trapani, 2001). In some documented instances of intraosseous replacement, such as the Bluefish, *Pomatomus saltatrix*, new tooth germs form directly in association with the oral epithelium (Bemis et al., 2005). The new tooth germ and associated cells then erode a replacement pore through which they move into the medullary cavity of the dentigerous bone while still connected to the oral epithelium by the dental lamina (Fig. 1). The new tooth continues to develop and eventually erupts, and replaces the functional tooth through bone remodeling. In fishes with a single row of teeth, tooth germs can enter the dentigerous bone from either the lingual or labial side of the jaw (Fig. 1). If there are multiple rows of teeth, then tooth germs can enter from both sides of the dentigerous bone (e.g., Atlantic Wolffish, *Anarhichas lupus*, Bemis and Bemis, 2015). This variation may be phylogenetically informative, but the position of new tooth germs and replacement pores has not been widely surveyed or considered in a phylogenetic context (Bemis et al., 2005; Thiery et al., 2017).

Cutlassfishes are pelagic ambush predators that primarily feed on cephalopods and bony fishes as adults (Martins et al., 2005). The Atlantic Cutlassfish, *Trichiurus lepturus*, occurs in warm, coastal shelf waters around the world (Nakamura and Parin,

1993). The heterodont dentition of *T. lepturus* consists of large, barbed, premaxillary and dentary fangs positioned anteriorly in the jaw, and laterally compressed dagger-shaped teeth posteriorly, which in larger individuals can also bear barbs (Fig. 2A). Morgan (1977: 73) described the dentition and tooth replacement patterns in *T. lepturus* and specified that "tooth development occurs in the dentigerous bones" (= intraosseous replacement) and that intraosseous development is an adaptation that prevents struggling prey from dislodging developing teeth. Morgan (1977) described the unusual intraosseous replacement that occurs for the premaxillary fangs, which develop horizontally and rotate into place. Here, we provide new anatomical and developmental data and phylogenetic context for intraosseous tooth replacement modes of *T. lepturus* based on a large series of individuals to document stages and variation. We also compare modes of tooth replacement in *T. lepturus* to those of related taxa to understand the phylogenetic distribution of these replacement modes.

MATERIALS AND METHODS.

Terminology. We use bone of attachment to refer to the tissue connecting the dentine of a tooth to the dentigerous bone (e.g., dentary; *sensu* Sire and Huysseune, 2003:236; also see Hall, 2015: fig. 1.1 – note that the basal bone of Hall, 2015 = dentigerous bone here). Ankylosis is achieved when the ligaments connecting the bone of attachment to the dentigerous bone are mineralized; such ankylosis corresponds to tooth attachment Type 1 of Fink (1981). We follow Tucker (1956) who used the term "fang" to refer to large teeth in the front of the premaxillae and dentaries in trichiurids. The term "fang" also has been used to describe large teeth in different groups of fishes (i.e., "fangs" in different taxa do

not necessarily look the same, see descriptions in Nakamura and Parin, 1990 for Gempylidae and Trichiuridae; Melo, 2009 for Chiasmodontidae; and Grande, 2010 for Lepisosteidae), however, all are united by their relatively large size in comparison to other teeth, and their anterior positions in the jaw. Morgan (1977) used the term "barb" to describe the hook-shaped enameloid cap of some but not all teeth in the dentition of *Trichiurus lepturus*, and we follow his usage here. In barbed teeth, there is an enameloid keel only on the anterior cutting edge of the tooth. In contrast, unbarbed teeth have prominent enameloid keels on both the anterior and posterior cutting edges. We use the term "locus" to refer to a single position on a dentigerous bone where teeth will, or have already erupted (Bemis et al., 2005). Typically, a locus in species with intraosseous tooth replacement is a position for multiple generations of teeth throughout an individual's lifetime; in *T. lepturus*, more loci can be added posterior to the existing loci as a fish grows.

We follow phylogenetic interpretations of Orrell et al. (2006: fig. 2), who concluded that billfishes are not part of Scombroidei, and that Bluefish, *Pomatomus saltatrix*, and Longfin Escolar, *Scombrolabrax heterolepis*, are at the base of a clade including Gempylidae, Trichiuridae, and Scombridae. Most recent molecular analyses (e.g., Betancur R et al., 2017) recover a monophyletic group containing *Trichiurus lepturus* + *Gempylus serpens*, two taxa studied here, but Miya et al. (2013) report a different and non-monophyletic arrangement; however, neither of these studies was designed to test monophyly of Gempylidae and Trichiuridae, and have low taxon sampling given the species diversity of each proposed family. Recently, Beckett et al. (2018) analyzed new morphological characters combined with mtDNA data from Miya et

al. (2013) and reported that "Gempylidae" is not monophyletic, and that Trichiuridae is a clade within "Gempylidae." In their strict consensus tree of morphological data (Beckett et al. 2018: fig. 13B) *Pomatomus saltatrix* and *Scombrolabrax heterolepis* are placed in a polytomy with Scombridae (represented by *Gasterochisma melampus*) and "Gempylidae" including Trichiuridae. For our analyses, we interpret that *G. serpens* and *T. lepturus* are members of a monophyletic group within Scombroidei.

Examined specimens of *Trichiurus lepturus*. We prepared 79 specimens of *Trichiurus lepturus*, ranging from 514 mm to 1110 mm TL (TL = total length), caught by bottom trawl surveys conducted by the Northeast Fisheries Science Center (Politis et al., 2014). Specimens were fixed in 10% formalin (n=7) or frozen at sea (n=72). All specimens are deposited in the Nunnally Ichthyology Collection at the Virginia Institute of Marine Science (VIMS; Specimens Examined). We examined thirteen larval specimens ranging from 5 mm to 37 mm TL from the Southeast Area Monitoring and Assessment Program (SEAMAP/SML); these were collected during monitoring programs in the Gulf of Mexico. We also studied two juvenile specimens, 220 and 240 mm TL (VIMS 35823), collected in Chesapeake Bay.

Measurements and scoring. We dissected 72 specimens of *Trichiurus lepturus*, measured TL, recorded sex based on examination of gonads (M = male, F = female), and prepared dry skeletons (Bemis et al., 2004). For 15 specimens, we counted the number of loci, scored the replacement status of each locus, and the positions of replacement pores (*sensu* Bemis et al., 2005). As shown in Figure 2B, we used the replacement

classification of Bemis et al. (2005), which is: Absent (A, locus empty or shows broken remnants of previous tooth generation and the new tooth is developing within the bone); Incoming (I, tooth crown visible above the dentigerous bone but tooth is not ankylosed); Functional (F, tooth fully ankylosed around its circumference); or Eroding (E, ankylosis eroding around its circumference or at the base of the tooth). Both Absent and Incoming loci can be characterized as Replacing Loci (Fig. 2B); they are either wholly within the jaw or incompletely erupted, not ankylosed, and thus likely do not contribute to feeding. Functional and Eroding loci collectively make up Ankylosed Loci (Fig. 2B), and the teeth in such loci can be used in feeding. We measured tooth height (above the jaw) and base length (along the jaw) for Functional and Eroding teeth. We scored the presence of barbs on all Functional and Eroding teeth; if an Incoming tooth was sufficiently erupted to see a barb, then we scored it. Absent and Incoming loci in which the barb could not be seen were not scored. This scoring system yielded a minimal estimate of the number of barbed lateral teeth in the dentary, particularly for specimens in which the loci of the barbed region were in an early stage of a replacement wave. A replacement wave consists of two or more alternate loci with teeth in similar stages of development or progressive stages in a series (e.g., Functional teeth in loci 1, 3, 5 would be an example of three alternate loci within the same replacement wave). We graphically identified tooth replacement waves by connecting dashed lines between alternate loci in plots of locus condition.

Micro-computed tomography. We scanned three specimens with micro-CT: 1) the head of a specimen fixed in formalin and then dehydrated in ethanol before air drying (VIMS 35783); 2) a dry skeletal preparation of a premaxilla (VIMS 35776); and 3) a single

premaxillary fang (VIMS 35784). We used a GE 120 micro-CT scanner in the Biotechnology Resource Center Multiscale Imaging Facility at Cornell University to prepare data sets for VIMS 35783. Reconstructions prepared from these data sets have a resolution of 50 to 100 μm voxels. We used the facility's Xradia Versa XRM-500 nano-CT scanner to prepare data sets for VIMS 35776 and VIMS 35784, with resolutions of 5 to 20 μm voxels. We made 2-D orthogonal MPR (Multiplanar Reformatting) and 3-D volume reconstructions using OsiriX™ (version 5.8.5, 64-bit edition) DICOM imaging software (Rosset et al., 2004) on Apple Macintosh computers running OSX 10.8.5. To view internal anatomy of teeth and bones, we digitally dissected reconstructions within OsiriX™.

Histology and SEM. We decalcified portions of two formalin-fixed specimens using Formic Acid A (Humason, 1972; 20% formic acid), washed and dehydrated them for paraffin embedding, cut sections at 6 μm, and stained them with H&E (hematoxylin and eosin; Cornell Veterinary College Diagnostic Laboratory). For SEM study, we washed portions of dry skeletal specimen VIMS 35776 in several changes of household ammonia and water before dehydration in acetone and air drying. We mounted targeted parts of the specimen on stubs, sputter coated them with gold palladium, and imaged them with a JEOL NeoScope JCM-5000 SEM at the Paleontological Research Institution (PRI, Ithaca, NY).

Hardness testing. We performed hardness testing at the Cornell Center for Materials Research (CCMR) using a diamond indenter (Nanovea Series Digital Microhardness

Tester HWMMT-X3). Teeth from VIMS 35784 were embedded in epoxy and the surface was ground flat using a graded series of carborundum grits. We measured dimensions of the indentations to calculate Vicker's hardness (Bemis, 1984).

Comparative materials. We studied dry skeletal materials and preserved specimens of representative scombroids from 20 species in 18 genera (Specimens Examined). The intent of our comparisons is not to provide detailed studies of all scombroid dentitions, but to focus on modes of tooth replacement.

Photography. We photographed sections using an Olympus SZX12 microscope equipped with an Olympus DP70 digital camera. We used a Canon 5D Mark II digital camera to record color macrophotographs. Using Adobe Photoshop CS6, we adjusted images for color balance and contrast, and prepared plates and line drawings in Adobe Illustrator CS6.

RESULTS.

We found teeth in specimens >6 mm TL (e.g., SML 450916-000, 5 mm TL, lacks teeth). The silver-pigmented skin covering the tooth-bearing bones of the jaws is extremely thin (Fig. 3A). As a result, the major skeletal elements (Fig. 3B) are visible even with the skin intact. The long dentaries extend anteriorly beyond the premaxillae (Fig. 3), so that the mandibular symphysis is the most anterior point on the head. Elongate premaxillary and dentary fangs are approximately perpendicular to their dentigerous bones when they are

fully ankylosed. When the jaw is closed, the premaxillary fangs fit into recesses in the soft tissue between the rami of the lower jaw. The anteriormost premaxillary fangs fit anterior to a pair of distinct medial bony thickenings near the symphysis of the left and right dentary bones. The second or third functional premaxillary fangs insert posterior to these thickenings. Dentary fangs do not contact the premaxillary fangs because the dentary is longer. There is a small tooth on each premaxilla in front of the anteriormost fang, and a series of small teeth between and lateral to the premaxillary fangs (Fig. 3B). Posteriorly along the premaxilla is the series of teeth that we term lateral teeth. A corresponding series of lateral teeth is posterior to the dentary fangs, but the dentary lacks small teeth comparable to those in the anterior portion of the premaxilla.

Premaxillary fangs and replacement. Each premaxilla has three loci for large, barbed fangs (Fig. 4). Vascular dentine makes up most of the tooth, but a dense, outer enameloid layer forms a sharp blade along the anterior edges of the fangs, which we term a keel (Fig. 5). The keel is a smooth cutting edge, without serrations. In the premaxillary fangs, the enameloid keel continues into the barb and extends along the barb's posterior edge (Fig. 5A), but proximal to the barb, the posterior edge of the fang is rounded, without a keel or any evidence of dense mineralization. Diamond-indenter hardness testing showed that average Vickers Hardness (HV) of the barb is 213 HV (SD ± 44) in comparison to the shaft, which has a hardness of 53 HV (SD ± 3; Fig. 6).

In most specimens examined, no more than two of the three premaxillary loci had ankylosed, fully functional fangs (Fig. 4), with the other fang locus or loci undergoing replacement (Fig. 7). We observed some cases in which three functional fangs were

present (e.g., Fig. 7N, O). We interpret that the premaxillary fangs have an alternate replacement pattern. Replacement pores are located on the lingual side of the premaxilla. For example, two replacement pores (1RP and 3RP) are visible in Figure 4A; tooth germs have already migrated into the bone through these pores.

The premaxillary fangs exhibit intraosseous tooth replacement in which they develop horizontally along the axis of the premaxilla. The tip of the incoming fang (2I; Fig. 4A) faces posteriorly, and, as it develops, it grows out of the replacement pore through which its tooth germ originally migrated into the premaxilla. The tooth reaches full size before rotating into position and ankylosing. In Figure 4A, tooth 2I has nearly completed its development. As a premaxillary fang reaches full size, a channel erodes in the bone allowing the fang to rotate ventrally to a nearly perpendicular position before ankylosing to the premaxilla (Fig. 4B). Teeth that have recently rotated into place and have yet to ankylose to the dentigerous bone can be depressed by light pressure from a probe. The large channels created by new teeth rotating into place weaken the attachment of adjacent fangs from earlier generations, and their attachments begin to give way. In the two juvenile specimens examined (220 and 240 mm TL; VIMS 35823) horizontal tooth replacement of premaxillary fangs is evident.

Dentary fangs and replacement. Each dentary bears a single ankylosed barbed fang. A diastema separates the fang from the single row of lateral teeth along the dentary crest, and premaxillary fangs overlap the diastema (Fig. 3). Dentary fangs have a second mode of replacement (Figs. 7-9). All 92 specimens examined had two loci for dentary fangs (Fig. 7). One locus always had an ankylosed fang and the other locus was in a

replacement stage, yielding an alternate pattern of replacement. New tooth germs erode a well-developed replacement pore to enter the dentary on its labial side (Fig. 8). Once the tooth germ enters through the replacement pore, the new fang develops within the dentary and erupts vertically, directly into the locus (Figs. 8, 9). Dentary fangs never rotate unlike the developing premaxillary fangs. The replacement pore of a dentary fang remains open throughout the replacement process, and its diameter increases as the incoming tooth begins to erupt through it into position, until the tooth reaches its full height and ankyloses begins. The smooth surfaces of the replacement pore and eroding surface for the incoming fang are the result of osteoclast activity during erosion of the existing bone to accommodate the migrating tooth germ (Figs. 8, 9).

In the specimen shown in Figure 9, the dentary fang is ankylosed to the surrounding bone of the dentary, but its base is already being eroded. The skin of the lower jaw is exceptionally thin, and there are no pads flanking the labial surface of the ankylosed fang. Lingually, there is a thin, pad-like gum with adipose tissue deep to it.

Lateral teeth and replacement. The lateral teeth of the premaxilla and dentary are deeply socketed and ankylosed in a trench along the crest of the dentigerous bone (Fig. 4B). The lateral teeth are laterally compressed with cutting edges on their anterior and posterior surfaces, but only some teeth in the dentary are barbed.

Figure 10 plots the condition (A, I, F, E) for a series of 15 specimens ranging from 514 mm to 1103 mm TL. The total number of premaxillary loci for lateral teeth ranged from 15 (Fig. 10B) to 23 (Fig. 10L). The number of dentary loci for lateral teeth ranged from 16 (Fig. 10C) to 29 (Fig. 10N). Within each specimen, the number of loci for

lateral teeth in the premaxilla correlated with the number of loci for lateral teeth in the dentary ($r^2 = 0.86$). For example, specimens that have few premaxillary loci also have few dentary loci (Fig. 10C). The number of premaxillary and dentary loci correlates with TL ($r^2 = 0.76$, 0.79, respectively). No statistically significant relationship was found between number of loci of lateral teeth and sex of the individual, i.e., male and female specimens of similar lengths have similar numbers of loci. For example, two of the largest specimens examined are male and female (Fig. 10K and L, respectively), and they have similar numbers of loci for lateral teeth in the premaxilla and dentary.

The pattern of replacement waves indicated by the dashed lines in Figure 10 can be understood in the context of alternate tooth replacement and the four-part staging system (A, I, F, E). In particular, a tooth locus scored as eroding would soon have lost its tooth and then be scored as absent. For example, there are three premaxillary waves in the specimen shown in Figure 10 Part O. To understand how these three waves are coordinated, consider tooth loci 7, 9, 11 and 13. In the case of locus 9, the eroding tooth that was formerly there has been lost and thus locus 9 is scored as absent. Note that loci 7 and 11 are eroding. We interpret that a single eroding tooth in the middle of the first wave was lost at locus 9 because it eroded slightly faster than did the two adjacent loci (7 and 11) of the first wave. Similarly, the eroding tooth at locus 11 would soon have been lost, rendering this locus as absent. This would put locus 11 in complete alignment with the third tooth wave (i.e., loci 9, 13, 15, 17, 19). Such variation in replacement waves reflects the biological reality and timing of tooth replacement across individuals.

The base lengths of lateral teeth increase toward the middle of the series of loci in both the premaxilla and dentary, and decrease from that point posteriorly (Fig. 11A, B).

A similar pattern occurs for tooth height (Fig. 11A, B). The most posterior teeth in the series are smaller and slightly recurved (Fig. 3B). Because the alveolar margin of the premaxilla is concave, the absolute height increase and subsequent decrease is not evident except from tooth measurements. All teeth have enameloid caps, but barbs only occur on dentary teeth on the widest and tallest teeth in the middle of the series; all lateral teeth of the premaxillary and lateral teeth at the anterior and posterior ends of the dentary lack barbs. Larvae and juvenile specimens examined lack barbed lateral teeth in the dentary, but have barbed premaxillary and dentary fangs. The number of barbed lateral teeth in the dentary increases as a function of TL ($r^2 = 0.63$; range = 0-8 barbs). The teeth of larger specimens are larger (Fig. 11). Thus, over ontogeny, individuals increase both the number of loci and tooth size at a given locus. For example, in the specimen shown in Figure 11B, the eroding tooth at locus 11 indicated by an arrow is smaller in height and base length than the functional teeth adjacent to it in loci 10 and 12. This is because the adjacent functional teeth are from a later wave and thus larger than the eroding tooth between to them.

Despite differences in tooth shape (e.g., barbed or not barbed) all lateral teeth in the premaxilla and dentary have the same replacement mode (Figs. 10-14). For both the premaxilla and dentary, the numbers of Replacing Loci are approximately equal to those of Ankylosed Loci. In the 15 scored specimens, 573 premaxillary loci were scored: 51% were Replacing Loci; 49% were Ankylosed Loci. Of 717 dentary loci, 54% were Replacing Loci; 46% were Ankylosed Loci. There is no significant difference between the percentages of Replacing Loci and Ankylosed Loci in either the premaxilla or the dentary, and this indicates an almost perfectly alternate tooth replacement pattern across

the entire sample. The alternate tooth replacement pattern is evident in most specimens, with Incoming (I) or Absent (A) alternating with Functional (F) or Eroding (E) teeth (Fig. 12A).

Replacement waves for the lateral teeth in 15 specimens are indicated by dashed lines connecting loci in the same replacement wave (Fig. 10). For example, in a 514 mm TL specimen (Fig. 10A) there is a long replacement wave in the premaxilla consisting of five Absent Loci (1, 3, 5, 7, and 9), followed by two Incoming Loci (11, 13), and two Functional Loci (15, 17). A second replacement wave consists of six Functional Loci at positions 2, 4, 6, 8, 10, and 12. A third and very short replacement wave is indicated by Absent Loci 14 and 16. The oldest tooth in a given replacement wave is at its posteriormost locus. The number of replacement waves in the premaxilla ranged from 2-6 with a mode of 3 (Fig. 10). The number of replacement waves in the dentary ranged from 3-7 with a mode of 4 (Fig. 10).

Ankylosis is not complete until after an Incoming tooth erupts, but once the ankylosis develops, it is strong. For example, ankyloses at the bases of the fangs and lateral teeth (Fig. 12A) are the densest tissues of the premaxilla. In the case of lateral teeth, incoming teeth develop within the bone, and erode bone of attachment (cone-shaped collars at the base of each functional tooth) as they erupt (Fig. 12A). Constant processes of ankylosis and erosion remodel the jaws to accommodate tooth development, growth, and attachment. For example, the ankylosis of a functional tooth is eroded from both sides as new incoming teeth erupt; the ankyloses for the newly erupted teeth will not develop until later (Fig. 12B).

Three waves of lateral teeth can be present at the same time. Near the top of the section shown in Figure 13, an Absent Locus is flanked by two Functional Loci. A new tooth germ, the youngest tooth, is migrating deep into the trench, passing between the two functional teeth and still connected to the oral epithelium by its dental lamina (Fig. 13). Simultaneously, two developing teeth, intermediate in age between the tooth germ and the two functional teeth, have mineralized portions of the vascular dentine and keel but have not yet erupted. The two functional teeth, which are the first wave shown, would soon have been lost. The two developing teeth that are part of the second wave would have erupted into the Absent Loci adjacent to the Functional Loci. The tooth germ, which is the third wave visible, would have continued to sink beneath the functional tooth to its left, and developed to eventually replace it.

Unlike the obvious replacement pores for premaxillary and dentary fangs, the replacement pores for lateral teeth are harder to define. Because the new tooth germ and the incoming tooth together erode bony tissues at an Absent Locus between ankylosed teeth, there is extensive and continuous remodeling of bone around each replacement pore in the trench (Figs. 4B, 12B, 13).

Phylogenetic comparisons. We examined tooth replacement patterns in scombroids (see Specimens Examined) and highlight several specific comparisons here using Figure 14.

Pomatomidae. The Bluefish, *Pomatomus saltatrix*, lacks fangs in both the premaxilla and dentary (Fig. 14A). Tooth replacement is alternate throughout the jaw (Bemis et al. 2005). New tooth germs for the teeth of *P. saltatrix* migrate into the dentigerous bone via

replacement pores on the labial side of the premaxilla and the lingual side of the dentary as opposed to entering via a trench (Fig. 14A). In the case of *P. saltatrix*, a replacement pore is largest just after it has admitted a tooth germ into the dentigerous bone. This is because the tooth germ migrates through the enlarged pore to reach its position directly underneath the tooth that it will replace. Subsequently, the replacement pore becomes smaller. The new tooth germ that entered the jaw continues to develop below the older tooth that it will replace, and as it grows, it enters the older tooth's pulp cavity. There is a pattern of replacement pore sizes in relation to the tooth condition (A, I, F, or E) at each locus along the jaw. Large replacement pores are associated with Functional teeth and small pores with Absent Loci; a pore may close completely after the tooth germ has migrated into the jaw. The large pores are the youngest because a tooth germ has just entered through the pore; the pore will eventually be closed over as the surrounding bone is remodeled. A new tooth of *P. saltatrix* does not erupt through its replacement pore (Bemis et al., 2005). In contrast, replacement pores remain open in all three replacement modes in *Trichiurus lepturus*, and new teeth erupt through them.

Scombrolabracidae. *Scombrolabrax heterolepis* has distinctive premaxillary and dentary fangs (Fig. 14B). The fangs develop in loci that we presume to be homologous to the fang loci of *Trichiurus lepturus* because the replacement pores are on the lingual side of the premaxilla, and the labial side of the dentary. The premaxillary fangs develop vertically and do not rotate into place. Pores for dentary fangs are located more anteriorly and ventrally than in *T. lepturus*, and dentary fangs erupt vertically. Like *T. lepturus*, the

lateral teeth of *S. heterolepis* replace via a trench. Tooth replacement is alternate throughout the jaws.

Trichiuridae + "Gempylidae". Other trichiurids and "gempylids" (Fig. 14C; Specimens Examined) show patterns of tooth replacement similar to *Trichiurus lepturus*. The 2-3 premaxillary fangs on each ramus develop horizontally from replacement pores located on the lingual surface of the premaxilla; all three replacement modes are present. *Gempylus serpens* (Fig. 14C) has a remarkably similar dentition and replacement pattern to that of *T. lepturus*; the incoming fangs can be depressed with a probe before they ankylose to the bone. There are two loci for dentary fangs, which develop through replacement pores on the labial surface; new dentary fangs erupt vertically without rotating. Lateral teeth of the premaxillae and dentaries develop in trenches as in *T. lepturus*. Tooth replacement is alternate in all three modes. In some "gempylids" with smaller fangs, like *Promethichthys prometheus*, premaxillary fang development rotation is present, but the rotation is less extreme.

Scombridae. Scombrid teeth vary greatly in size and shape, but all taxa examined lack premaxillary and dentary fangs (Fig. 14D; Specimens Examined). The teeth of scombrids are replaced in a trench, using the same mode that we observed for the lateral teeth of *Trichiurus lepturus*. Replacement is alternate. The teeth of *Scomber scombrus* are among the smallest examined in this survey, however, they exhibit typical alternate replacement. There are no replacement pores on the labial or lingual surfaces.

DISCUSSION.

Although age and growth of *Trichiurus lepturus* have been studied in other regions (e.g., Kwok and Ni, 2000, South China Sea), comparable data do not exist for the western North Atlantic population. Such information would inform estimates of absolute rates of tooth replacement because more teeth are added as a fish grows. We infer from the strongly alternate replacement pattern that tooth replacement is closely regulated, with teeth replaced on a schedule rather than as they are damaged. A higher percentage of the ankylosed teeth are functional rather than eroding, which suggests that individual teeth are quickly lost once erosion begins but that teeth remain functional for extended periods of time. A similar interpretation was suggested for two other scombroids, *Scomberomorus cavalla* (Morgan and King, 1983: fig. 1) and *Pomatomus saltatrix* (Bemis et al., 2005: fig. 5).

The premaxillary fangs, dentary fangs, and barbed lateral teeth of *Trichiurus lepturus* have cutting edges along the keel and the posterior edge of the barb (Fig. 5). Unbarbed lateral teeth are compressed, with cutting edges on both the anterior and posterior surfaces of the tooth. CT scans and hardness testing (Figs. 5, 6) show that the barb and keel are much harder than the dentine of the shaft. The average Vickers hardness for the barb tip is 213 HV (SD ± 44; Fig. 6), somewhat lower than that of mammalian enamel (> 270 HV for humans; Gutiérrez-Salazar and Reyes-Gasga, 2003). The average Vickers hardness for the tooth shaft is 53 HV (SD ± 3), comparable to mammalian dentine (50-60 HV for humans, Gutiérrez-Salazar and Reyes-Gasga, 2003). Hardening and reinforcement of cutting edges and barbs likely have functional

implications for capturing and processing prey. There are no detailed studies on feeding behavior of *T. lepturus*, but Martins et al. (2005) reported field observations of feeding by large *T. lepturus* suggesting that they impale and cut prey items. These authors also reported ontogenetic shifts in diet: larvae (<5 cm) feed primary on calanoid copepods, juveniles (5-30 cm) feed on small zooplanktonic crustaceans, subadults (30-70 cm) feed on euphausiids and small fishes like anchovies, and large adults (70-160 cm) cannibalize other *T. lepturus,* feed on sciaenids, cephalopods, and shrimps, as well as anchovies and euphausiids. Despite these ontogenetic changes in diet, barbed and keeled teeth are present in larval *T. lepturus.* De Schepper et al. (2008) suggested that rapid closing of the jaws and a powerful bite help to ensure prey capture; their study documented both attributes in *T. lepturus*. Long jaws facilitate rapid closing and increased gape, which allows *T. lepturus* to capture large prey (De Schepper et al., 2008).

We found three modes of tooth replacement in *Trichiurus lepturus* related to the location of the tooth locus in the jaw (Fig. 15). Mode 1 relates to replacement of premaxillary fangs via horizontal development of replacement fangs and rotation into place before ankylosis; the replacement pores are located on the lingual surface of the premaxilla. In Mode 2, dentary fangs develop from tooth germs that enter replacement pores on the labial surface of the dentary, migrate deeply beneath the functional tooth, develop vertically, and erupt directly into position before ankylosis. Lateral teeth develop via Mode 3: new tooth germs form in soft tissues in a trench along the crest of the dentigerous bone and then migrate into the bone between adjacent Functional Loci (Fig. 13). The tooth germs of lateral teeth develop vertically beneath existing teeth and erupt directly into position before ankylosis. In all three modes, tooth replacement is alternate

and very strong ankyloses develop. We found no reports that document such distinctly different modes of tooth replacement in one species of teleost (e.g., Berkovitz and Shellis, 2017).

We surveyed 20 species of scombroids (Fig. 14; Specimens Examined) to explore the phylogenetic distribution of the three tooth replacement modes found in *Trichiurus lepturus* (Fig. 16). Orrell et al. (2006) placed *Pomatomus saltatrix* at the base of Scombroidei, and it shares many features of tooth replacement with other scombroids (e.g., alternate tooth replacement, strong ankyloses of teeth, and intraosseous tooth replacement; Bemis et al., 2005, Johnson, 1986). However, these features occur in many other percomorph taxa and are likely plesiomorphic to Scombroidei (Fig. 16). *Scombrolabrax heterolepis* has premaxillary and dentary fangs, so we can compare all three replacement modes to those observed in *T. lepturus*. A key difference is that the relatively shorter premaxillary fangs of *S. heterolepis* do not rotate during their development. In *T. lepturus* and *Gempylus serpens*, all three tooth replacement modes are present and very similar. In *Scomber scombrus*, however, premaxillary and dentary fangs are absent, meaning that only replacement Mode 3 occurs. Key differences among the taxa summarized in Figure 16 include the opposite location of replacement pores in *P. saltatrix* compared to the fang pores of *S. heterolepis*, *T. lepturus*, and *G. serpens*; rotation of the premaxillary fangs in *T. lepturus* and *G. serpens*; and the absence of fangs in *S. scombrus*, which we interpret as a phylogenetic loss. Although there is great variation in the dentitions of scombroids, such as the shapes and details of the teeth (e.g., size, keels, barbs, serrations, etc.), the replacement modes, especially within clades, are conserved.

Dental lamina and replacement pores. The source of epithelial cells for new tooth formation can either be from the preceding generation of teeth, a condition known as a successional dental lamina (Huysseune, 2006), or the epithelium can enter directly through replacement pores that extend the dental lamina from its initial site in the oral epithelium (Bemis et al. 2005, Thiery et al. 2017). Huysseune (2006) described a successional dental lamina in the pharyngeal jaw of *Danio rerio*, which has extraosseous tooth replacement, in which a new tooth germ is derived in part from the epithelium of a predecessor tooth, i.e., there is an epithelial strand connecting the new tooth germ with its predecessor. Such a successional dental lamina occurs when the new tooth germ is part of an established tooth family (Huysseune, 2006). In contrast, the dental lamina in *Trichiurus lepturus* derives directly from the oral epithelium and is not connected to that of a predecessor tooth. We term this a direct dental lamina to distinguish it from the successional lamina described by Huysseune (2006). Such a direct dental lamina occurs in other species with intraosseous tooth replacement in the oral jaws (e.g., Bemis et al., 2005, Bemis and Bemis, 2015, Thiery et al., 2017) although this is our first use of the term direct dental lamina. We think that characters related to the type of tooth replacement (extraosseous vs intraosseous), the position of the dental lamina (successional vs direct), the occurrence of replacement pores (present or absent), and the position of replacement pores (lingual side, labial side, or crest of dentigerous bone) have phylogenetic signals. Until more taxa are surveyed, however, it is not possible to establish whether the direct dental lamina is part of a character complex linked to

intraosseous tooth development or whether it should be interpreted as a separate character.

Coupling of tooth formation and bone erosion processes. The locations where tooth germs enter the bone influence subsequent developmental processes related to bone erosion and remodeling, and, by extension, are directly related to functional anatomical considerations such as the strength of the dentigerous bones. By eroding into the side of the dentigerous bone, a tooth germ of *Pomatomus saltatrix* invades directly into the base of the functional tooth (and eventually its pulp cavity) that it will replace. This process links new tooth formation to erosion of the old tooth (Bemis et al., 2005: figs. 9, 10). In contrast, tooth germs for the lateral teeth of *Trichiurus lepturus* erode into bone from the trench along the crest of the dentigerous bone in association with an Absent Locus. Simultaneously, a developing tooth nears eruption into that locus (Fig. 13). Such coupling of tooth germ entry and eruption minimizes bone erosion, and allows a passage for the incoming tooth. As a result, much of the bone eroded during lateral tooth germ migration of *T. lepturus* is bone of attachment, not the parallel-fibred bone through which the tooth germs of *P. saltatrix* pass. In both cases, erosion depends on osteoclasts, but the patterns of development are different. Differences between the Bluefish Type and Cutlassfish Type of tooth replacement (Fig. 17) are not simply the result of moving the site of origin of tooth germs because the mechanisms by which tooth germs enter the bone are coupled to subsequent developmental processes of bone erosion, remodeling, and tooth ankylosis. The differences between *P. saltatrix* and *T. lepturus* show that there

are multiple ways for intraosseous tooth replacement to yield alternate tooth replacement with strong ankyloses of teeth.

Evolution of intraosseous replacement in *Trichiurus lepturus*. Developing tooth germs can be protected from potential damage during feeding by soft tissues and/or bone (Morgan, 1977). In the case of *T. lepturus*, the skin and oral mucosa are too thin to offer much protection to tooth germs (Fig. 8A). Tooth germs developing in a trench are better protected than they would be if they entered the bone on either its lingual or labial side. In the case of the premaxillary fangs, horizontal replacement may protect large teeth as they develop, but it is also possible that such horizontal development is related to space constraints. The jaws of *T. lepturus* are thin and lightly built of parallel-fibred bone. More bone is present near the premaxillary symphysis, but it is still insufficient to allow vertical development of elongate fangs, particularly because there are three fang loci in this compact region. Perhaps the small overall height of the premaxilla relative to its long fangs constrains fang development. If so, then rotational fang development is a mechanism for developing large premaxillary fangs. Dentary fangs develop vertically: they are shorter than premaxillary fangs, and there are only two loci, so there is more space and better protection for developing fangs within the bone prior to their eruption.

Although yet to be formally surveyed, we have observed horizontal rotation during replacement of large fangs in other families of teleosts such as Cynodontidae (intraosseous) and Alepisauridae (extraosseous). Horizontal tooth development and rotation into the functional position also occurs in snakes. For example, replacement teeth in the lower jaw of the Rhinoceros Horned Viper (*Bitis nasicornis*) develop in a

horizontal position; the new teeth rotate upon eruption into the functional position before ankylosis (Berkovitz and Shellis, 2017: fig. 7.21). A similar replacement mode occurs in elapid snakes (Berkovitz and Shellis, 2017: 216). Rotational development of teeth in snakes convergently resembles the condition in Alepisauridae because in both taxa tooth development is extraosseous.

Replacement premaxillary fangs of trichiurids and "gempylids" have been misinterpreted in some taxonomic works, with incoming fangs described as "depressible teeth" (e.g., Tucker, 1956; Ho et al., 2017). These teeth are merely a stage (incoming) during the development of premaxillary fangs. The number of incoming premaxillary fangs varies over time and needs to be viewed in the context of tooth replacement overall.

Intraosseous tooth replacement is a complex and variable process that has evolved repeatedly within teleosts. Key processes include the sites of formation of new tooth germs and points of entry into bones, whether teeth develop horizontally or immediately beneath the tooth that they will replace, and how erosion, tooth eruption, and ankylosis occur. These processes can differ, but still yield similar dentitions (Fig. 17). In the modes of tooth replacement described to date, details vary, and the full implications of such differences remain unexplained. Further descriptions of the diversity of tooth replacement modes of teleosts will contribute to a better understanding of phylogenetic patterns as well as the functional anatomy and development of teeth.

ACKNOWLEDGEMENTS

We thank J. Galbraith, H. Cook, J. Kircun of the Northeast Fisheries Science Center (NEFSC) who collected many of the specimens examined, and we are grateful for the wealth of specimens and information available from the NEFSC Ecosystems Survey Branch. We thank T. Hughes, C. Copeland, and C. Fox for help preparing skeletal material. We thank S. Huber, VIMS, for cataloging and curating new specimens collected for this project, and the following individuals for loans of comparative material: D. McElroy, NEFSC; C. Dardia, CUMV; T. Cullins, SEAMAP and L. Habegger, Florida Southern College; R. Arrindale, B. Brown, and T. Vigliotta, AMNH; M. Arce and M. Sabaj, ASNP; K. Murphy, S. Raredon, USNM. A. S. Martins provided valuable information about cutlassfish diet. M. Riccio and T. Porri, Cornell University Biotechnology Resource Center, performed CT scans. W. Allmon, Paleontological Research Institution, provided access to SEM facilities. We also thank M. Slade, Cornell Veterinary College Diagnostic Laboratory, and P. Carubia of Cornell Center for Materials Research (CCMR, facilities supported by NSF MRSEC program, DMR-1120296). B. Collette, N. Schnell, and M. Vecchione reviewed an earlier version of the paper. Research support provided by NSF Graduate Research Fellowship Program, Nancy S. and Henry George Fellowship, Cornell University Jane E. Brody Undergraduate Research Grant, Morley Student Research Grant, and Tontogany Creek Fund. This paper is Contribution No. xxxx of the Virginia Institute of Marine Science, College of William & Mary.

LITERATURE CITED

Bemis, W. E. (1984). Morphology and growth of lepidosirenid lungfish tooth plates (Pisces: Dipnoi). *Journal of Morphology*, 179, 73-93. DOI:10.1002/jmor.1051790108.

Bemis, K. E. and W. E. Bemis. (2015). Functional and developmental morphology of tooth replacement in the Atlantic Wolffish, *Anarhichas lupus* (Teleostei: Zoarcoidei: Anarhichadidae). Copeia, 103(4), 886-901. DOI: 10.1643/OT-14-141.

Bemis, W. E., E. J. Hilton, B. Brown, R. Arrindell, A. M. Richmond, C. D. Little, L. Grande, P. L. Forey, and G. J. Nelson. (2004). Methods for preparing dry, partially articulated skeletons of osteichthyans, with notes on making Ridewood dissections of the cranial skeleton. *Copeia*, 2004(3), 603-609. DOI:10.1643/CI-03-054R1.

Bemis, W. E., A. Giuliano, and B. McGuire. (2005). Structure, attachment, replacement and growth of teeth in Bluefish, *Pomatomus saltatrix* (Linnaeus, 1766), a teleost with deeply socketed teeth. *Zoology*, 108, 317-327. DOI: 10.1016/j.zool.2005.09.004.

Berkovitz, B. and P. Shellis. (2017). The Teeth of Non-Mammalian Vertebrates. Elsevier, Amsterdam.

Betancur-R, R., E. O. Wiley, G. Arratia, A. Acero, N. Bailly, M. Miya, G. Lecointre, and G. Ortí. (2017). Phylogenetic classification of bony fishes. *BMC Evolutionary Biology*, 17 (162),1-40. DOI: 10.1186/s12862-017-0958-3.

Collette, B. B., T. Potthoff, W. J. Richards, S. Ueyanagi, J. L. Russo, and Y. Nishikawa. (1984). Scombroidei: Development and relationships. In: Ontogeny and Systematics of Fishes, ASIH Special Publication 1, 591-620.

Conway, K.W., N. G. Bertrand, Z. Browning, T. W. Lancon, and F. J. Clubb Jr. (2015). Heterodonty in the New World: An SEM Investigation of oral dentition in the Clingfishes of the subfamily Gobiesocinae (Teleostei: Gobiesocidae). *Copeia*, 103(4), 973-998. DOI: 10.1643/OT-15-234.

De Schepper, N., S. V. Wassenbergh, and D. Adriaens. (2008). Morphology of the jaw system in trichiurids: trade-offs between mouth closing and biting performance. *Zoological Journal of the Linnean Society*, 152, 717-736. DOI: 10.1111/j.1096-3642.2008.00348.x.

Grande, L. (2010). An Empirical Synthetic Pattern Study of Gars (Lepisosteiformes) and Closely Related Species, Based Mostly on Skeletal Anatomy. The Resurrection of Holostei, ASIH Special Publication 6, 1-871.

Gutiérrez-Salazar, M. del Pilar, and J. Reyes-Gasga. (2003). Microhardness and chemical composition of human tooth. *Materials Research*, 6, 367-373. DOI: 10.1590/S1516-14392003000300011.

Francillon-Vieillot H., V. de Buffrénil, J. Castanet, J. Géraudie, F. J. Meunier, J. Y Sire, L. Zylberberg, and A. de Riclès. (1990). Microstructure and Mineralization of Vertebrate Skeletal Tissues. In Skeletal Biomineralization: Patterns, Processes and Evolutionary Trends. J. G. Carter, ed. Van Nostrand Reinhold, New York, pp 471-530.

Hall, B. K. (2015). Bones and Cartilage: Developmental and Evolutionary Skeletal Biology. 2nd Edition. Academic Press, Amsterdam.

Ho, H.-C., H. Motomura, H. Hata and W.-C. Jiang. (2017). Review of the fish genus *Epinnula* Poey (Perciformes: Gempylidae), with description of a new species from the Pacific Ocean. *Zootaxa*, 4363(3), 393-408. DOI: 10.11646/zootaxa.4363.3.5.

Humason, G. L. (1972). Animal Tissue Techniques. W. H. Freeman, San Francisco.

Huysseune, A. (2006). Formation of a successional dental lamina in the zebrafish (*Danio rerio*): support for a local control of replacement tooth initiation. *International Journal of Developmental Biology*, 50, 637-643.

Huysseune, A. and P. E. Witten. (2006). Developmental mechanisms underlying tooth patterning in continuously replacing osteichthyan dentitions. *Journal of Experimental Zoology*, 306B, 204-215. DOI: 10.1002/jez.b.21091.

Johnson, G. D. (1986). Scombroid phylogeny: An alternative hypothesis. *Bulletin of Marine Science*, 39(1), 1-41.

Kwok, K. Y. and I-H. Ni. (2000). Age and growth of cutlassfishes, *Trichiurus* spp., from the South China Sea. *Fishery Bulletin*, 98(4), 748-758.

Martins, A. S., M. M. Haimovici, and R. Palacios. (2005). Diet and feeding of the cutlassfish *Trichiurus lepturus* in the subtropical convergence ecosystem of southern Brazil. *Journal of the Marine Biological Association of the United Kingdom*, 85, 1223–1229.

Melo, M. R. S. (2009). Revision of the genus *Chiasmodon* (Acanthomorpha: Chiasmodontidae), with the description of two new species. *Copeia*, 2009 (3), 583-608. DOI:10.1643/CI-08-048.

Miya, M., M. Friedman, T. P. Satoh, H. Takeshima, T. Sado, W. Iwasaki, Y. Yamanoue, M. Nakatani, K. Mabuchi, J. G. Inoue, J. Yde Poulsen, T. Fukunaga, Y. Sato, M. Nishida. (2013). Evolutionary origin of the Scombridae (tunas and mackerels): Members of a Paleogene adaptive radiation with 14 other pelagic fish families. *Plos One* 8(9), e73535. DOI:10.1371/journal.pone.0073535.

Morgan, E.C. (1977). Dentitional phenomena and tooth replacement in the scabbard fish *Trichiurus lepturus* Linnaeus (Pisces: Trichiuridae). *Texas Journal of Science*, 29, 71–77.

Morgan, E. C. and W. K. King. (1983). Tooth replacement in King Mackerel, *Scomberomorus cavalla* (Pisces: Scombridae). *The Southwestern Naturalist*, 28(3), 261-269.

Nakamura, I. and N. V. Parin. (1993*).* FAO Species Catalogue Vol. 15 Snake Mackerels and Cutlassfishes of the World (Families Gempylidae and Trichiuridae): An annotated and illustrated catalogue of the snake mackerels, snoeks, escolars, gemfishes, sackfishes, domine, oilfish, cutlassfish, hairtails and frostfishes known to date. Food and Agriculture Organization, Rome.

Orrell, T. M., B. B. Collette, and G. D. Johnson. (2006). Molecular data support separate scombroid and xiphioid clades. *Bulletin of Marine Science*, 79(3), 505-519.

Politis, P. J., J. K. Galbraith, P. Kostovick, and R. W. Brown. (2014). Northeast Fisheries Science Center bottom trawl survey protocols for the NOAA Ship Henry B.

Bigelow. US Department of Commerce, Northeast Fish Sciences Center Reference Document 14-06; 138 p. http://nefsc.noaa.gov/publications/.

Rosset, A., L. Spadola, and O. Ratib O. (2004). OsiriX: An open-source software for navigating in multidimensional DICOM images. *Journal of Digital Imaging* 17, 205-216.

Sabaj M. H. (Ed.). (2016). Standard symbolic codes for institutional resource collections in herpetology and ichthyology: An Online Reference. Version 6.5 (accessed 24 March 2018). Electronically accessible at http://www.asih.org, American Society of Ichthyologists and Herpetologists, Washington, D.C.

Thiery, A. P., T. Shono, D. Kurokawa, R. Britz, Z. Johanson, and G. Fraser. (2017). Spatially restricted dental regeneration drives pufferfish beak development. *Proceedings of the National Academy of Sciences of the United States of America*, 114 (22), E4425–E4434. DOI: 10.1073/pnas.1702909114.

Trapani, J. (2001). Position of developing replacement teeth in teleosts. *Copeia*, 2001(1), 35–51. DOI:10.1643/0045-8511(2001)001[0035:PODRTI]2.0.CO;2.

Tucker, D. W. (1956). Studies on the trichiuroid fishes – 3: A preliminary revision of the family Trichiuridae. *Bulletin of the British Museum of Natural History and Zoology*, 4, 73.

Figure Legends

Figure 1. Overview of intraosseous replacement of oral teeth based on Bluefish, *Pomatomus saltatrix*. During intraosseous tooth replacement, tooth germs migrate into dentigerous bones through a replacement pore. Location of replacement pores varies within teleosts: they can occur, for example, on the lingual or labial surfaces of the bones. In Bluefish, new tooth germs form on the labial side of the premaxilla and the lingual side of the dentary.

Figure 2. Morphological data and terminology used in this study. **A.** Diagram showing four types of teeth in the oral jaws of *Trichiurus lepturus*. **B.** Diagram of developing teeth based on Morgan and King (1983), simplified and relabeled to match tooth classification system of Bemis et al. (A, I, F, E; 2005) used here. Replacing Loci are those scored A or I. Ankylosed Loci are those scored F or E.

Figure 3. Head and dentition of adult specimens of *Trichiurus lepturus*. **A.** Lateral view of freshly caught specimen to show external anatomy of head with intact soft tissues. VIMS 35902, 1045 mm SL. **B.** Lateral view of cranial skeleton to show general arrangement of dentigerous bones and teeth (right side of specimen is shown; image has been reversed so that anterior faces left). VIMS 35789, 964 mm TL, F.

Figure 4. Micro-CT reconstruction of dentition and tooth replacement in right premaxilla. **A.** Lingual view, anterior to left. Two functional ankylosed fangs are present (1F, 3F), each with a replacement pore (1RP, 3RP) posterior to the corresponding fang. The incoming fang at the second locus (2I) is horizontal and aligned with the ramus of the premaxilla. A series of small teeth extend laterally

between the three fang loci; a single small tooth is located at the anterior tip of the premaxilla. Incoming lateral teeth (I) alternate with functional lateral teeth (F); note that the incoming lateral teeth are just beginning to erupt in the anterior part of the series and have almost completed eruption posteriorly. This difference reflects a replacement wave. Arrows enameloid indicate keel(s) of teeth; in barbed teeth, there is a keel only on the anterior cutting edge of the tooth. Unbarbed teeth have enameloid keels on both the anterior and posterior cutting edges. **B.** Palatal (= ventral) view of the same specimen shown in part A. The incoming fang (2I) is eroding a channel in the premaxilla, through which the fang will rotate into position. The incoming lateral teeth are erupting via the trench along the crest of the premaxilla. VIMS 35776, 540 mm TL, M.

Figure 5. Micro-CT reconstruction and virtual dissection of a fang from the left premaxilla. Lighter colors indicate greater tissue density. **A.** Anterior, posterior, and lateral views together with a sagittal section (left to right) of the fang showing different densities of mineralized tissues. A sharp, and dense enameloid keel is present on the anterior edge; there is no comparable mineralized tissue along the posterior edge except distally in the region of the barb. Arrows marked B indicated the plane of the virtual dissection shown in Part B. **B.** Virtual dissection of the shaft of the fang showing vascular dentine and comparative density of mineralized tissues in the keel, barb, and tooth shaft. VIMS 35784, 1034 mm TL, F.

Figure 6. Diamond indenter hardness testing of barb and tooth shaft of an epoxy embedded premaxillary fang. **A.** Overview of fang showing region where

measurements were made. **B.** Close up showing positions of indentations and Vicker's Hardness (VH) values. Values for the enameloid of the barb ranged from 91-267 VH; dentine of the shaft was softer, with values ranging from 58-62 VH. VIMS 35784, 1034 mm TL, F.

Figure 7. Condition of fangs at each locus in the left and right premaxilla, and left and right dentary for 15 individuals arranged by TL scored as Absent, Incoming, Functional or Eroding. Replacement status of the fang loci in the left ramus is often opposite to that in the right ramus when teeth are considered Ankylosed or Replacing. **A.** VIMS 35770, 514 mm TL, M. **B.** VIMS 35874, 535 mm TL, M. **C.** VIMS 35769, 550 mm TL, M. **D**. VIMS 35798, 601 mm TL, M. **E.** VIMS 35774, 650 mm TL, F. **F.** VIMS 35778, 695 mm TL, M. **G**. VIMS 35777, 715 mm TL, M. **H**. VIMS 35780, 785 mm TL, F. **I.** VIMS 35791, 911 mm TL, M. **J.** VIMS 35795, 948 mm TL, F. **K.** VIMS 35790, 1000 mm TL, M. **L.** VIMS 35787, 1005 mm TL, F. **M**. VIMS 35788, 1037 mm TL, F. **N**. VIMS 35794, 1040 mm TL, M. **O**. VIMS 35779, 1103 mm TL, F.

Figure 8. Scanning electron micrograph of fang and fang replacement at tip of left dentary. The functional fang is ankylosed to the bone and a replacement pore has developed at its base. An incoming fang immediately posterior to it is erupting through its replacement pore. Note the smooth edges of the replacement pore and smooth eroding surface surrounding the incoming fang. Anterior to left. VIMS 35776, 540 mm TL, M.

Figure 9. Histological section (6 μm) of dentary stained with hematoxylin and eosin showing a dentary fang developing directly beneath the ankylosed, functional

fang that it will replace. Dashed lines indicate the region of ankylosis between the vascular dentine of the fang and bone. Bone immediately adjacent to the dashed line is bone of attachment, which can be differentiated from the parallel-fibred bone of the dentary by its irregular vascular channels. Asterisks (*) indicate position of osteoclast resorption of dentine and bone to accommodate growth and eventual eruption of developing fang. Note the extremely thin skin surrounding the labial surface of the dentary. To the lingual side of the fang, a small pad of gum tissue is underlain by adipose. Due to plane of section, only one dentary locus and its replacement are visible in this image. VIMS 35894 (KEB2015-0060), 718 mm TL, F.

Figure 10. Condition of lateral teeth at each locus in the left premaxilla and left dentary scored as Absent, Incoming, Functional or Eroding for 15 individuals arranged by TL. Dashed lines connect loci within a replacement wave. Data for the premaxilla is shown on the left side, and corresponding data for dentary is shown on the right. Dentary teeth bearing barbs indicated with B. **A.** VIMS 35770, 514 mm TL, M. **B.** VIMS 35874, 535 mm TL, M. **C.** VIMS 35769, 550 mm TL, M. **D**. VIMS 35798, 601 mm TL, M. **E.** VIMS 35774, 650 mm TL, F. **F.** VIMS 35778, 695 mm TL, M. **G**. VIMS 35777, 715 mm TL, M. **H**. VIMS 35780, 785 mm TL, F. **I.** VIMS 35791, 911 mm TL, M. **J.** VIMS 35795, 948 mm TL, F. **K.** VIMS 35790, 1000 mm TL, M. **L.** VIMS 35787, 1005 mm TL, F. **M**. VIMS 35788, 1037 mm TL, F. **N**. VIMS 35794, 1040 mm TL, M. **O**. VIMS 35779, 1103 mm TL, F.

Figure 11. Dimensions of teeth in left premaxilla and dentary in two specimens. Tooth base length and tooth height are expressed as a function of locus number. Only

two stages of teeth are shown (functional in red and eroding in brown) because it is not possible to accurately measure Absent or Incoming loci. Arrow indicates an eroding tooth at locus 11 from a previous wave that is smaller than the subsequent wave of functional teeth at its flanking loci 10 and 12. The presence of barbs on teeth is indicated with B. **A.** VIMS 35769, 514 mm TL, M. **B.** VIMS 35779, 1103 mm TL, F.

Figure 12. X-ray views of ankylosis and erosion of teeth and bone. **A.** Conventional x-ray of right premaxilla viewed from lingual surface showing alternate tooth replacement of lateral teeth with Incoming Loci (I) located between Functional Loci (F). Note the dense ankylosis of two premaxillary fangs and the cone shaped collars of the bone of attachment surrounding the bases of the functional lateral teeth, which ankylose the teeth to the dentigerous bone. VIMS 35787, 1005 mm TL, F. **B.** Frontal section of right premaxilla reconstructed from CT dataset to show ankylosis and erosion in relation to a functional tooth. The indicated tooth is ankylosed to the premaxilla, and, flanking it, are two incoming teeth not yet ankylosed. Erosion occurs to allow the incoming tooth to erupt. VIMS 35776, 540 mm TL, M.

Figure 13. Histological section (6 μm) of dentary stained with hematoxylin and eosin showing three waves of teeth. Two functional teeth, ankylosed to adjacent bone, flank an Absent Locus. A new tooth germ, still connected to the oral epithelium by its dental lamina, migrates deeply into the jaw between the two functional teeth. Simultaneously, a developing tooth is positioned to erupt through the same

opening; traces of its dental lamina are present. Note the enameloid cap of the developing tooth. VIMS 35894 (KEB2015-0060), 718 mm TL, F.

Figure 14. Comparisons of teeth and tooth replacement in scombroids (*sensu* Orrell et al. 2006). All four of these taxa exhibit alternate tooth replacement in the oral jaws. **A.** *Pomatomus saltatrix*. The large teeth of the dentary and premaxilla are homodont and no fangs are present. Replacement pores for the premaxilla are on the labial side; those for the dentary are on the lingual side. In both cases, large replacement pores are beneath ankylosed teeth. Small pores, if present, are beneath replacing teeth. CUMV 97588. **B.** *Scombrolabrax heterolepis*. A single pair of premaxillary fangs is present; dentary fangs are present but small (not visible in this photograph). The lateral teeth are similar to those of *Trichiurus* and replace via a trench. AMNH 211557, est. 200 mm SL. **C.** *Gempylus serpens*. Three premaxillary fang loci and two dentary fang loci are present as in *Trichiurus* and the replacement modes are similar to those of *Trichiurus*. The lateral teeth replace via a trench. Skull of AMNH 90898; inset showing lingual view of right premaxilla of AMNH 90897. **D.** *Scomber scombrus*. No fangs are present and all teeth are replaced via a trench. AMNH 55859, est. 355 mm SL.

Figure 15. Summary of the three modes of tooth replacement in *Trichiurus lepturus*.

Figure 16. Simplified phylogeny for Scombroidei based on Orrell et al. (2006) highlighting differences in tooth development in Bluefish + scombroids. Derived features that are putative synapomorphies are indicated in pink boxes. Symplesiomorphies are indicated at the base in a yellow box.

Figure 17. Two types of tooth replacement exemplified by Bluefish (*Pomatomus saltatrix*) and Atlantic Cutlassfish (*Trichiurus lepturus*). Arrows indicate locations where tooth germs enter the bone; dotted lines indicate path of the tooth germ within the bone. Both types couple bone erosion and deposition in highly dynamic processes. Key differences relate to the position of the replacement pores and the migration pathway of tooth germs once they enter the bone, which affects how erosion proceeds.

SPECIMENS EXAMINED. We studied specimens preserved in alcohol (A), decalcified-and-stained sections (DSS), dried osteological preparations (SD). All specimens examined are single specimens lots unless otherwise indicated. Total lengths (TL) are listed, if available. Institutional abbreviations follow Sabaj (2016).

Trichiuridae:

Trichiurus lepturus: VIMS 35769 SD, 550 mm TL; VIMS 35770 SD, 514 mm TL; VIMS 35771 SD, 659 mm TL; VIMS 35772 SD, 614 mm TL; VIMS 35773 SD, 710 mm TL; VIMS 35774 SD, 650 mm TL; VIMS 35775 SD, 619 mm TL; VIMS 35776 SD, 540 mm TL; VIMS 35777 SD, 715 mm TL; VIMS 35778 SD, 695 mm TL; VIMS 35779 SD, 1103 mm TL; VIMS 35780 SD, 795 mm TL; VIMS 35781 SD, 670 mm TL; VIMS 35782 SD, 630 mm TL; VIMS 35783 SD, est. 570 mm TL; VIMS 35784 SD, 1034 mm TL; VIMS 35785 SD, 1068 mm TL; VIMS 35786 SD, 962 mm TL; VIMS 35787 SD, 1005 mm TL; VIMS 35788 SD, 1037 mm TL; VIMS 35789 SD, 964 mm TL; VIMS 35790 SD, 1000 mm TL; VIMS 35791 SD, 911 mm TL; VIMS 35792 SD, 1000 mm TL; VIMS 35793 SD, 1081 mm TL; VIMS 35794 SD, 1040 mm TL; VIMS 35795 SD, 948 mm TL; VIMS 35796 SD, est. 560 mm TL; VIMS 35797 SD, 806 mm TL; VIMS 35798 SD, 601 mm TL; VIMS 35799 SD, 590 mm TL; VIMS 35835 SD, 650 mm TL; VIMS 35836 SD, 668 mm TL; VIMS 35837 SD, 672 mm TL; VIMS 35838 SD, 670 mm TL; VIMS 35839 SD, 650 mm TL; VIMS 35840 SD, 598 mm TL; VIMS 35841 SD, 650 mm TL; VIMS 35842 SD, 653 mm TL; VIMS 35843 SD, 580 mm TL; VIMS 35844 SD, 575 mm TL; VIMS 35845 SD, 593 mm TL; VIMS 35846 SD, 640 mm TL; VIMS 35847 SD, 620 mm TL; VIMS 35848 SD, 745 mm TL; VIMS 35849 SD, 556 mm TL; VIMS 35850

SD, 620 mm TL; VIMS 35851 SD, 570 mm TL; VIMS 35852 SD, 640 mm TL; VIMS 35853 SD, 566 mm TL; VIMS 35854 SD, 630 mm TL; VIMS 35855 SD, 560 mm TL; VIMS 35856 SD, 630 mm TL; VIMS 35857 SD, 608 mm TL; VIMS 35858 SD, 553 mm TL; VIMS 35859 SD, 640 mm TL; VIMS 35860 SD, 584 mm TL; VIMS 35861 SD, 675 mm TL; VIMS 35862 SD, 1050 mm TL; VIMS 35863 SD, 830 mm TL; VIMS 35864 SD, 873 mm TL; VIMS 35865 SD, 759 mm TL; VIMS 35866 SD, 1041 mm TL; VIMS 35867 SD, 946 mm TL; VIMS 35868 SD, 940 mm TL; VIMS 35869 SD, 1045 mm TL; VIMS 35870 SD, 1068 mm TL; VIMS 35871 SD, est. 985 mm TL; VIMS 35872 SD, 906 mm TL; VIMS 35873 SD, 916 mm TL; VIMS 35874 SD, 535 mm TL, VIMS 35894 A, n=3, 600 mm TL, 641 mm TL, 718 mm TL; VIMS 35901 A, n=2, TL unknown; VIMS 35823 A, n=2, 240 mm TL, 220 mm SL

SML 450916-000 A, n=4, 5.7 mm TL, 5.8 mm TL, 5.9 mm TL, 5.9 mm TL; SML 39772-000 A, 39 mm TL; SML 18590-000 A, 22.6 mm TL, SML 300582-000 A, n=2, 22.13 mm TL, 28.90 mm TL; SML 18583-000 A, 10.6 mm TL, SML 450839-000 42537 A, 49.6 mm TL

Lepidopus caudatus: AMNH I-91527 SD; AMNH I-98413 SD

Gempylidae:

Lepidocybium flavobrunneum: AMNH I-214575 SD; AMNH I-93584 SD

Neoepinnula americana: VIMS 35898 A (2) 184 mm TL, 206 mm TL; VIMS 35900 A (3) 178 mm TL, 184 mm TL, 182 mm TL; VIMS 35903 A (2) 155 mm TL, 121 mm TL

Nesiarchus nasutus: VIMS 35895, A 315 mm TL

Gempylus serpens: AMNH I-90897 SD; AMNH I-90898 SD; AMNH I-216465 SD

Promethichthys prometheus: AMNH I-210600 SD; VIMS 35896 A 345 mm TL; VIMS 35897 A 203 mm TL; VIMS 35899 A, n=2, 225 mm TL, 211 mm TL

Rexea solandri: AMNH I-91984 SD; AMNH I-214360 SD

Scombridae:

Acanthocybium solanderi: AMNH I-79804 SD; AMNH I-57641 SD

Auxis rochi: AMNH I-88912 SD; AMNH I-56704 SD

Auxis thazard: AMNH I-56712SD

Euthynnus affinis: AMNH I-217951 SD; AMNH I-217948 SD

Gasterochisma melampus: AMNH I-98426 SD; AMNH I-93480 SD; AMNH I-093411 SD

Grammatorcynus bicarinatus: AMNH I-214132 SD

Katsuwonus pelamis: AMNH I-219988 SD

Scomberomorus maculatus: CUMV 79384 SD

Scomberomorus cavalla: AMNH I-79721 SD

Scomber scombrus: AMNH I-55859 SD, n=5

Thunnus atlanticus: AMNH I-79718 SD; AMNH I-79802 SD; AMNH I-79801 SD

Scombrolabracidae:

Scombrolabrax heterolepis: AMNH I-79557 SD; AMNH I-218211 SD; AMNH I-211557 SD

Pomatomidae:

Pomatomus saltatrix: CUMV 97588 SD; CUMV 97589 SD; CUMV 97590 SD; CUMV 97591 SD

CHAPTER 3. Comparative Anatomy and Ontogeny of Ocean Sunfishes (Tetraodontiformes: Molidae)

*Katherine E. Bemis[1, 2], James C. Tyler[3], Eric J. Hilton[1], and William E. Bemis[4,5]

[1]Department of Fisheries Science, Virginia Institute of Marine Science, William and Mary, Gloucester Point, Virginia, USA

[2]Department of Vertebrate Zoology, National Museum of Natural History, Smithsonian Institution, Washington, District of Columbia, USA

[3]Department of Paleobiology, National Museum of Natural History, Smithsonian Institution, Washington, District of Columbia, USA

[4]Department of Ecology and Evolutionary Biology, Cornell University, Ithaca, NY, USA

[5]Cornell University Museum of Vertebrates, Ithaca, NY, USA

*Corresponding author

Suggested running head: Anatomy of Molidae

Abstract

This chapter reviews literature on the comparative anatomy of Ocean Sunfishes (Molidae) and presents new findings based on our studies. We document similarities and differences among the three living genera, *Ranzania, Masturus*, and *Mola* using an organ system approach to examine: general body form and external anatomy; skeleton; integument; brain and sense organs; digestive organs; heart and circulation; respiratory system; excretory system; and endocrine organs. Other chapters in this book address muscles and reproduction; therefore, these organ systems are not covered here. Molids have many anatomical specializations such as the formation of the clavus from dorsal- and anal-fin elements, enlarged gills with unusual skeletal supports, a heart with thick walls and more valves than other teleosts, ontogenetic loss of the swimbladder, enlarged kidneys and a well-developed urinary bladder, reduced otoliths, and a spinal cord contained completely within the braincase. Tagging studies on locomotion and diving behavior demonstrate that molids move efficiently over horizontal and vertical distances in the water column, and this new information helps to interpret some of the many unusual features of molid anatomy. This synthesis will help guide further comparative anatomical studies of ontogenetic series and adult specimens of Molidae.

Introduction

This chapter includes both a review of prior work and original contributions toward a synthesis on the anatomy of Molidae beginning with external anatomy and general body form followed by sections on eight of the ten organ systems (Liem et al. 2001: table 1.1); muscular and reproductive systems are treated elsewhere in this book (see Davenport et al. and McBride et al. in this book, respectively). The rich history of anatomical studies of molids offers extensive detail on many organ systems. Because of their unusual anatomy, molids are illustrated in some of the earliest works on fishes (e.g., Rondelet 1554, Gesner 1558; see Johnson and Britz 2005: fig 1). Tyler (1980) reviewed early anatomical work on molids; herein, we highlight just a few of these. One of the broadest early works on molid anatomy is Harting (1865), who described and illustrated external features, as well as anatomical aspects of bones, integument, brain, eye, ear, and gills. Harting's detailed observations were those of a microscopist who employed the most advanced techniques of his time. Steenstrup and Lütken (1898) summarized early works on molids and provided new information on the general osteology and ontogeny of molids, including a striking illustration of the skeleton of a *Mola* sp. in lateral view and a series of juveniles (Steenstrup and Lütken 1898: fig. 2, fig. 4). A series of papers by Rosén (1912–1916) offered the first comparative organ system approach to tetraodontiforms, including observations on molids. Widely cited accounts by Gregory and Raven (1934) and Raven (1939a, b) provided an anatomical framework and easily interpreted illustrations that incorporated skeletal and soft tissue anatomy (e.g., bones, muscles, and gastrointestinal tract) for each of the three extant molid genera, *Ranzania*, *Masturus*, and *Mola*. Fraser-Brunner (1951) synthesized anatomical information with

systematic interpretation for Molidae. In 1980, Tyler published a monograph on the skeletal anatomy of tetraodontiforms, providing osteological descriptions and illustrations of representatives of each of the extant genera placed in the context of the anatomy of other Tetraodontiformes and their systematic relationships. In addition to these larger works, there are many specialized reports on specific aspects of the unusual anatomy of molids that also informed our review. Progress in understanding evolutionary relationships within tetraodontiforms based on anatomical systems other than the skeleton (e.g., muscles, Winterbottom 1974; larvae, Leis 1984), incorporation of fossils (Santini and Tyler 2003, Arcila and Tyler 2017), combined with genetic studies (e.g., Yamanoue et al. 2004, 2008, Bass 2005, Yoshita et al. 2009) and new anatomical studies including studies of ontogeny (e.g., Britz and Johnson 2005a, Johnson and Britz 2005, Konstantinidis and Johnson 2012) continue to inform our understanding of molid anatomy. Advances in behavioral and tracking studies indicate that older ideas about molids and their functional biology and ecology need to be reconsidered: molids are not sluggish or inactive but, instead, are visual, rapidly diving fishes of the pelagic realm (e.g., Watanabe and Sato 2008, Houghton et al. 2009, Dewar et al. 2010, Nakamura et al. 2015). Recent taxonomic studies and descriptions of new species of molids (Nyegaard et al. 2018a, Sawai et al. 2018) are encouraging researchers to examine and restudy anatomical differences within Molidae.

Molidae has long been recognized as a monophyletic group supported by both morphological (e.g., Tyler 1980, Santini and Tyler 2002) and molecular data (e.g., Betancur-R et al. 2017), and by combined analyses (e.g., Arcila and Tyler 2017). Figure 1 summarizes current taxonomic and phylogenetic information for the five living species of

Molidae. The three valid species of *Mola* recognized by Nyegaard et al. (2018a) form a clade that is sister to *Masturus lanceolatus*. The monotypic *Ranzania laevis* is sister to *Masturus lanceolatus* + *Mola* based on anatomical character data (Fraser-Brunner 1951, Tyler 1980, Santini and Tyler 2002) and molecular data (e.g., Yamanoue et al. 2004, Bass et al. 2005, Alfaro et al. 2007).

Although there has been great interest in molid anatomy for several centuries, comparative anatomical information for the three extant genera is incomplete. This may be because specimens occur unpredictably in many parts of the world, making it difficult to reliably obtain fresh material for study. Also, researchers tend to study and only retain smaller specimens because of the logistical challenges of handling, dissecting, and storing large adults. When large specimens are dissected, they often are not retained for logistical reasons, making it difficult to corroborate some published observations. Those larger specimens that have been retained are often stored as dry skeletons or dissected portions of a specimen, which does not facilitate comparisons between individuals or taxa. For example, Gregory (1933: 294) stated: "the examination of dried skulls reveals only a sorry mess of distorted fragments." Most anatomical descriptions since Cuvier (1805a-e) have been based on specimens interpreted by the authors as *Mola mola*. Progress in understanding diversity within the genus *Mola* (e.g., Nyegaard et al. 2018a, b, Sawai et al. 2018) calls into question whether some earlier accounts are actually of *M. mola* because voucher specimens were rarely deposited in natural history collections. Finally, taxonomic confusion in the 19th century about the diagnosis and limits of the genus *Orthagoriscus* (used at various times primarily for *Mola*, although also used for *Masturus* + *Mola*; some other early authors also included *Ranzania* in *Orthagoriscus*)

means that it is often impossible to know with certainty even the generic identities of some specimens studied long ago (Fricke et al. 2019).

In the chapter, we combine information and figures from literature accounts with new data from dissections, micro-CT scans, and histological studies to develop an overview of the anatomy of Molidae.

Methods

New specimens were collected by NOAA Northeast Fisheries Science Center (Politis et al. 2014) and NOAA Pacific Islands Fisheries Science Center. Specimens were fixed in 10 percent formalin (n = 8) or frozen at sea (n = 2). New specimens are deposited in the Nunnally Ichthyology Collection at the Virginia Institute of Marine Science (VIMS) and Cornell University Museum of Vertebrates (CUMV). We also studied an additional 46 specimens in collections at ANSP, AUS, CAS, MCZ, OS, UF, USNM, and VIMS. Collection abbreviations follow Sabaj (2019). Lengths of examined specimens reported as total lengths (TL); lengths from the literature are included as standard lengths (SL) and notochord lengths (NL).

Keys for larval and juvenile specimens of *Mola* require updating because Nyegaard et al. (2018a) and Sawai (2018) recognized and clarified the taxonomic status of *Mola tecta* and *M. alexandrini*. Larval and juvenile specimens of *Mola* were identified to species based on locality. For example, MCZ 61454, MCZ 41675, MCZ 87065, MCZ 41503, and VIMS 40710 were collected in the western North Atlantic, where only *M. mola* is known; specimens from coastal Australia could only be identified to *Mola* sp. because all three species of *Mola* occur in these waters. Our identifications should be reviewed when new systematic studies of larval *Mola* are prepared.

We micro-CT scanned specimens using either a GE 120 micro-CT or the Xradia Versa XRM-500 nano-CT in the Biotechnology Resource Center Multiscale Imaging Facility at Cornell University. Reconstructions prepared from these datasets have a resolution of 7–100 μm voxels. We studied 2D orthogonal MPR (multiplanar reformatting) and 3D volume reconstructions using Horos DICOM imaging software on Apple Macintosh computers, and Avizo on a Windows Workstation. To view internal anatomy of teeth and bones, we digitally segmented reconstructions within Horos and Aviso.

We decalcified portions of two formalin-fixed specimens, washed and dehydrated them for paraffin embedding, cut sections at 6 μm, and stained them with H&E (hematoxylin and eosin; Cornell Veterinary College Diagnostic Laboratory). We photographed sections using an Olympus SZX12 microscope equipped with an Olympus DP70 digital camera or a Zeiss SteREO DiscoveryV20 microscope. We used a Canon 5D Mark II digital camera to record color macrophotographs. Using Adobe Photoshop CC, we adjusted images for color balance and contrast, and prepared plates and line drawings in Adobe Illustrator CC.

General Body Form and External Anatomy

The most distinctive external morphological feature of molids is the clavus, the structure at the posterior part of the body sometimes called a "pseudocaudal fin." The term "clavus" derives from the Latin word *clavus*, for rudder (Fraser-Brunner 1951: 90). Anatomically it refers to the truncated vertebral column and modified median fins that form the rudder-like structure, features discussed in the section on the skeleton.

Adults

Figure 1 shows general body form and overall external appearance of the five living species of Molidae. *Masturus lanceolatus* and the three species of *Mola* are among the heaviest teleosts, with the largest record for *M. alexandrini* being 2,300 kg and 272 cm TL (Sawai et al. 2018). *Ranzania laevis* is smaller than other molids, with a maximum size of 90 cm TL, rarely exceeding 70 cm TL (Schmidt 1921a:1, Fraser-Brunner 1951: 98). *Ranzania laevis* is elongate and more streamlined than either *Masturus lanceolatus* or *Mola* (Fig. 2). In all three genera of molids, the bodies are laterally compressed, but distinctly more so in *R. laevis* than in *Masturus* or *Mola*. The dorsal part of the body of *R. laevis* is rounded, and widens up to the pectoral girdle, where the body tapers ventrally to end in a ventral keel. *Masturus lanceolatus* and *Mola,* being less laterally compressed, do not taper so distinctly in the specimens we examined. However, Gregory and Raven (1934: 145) reported that "the body is deep and keel-like below with a knife-like lower edge in front of the vent" in a fresh specimen of *M. mola* that they dissected.

The lips and mouth of *Ranzania laevis* form an oval funnel (Fig. 3A, B), with a vertical orientation; the beak is set inside the tubular mouth. Some authors report that the mouth can be closed to form a vertical slit (Fraser-Bruner 1951: fig 4; Ebenezer and Joel 1984). However, other observers report that the lips are relatively inflexible and remain permanently open (Fitch 1969, Robinson 1975, Smith et al. 2010). Smith et al. (2010) report that both living and unpreserved specimens have inflexible and permanently open mouths. We have only examined preserved specimens of *R. laevis*, but agree that the lips are inflexible. Whether the funnel-like mouth functions primarily in feeding or respiration is unknown. In *Masturus lanceolatus* the lips are not as extended, and instead form an

inflexible opening with a horizontal orientation (Fig. 3C, D). By comparison, the lips of *Mola* are flexible and somewhat horizontally oriented (Fig. 3E, F).

The paired nostrils of all three genera of molids are minute and flush with the surrounding surface rather than upraised and have both incurrent and excurrent openings (Fig. 3A, C, E). In the specimens we examined, the narial openings are largest in *Mola*, and closest to the eye (Fig. 3E). *Ranzania laevis* and *Masturus lanceolatus* have such small openings that it is difficult to even locate them with the naked eye (Fig. 3A, C). The eyes are large relative to body size in all three genera. The lateral line is inconspicuous but present, as elegantly demonstrated by Nakae and Sasaki (2006). See sections on brain and sense organs for more information on these topics.

The pectoral fin in *Ranzania laevis* is relatively long and falcate (Fig. 2A), and when adducted, it fits into a shallow depression in the body, whereas in *Masturus* and *Mola* this fin is slightly shorter, more rounded (Fig. 2B, C).

Externally, the posterior margin of the body of *Ranzania laevis* is truncate and slightly oblique (Tyler 1970). In contrast, the posterior end of the body of *Masturus lanceolatus* and *Mola* is rounded or slightly scalloped (Tyler 1980). The central region of the clavus of *M. lanceolatus* forms a distinctly elongate caudal lobe (Fraser-Brunner 1951, Tyler 1970, 1980). This lobe may be supported by caudal fin rays as illustrated by Tyler (1980); notably, *M. lanceolatus* is the only molid to have a claval extension during early ontogeny (Fig. 4F, 6B).

The anterior portions of the dorsal and anal fins in molids (i.e., the portions of the fins anterior to the clavus) are approximately mirror images of each other: tall, stiff, and set far back on the body (Winterbottom 1974, Tyler 1980, Nyegaard et al. 2018a).

Watanabe and Sato (2008: fig 3a, b) found that the dorsal and anal fins of *Mola mola* change shape during ontogeny, causing a decrease in the aspect ratio of the dorsal and anal fins with growth. Despite these changes, the dorsal and anal fins are symmetrical with each other throughout ontogeny. The dorsal-, anal-, and pectoral-fin rays are extensively branched in all three genera of molids but there are few cross-striations, and these are confined to the distal ends of the rays (Tyler 1980). In *Ranzania laevis,* the rays in the dorsal and anal fins and especially the clavus are highly branched distally, whereas in *Masturus lanceolatus* and *Mola* these rays are only branched in single to triple dichotomies.

The species of *Mola* have prominent dermal ossicles along the edge of the clavus between the distal ends of the claval fin rays; neither *Masturus lanceolatus* nor *Ranzania laevis* have large dermal ossicles in the clavus. Differences in claval ossicles are diagnostic at the species level within the genus *Mola* (Sawai et al. 2018, Nyegaard et al. 2018a). The band of smaller scales adjacent to the bases of the dorsal and anal fins and the clavus allows the clavus to flex (see Sawai et al. 2018 and Nyegaard et al. 2018a for discussion of the band as a species-diagnostic feature).

Larvae

All molids undergo a remarkable metamorphosis from larvae to adults (Figs. 4-6). Since the 18th century (e.g., Koelreuter 1766: plate VIII, figs. 2, 3) zoologists have studied small, spiny fishes thought to be related to molids. Various names have been applied to larval molids (e.g., *Mola*, *Diodon*, *Orthagoriscus*, *Ostracion, Pallasia*, *Molacanthus*). For example, Putnam (1871) believed that the small molids that he studied belonged in their own genus, *Molacanthus*, a view that was supported by Gill (1884:

426), who elevated *Molacanthus* to its own subfamily and described them as "pelagic fishes of very small size." As knowledge of larvae improved and additional specimens were discovered to fill in gaps in ontogenetic series, specimens have been better tied to adults (Steenstrup and Lütken 1863, Schmidt 1921a). Schmidt (1921a) reviewed the history of larval and juvenile molid identification and assigned the spiny larvae to the genus *Mola*. Recent descriptions and reinterpretations of species level diversity within *Mola* (Nyegaard et al. 2018a, b, Sawai et al. 2018), have yet to be extended to larval and juvenile forms, and morphological diversity of larvae and juveniles of *Mola* has yet to be tied to each of the three valid species.

Larval development is best understood for *Ranzania laevis* because specimens are readily available (Fig. 4A-C; Leis 1977). Larval *Masturus lanceolatus* (Fig. 4D-F) and especially larvae of *Mola* are rare (Fig. 4G-I). All molid larvae are initially round (Figs. 4, 5). Molid larvae do not show notochordal flexion; instead, the caudal section of the body atrophies distally resulting in the formation of the clavus (Leis 1977, Johnson and Britz 2005). At about 2 mm, large pyramidal spines develop (Lyczkowski-Shultz 2005). In *R. laevis*, the spines decrease in size shortly after the dorsal-and anal-fin rays ossify. Leis (1977: 456) interpreted that ossification of fin rays allowed the fish to swim, making protective spines unnecessary. Spines persist in larval *Masturus* and *Mola* during a phase termed the "*Molacanthus*" stage, during which the body is deep and laterally compressed, with a ventral keel (Fig. 4-5; Lyczkowski-Shultz 2005, Leis 1984).

Sexual dimorphism

Fraser-Brunner (1951: 117) reported that when *Mola mola* exceed about 2 ft (= ~60 cm) in length, sexual dimorphism is apparent. He described the "bony tubercle"

producing a pronounced snout in males that projects forward, while females are reported to have a snout that projects upward, resulting in females having a deeper head, with the front of the snout nearly vertical. He also described sex-related differences in the clavus lobes and clavus length (Fraser-Brunner 1951: 117; see side by side illustrations of male and female specimens of similar length in Roon and Pelkwijk 1939: fig. 1). With recent advances in understanding species diversity in *Mola* it would be pertinent to revisit sexual dimorphism. Sexual dimorphism has not been described for *Ranzania laevis* or *Masturus lanceolatus*.

Skeleton

The skeleton of molids is the most studied organ system and has been a rich source of characters for systematic analyses, both within molids and among families of tetraodontiforms. A dominant theme of molid skeletons is reduction, with the acknowledgment that reduction (e.g., in number of vertebrae) is characteristic of tetraodontiforms generally. The skeleton of molids is reduced in two additional ways. The first reduction is manifest in the tissues of the skeletal system, including the fibrous nature of the bones and their reduced mineralization. The second relates to loss or reduction of individual skeletal elements beyond those already lost in many tetraodontiforms (e.g., ribs, pelvic girdle, and pelvic fins). For instance, in all molids the coronomeckelian (= sesamoid articular of Tyler 1980) is lost entirely and the exoccipitals are reduced in size to the point that they do not form condyles and are excluded from the foramen magnum by a dorsal extension of the basioccipital. The interopercle is lost in *Masturus* and greatly reduced in *Mola* (a short "needlelike" bone in *Mola*; Tyler 1980)

and *Ranzania laevis*; indeed all opercular elements except the preopercle are relatively small.

The most comprehensive analysis of the skeleton in molids was presented by Tyler (1980; Fig. 7), although aspects of skeletal anatomy are treated in many historical papers including Leydig (1857), Kolliker (1859, 1860), Harting (1865), Goette (1879), Trois (1883-1884), Steenstrup and Lütken (1898), Stephan (1900), Supino (1904), Nowikoff (1910), Kaschkaroff (1914a, b, 1916, 1925), and Studnicka (1916). The following overview is not intended to be a comprehensive osteology of the family. Rather, we briefly describe the molid skeleton, based largely on Tyler (1980) and recent studies (e.g., Britz and Johnson 2005a, Johnson and Britz 2005, Konstantinidis and Johnson 2012) that highlight features unique to Molidae and key variation within the family. Following introductory remarks on the condition of bone in molids, our treatment of the molid skeletal system follows the regional organization that has been used in previous osteological studies of actinopterygian fishes (e.g., Grande and Bemis 1998, Hilton 2002, and Hilton et al. 2011) and here adapted to the peculiar morphology of molids.

Comments on molid bones as tissues

The bones of *Ranzania laevis* are thicker and better ossified than the bones of *Masturus lanceolatus* and *Mola*, which have a dense, moderately spongy texture (Raven 1939a, Carnevale and Santini 2007). We found the bones of *Masturus lanceolatus* and *M. mola* to have a very peculiar texture and mineralization. They can be cut easily with a scalpel, almost as though they are composed entirely of softer connective tissue. This peculiarity has attracted attention since Harting (1865), but there is still a great deal to

learn about the composition of molid bones. Raven (1939a: 4) speculated that better ossification of the skeleton is a plesiomorphic character for molids that is retained by *R. laevis*, perhaps because of its smaller size.

Cranial skeleton

Following the general organization of Grande and Bemis (1998), information on the cranial skeleton is treated as follows: Skull roof and neurocranium; infraorbital bones and sclerotic ring; jaws and oral dentition; pharyngeal dentition; suspensorium and opercular series; ventral portions of the hyoid arch; and gill arches.

Skull roof and neurocranium

The skull roof of molids is dominated by the paired frontals in all three genera (Fig. 8). These bones extend much of the length of the braincase, and serve as a dorsal complement to the parasphenoid, which lies along most of the ventral length of the neurocranium. The pterotic is relatively large in all three genera, and is greatly expanded posteriorly in *Ranzania laevis*. The supraoccipital varies within the family. In *Masturus lanceolatus* and *Mola*, the supraoccipital bears a prominent dorsally directed rounded crest, whereas in *R. laevis*, in which the supraoccipital is generally larger than in the other two genera because it extends more anteriorly on the skull roof, there is a greatly exaggerated posterior extension to the supraoccipital crest. There are also posteriorly directed crests on the epioccipital (Fig. 8). As with the supraoccipital crest, the epioccipital crest in *R. laevis* is thin and greatly expanded posteriorly. Although prominent, the epioccipital crests in *Masturus lanceolatus* and *Mola* are shorter and rounded. The epioccipital crest in *Mola* is distinctly bent and horn-like. The basioccipital

of all molids is greatly enlarged and extends dorsally as the only bone to surround the foramen magnum, removing the exoccipitals from this position.

The median element in the orbit of molids was identified as the basisphenoid by Tyler (1980), but Britz and Johnson (2012) considered it to be a modified pterosphenoid because they considered it was associated with marginal portions of the neurocranium. However, because it is a median element, separate from the paired pterosphenoids (although in close proximity, being separated by a thin cartilage in *Mola* and *Masturus*, and widely separated from the pterosphenoid in *Ranzania laevis*), we accept Tyler's interpretation that it is a basisphenoid.

The ethmoid region of molids comprises a mesethmoid dorsally, which is positioned anterior and dorsal to the parasphenoid; paired lateral ethmoids, which define the anterior margin of the orbit; and the median vomer, which is anteroventral to the parasphenoid. Tyler (1980: 384) noted that the vomer is unossified in *Ranzania laevis*, although it was reported as present in an ontogenetic study by Konstantinidis and Johnson (2012). Tyler (1980) described the vomer as ventrally "articulated by fibrous tissue" with the ethmoid, palatine, and parasphenoid. Konstantinidis and Johnson (2012) found an autogenous, ossified vomer in a 2.5 mm NL specimen of *R. laevis*. In the next stage available to those authors, the vomer was expanded anterodorsally, but it was unclear whether an autogenous mesethmoid was present.

Infraorbital bones and sclerotic ring

Molids lack infraorbital bones. The sclera is supported by stout connective tissue that does not ossify. See the section on vision.

Jaws and oral dentition

The oral jaws of all three genera of molids bear a beak and lack a coronomeckelian. The anguloarticular (labeled as articular in figures in Tyler 1980) is much smaller than the dentary, and is restricted to the dorsal margin of the lower jaw in lateral view, although it spreads medially from the point where it contributes to the articular surface with the quadrate (i.e., the dentary forms the entire ventral margin of the lower jaw, from the tip of the jaw to its point of contact with the retroarticular). The retroarticular (labeled as angular in figures in Tyler 1980) is small in molids, being restricted to the posteroventral corner of the lower jaw (Fig. 8).

In extant species of molids, the premaxillary bones and the dentary bones are indistinguishably fused at their midlines and no sutures are visible (Figs. 10A-C; see Carnevale et al. this volume and Tyler and Bannikov (1992) for discussion of this condition in fossil molids). Bundles of more densely ossified tissue lie more or less perpendicular to the beak but do not cross the symphysis (Figs. 10A, C). The rest of the jaw is composed of poorly mineralized material, similar to the other cranial bones of molids.

Beaks in tetraodontoids are initially formed by the fusion of isolated dental elements; new material is added from beneath to replace material worn away at the surface (Bemis et al. 2017). In molids, the fused premaxillary bones support a beak along the margin of the upper jaw (Fig. 9A); the fused dentary bones likewise support a beak (Figs. 9A, 11). Relative to the dentigerous bones, the beak is highly mineralized (Figs. 9, 10B). In both the upper and lower jaws, the beak is continuous between the right and left sides (Figs. 9A, C), and their margins continue laterally along the crests of the bones

(Fig. 9D). The beak of *M. mola* is composed of tall columns of osteodentine (Figs. 9E, 10C); there is no enameloid tissue. The osteodentine is identified by the long tubular canals for blood vessels. At higher magnification, individual dentine tubules are evident radiating through the osteodentine. The beak of *M. mola* is never completely lost and, as it wears away at its masticating surface, new mineralized tissue is added from a single, large, well-vascularized pulp cavity at its base (Figs. 9E, 10C). A peculiarity of molids in comparison to other tetraodontoids is the absence of tooth germs entering the dentigerous bones to supply new dental material for the beak (Fig. 10C). We did not identify tooth germs in the jaws of *M. mola* that contribute to the beak at any developmental stages based on our dissections, micro-CT scans, and histological studies of ground and paraffin sections (Figs. 9E, 10C). There also do not appear to be separate tooth germs in specimens that we studied for *Ranzania laevis*; we have not yet studied the condition in *Masturus lanceolatus*.

Posterior to the beak in both the upper and lower jaws are mineralized dental surfaces termed triturating teeth (= *sensu* Tyler 1980, for enlarged and especially sturdy interior teeth with grinding or crushing surfaces in tetraodontoids; Figs. 10A, B, 11, 12). Triturating teeth located most anteriorly are integrated with the biting edge of the beak, whereas those located more posteriorly are separate teeth at their distal points, but connected at their bases to the same osteodentine base that supports the beak (Fig. 11C). Folded oral pads of soft tissue surround the individual triturating teeth in *M. mola* (Fig. 11A, C). Many, but not all triturating teeth are visible between the pads; some triturating teeth visible in Figure 11B are completely covered by pads and thus not visible at the surface (Fig. 11A). The epithelium of the oral pads is folded into deep crypts (Fig. 11C).

Triturating teeth of molids change in number, size, and distribution on the jaws during ontogeny (Fig. 12). The smallest specimen of *M. mola* in the series shown in Figure 12 (7 mm TL, Fig. 12A) has a beak, but it has not yet developed the paired triturating teeth seen in slightly larger specimens (e.g., 13 mm TL, Fig. 12B, 55 mm TL, Fig. 12C). In a larger specimen, (400 mm TL, Fig. 12D), three to four rows of triturating teeth are spread from left to right along the jaw. A still larger specimen (466 mm TL, Fig. 12E) has fewer and relatively smaller triturating teeth, and in a specimen 1500 mm TL (Fig. 12F), the triturating teeth are reduced to small, indistinct mineralized structures continuous with the beak.

Pharyngeal dentition

All molid genera have long, recurved pharyngeal teeth borne on pharyngobranchials 2-4 (Fig. 13). Between these teeth are thick pads of tissue (Fig. 13). Among others, Harting (1865: plate 3, fig. 7), Suyehiro (1942: 193, fig. 140), Steenstrup and Lütken (1898: 94, unnumbered figure) and Berkowitz and Shellis (2017: figure 4.114) have highlighted the pharyngeal dentition of molids. Suyehiro (1942) interpreted that the long, recurved pharyngeal teeth are related to the diet of jellyfish. No histological studies of pharyngeal teeth are available so it is unknown if, like the oral dentition, the pharyngeal teeth also lack enameloid.

Suspensorium and opercular series

As in many but not all tetraodontiforms, the anterior articulation between the suspensorium and the ethmoid region of molids is immobile (Breder and Clark 1947). The large palatine of molids has an extension that reaches posteriorly nearly one third the length of the parasphenoid (Figs. 7A, 8A, 9A). The palatine is firmly attached to the

ethmoid bones, vomer, and parasphenoid dorsally, and to the more posteroventral portions of the suspensorium through "fibrous tissue" (Tyler 1980: 371); it also serves as the articulation surface for the maxilla. In a 2.5 mm NL specimen of *Ranzania laevis*, Konstantinidis and Johnson (2012) describe the palatine as bearing two crests of membrane bone, which are the main anterodorsal component of the maxillary process, which articulates with the maxilla, and the posterodorsal crest, which at this early stage is already firmly attached to the lateral ethmoid and parasphenoid.

Posterior to the palatine, the suspensorium of molids contains the typical elements of the teleostean suspensorium, including the ectopterygoid, endopterygoid, metapterygoid, and quadrate, and the bones of the hyosymplectic cartilage, which are the hyomandibula and the symplectic (contrary to Raven 1939a, who reported the symplectic to be absent). The hyomandibula is particularly large, and its broad, dorsal head articulates with the sphenotic and prootic anteriorly and the pterotic posteriorly (Tyler 1980); the anterior portion of this articulation is larger in *Ranzania laevis* than in *Mola* and *Masturus*, in which the articulation is dominated by the pterotic (Figs. 7A, 8A, 9A). The ventral shaft of the hyomandibula tapers strongly. Raven (1939a:4) was impressed by the form of the hyomandibula in *R. laevis*, describing it as: "Perhaps the most striking modification of the skull bones is to be seen in the hyomandibular, which is produced backward as a long flange overlying the dorsal part of the gill chamber…It appears that the flange on the hyomandibular of *R. laevis*, braced as it is, prevents the collapse of the branchial chamber, an office usually performed by the opercula…" An elongate symplectic, contacting the quadrate anteriorly, is present in *R. laevis*; the symplectic in *Masturus lanceolatus* and *Mola* is relatively shorter.

The opercular bones of molids are highly modified. In all three genera, the preopercle is the largest bone of the opercular series; it forms a gently curving element in close contact with the posterior margin of the suspensorium (Figs. 7A, 8A, 9A). The more posterior bones of the opercular series are small relative to other bones of the skull, and to the head in general. Dorsally, the opercle is a small, somewhat rectangular (*Ranzania laevis* and *Mola*) or nearly oval element. The subopercle of all molids is straight (*R. laevis*) or sigmoid (*Mola* and *Masturus*); it extends anteriorly to varying degrees along the medial surface of the preopercle. It is longest in *R. laevis*, in which it reaches the level of the ventral tip of the hyomandibula (Fig. 7A) and shortest in *Masturus*, in which it just overlaps the ventral flange of the subopercle (Figs. 8A, 9A). The interopercle is lost in *Masturus* and present only as a short "needlelike" bone in *Mola* that is far removed from the subopercle. In *R. laevis* the interopercle remains in contact with the subopercle, and is visible in lateral view at the anterior tip of the preopercle.

Ventral portion of the hyoid arch and branchiostegals

Ventral components of the hyoid arch of molids include a median basihyal, dorsal and ventral hypohyals, anterior and posterior ceratohyals (= ceratohyal and epihyal, respectively, of Tyler 1980), and an interhyal. The branchiostegals, which are dermal components of the opercular series, are closely associated with the ventral portion of the hyoid arch as is typical for actinopterygians, and therefore we include them in this section. The anterior and posterior ceratohyals of *Masturus* and *Mola* are similar to each other (Figs. 8B, 9B). In both, the anterior ceratohyal is rounded anteriorly, and broadly separated from the posterior ceratohyal (Tyler 1980). In contrast, the broad anterior

ceratohyal of *Ranzania laevis* tapers posteriorly as it approaches the posterior ceratohyal (Fig. 7B).

Ranzania laevis has five branchiostegals (Fig. 7A, B). There are six branchiostegals in *Masturus* (Fig. 8A, B) and *Mola* (Figs. 9A, B, 14). Of these, the posteriormost branchiostegal is relatively small and slender. Tyler (1980) suggested that *R. laevis* either lost the sixth branchiostegal or that it fused to form the enlarged posteriormost branchiostegal.

Gill arches

Ventral components of the molid gill-arch skeleton comprise two ossified basibranchials, three pairs of hypobranchials, and five pairs of ceratobranchials (Fig. 7C, 8C, 9C). In molids, the anterior basibranchial is intercalated between hypobranchial 1. The posterior basibranchial is positioned between the medial tips of hypobranchial 2 and extends posteriorly to beyond the medial tips of hypobranchial 3. Hypobranchial 1 is large relative to all other hypobranchials, with the third hypobranchial being much smaller than the rest, particularly in *Ranzania laevis*. In *Mola* and *Masturus lanceolatus*, the five ceratobranchials are approximately similar in size whereas in *R. laevis* the fifth ceratobranchial is more slender compared to the preceding elements. The ceratobranchials of *R. laevis* overall are slender compared to those of the other genera. Similarly, the epibranchials of *R. laevis* are slender bars of bone, whereas the epibranchials of *Mola* and *M. lanceolatus* vary in size, with epibranchial 4 being the largest, and of a distinctly triangular shape. There are three pharyngobranchials (pb2-4) in all molids, supporting three rows of elongate pharyngeal teeth.

Gill rakers are distributed along the anterior and posterior edges of all gill arches except the fifth arch, in which they are only present along the anterior edge. There are also gill rakers along the anterior edge of the first gill slit (Tyler 1980). See section on respiration for more information on soft tissues of the gills and their relationship to the arches.

Postcranial axial and appendicular skeleton

Our treatment of the postcranial axial and appendicular skeleton follows the general outline of Grande and Bemis (1998) and includes: vertebral column; dorsal and anal fins, skeletal supports, and clavus; pectoral girdle and fin; and pelvic girdle and fin.

Vertebral column

The vertebral column of molids is comparatively short, as reflected in the length of the notochord during development (Leis 1977, 1984). In an ontogenetic series of *Ranzania laevis*, Britz and Johnson (2005a) found that the first vertebra fuses with the basioccipital early in development, a fusion so complete that earlier authors usually did not include the first vertebra in their counts of vertebral numbers, meaning that previous vertebral counts may be incorrect by one abdominal vertebra. Britz and Johnson (2005a: fig. 2b) also showed that this fusion occurs in *Masturus lanceolatus*, and we confirmed it in an adult *Mola mola* (VIMS 35803, 1180 mm TL).

Given the ontogenetic fusion of the first vertebra into the skull and variation within the family, there has been confusion regarding the total number of vertebrae in molids. For instance, Cleland (1862), Steenstrup and Lütken (1898), and Kaschkaroff (1914a) stated that *Mola mola* has eight abdominal vertebrae and eight caudal vertebrae, whereas Tyler (1980: 375) reported that *M. mola* has nine caudal vertebrae. Britz and

Johnson (2005a) suggested that earlier authors may have misidentified their specimens and were reporting numbers for *Masturus lanceolatus*, which has only eight caudal vertebrae (Tyler 1970), or that the number of caudal vertebrae varies within *M. mola*. Fraser-Brunner (1951: 94) reported that *Mola* and *Masturus* have nine abdominal vertebrae and eight caudal vertebrae, but he provided no evidence for these counts. Tyler (1980: 379) speculated that "Fraser-Brunner's counts of nine abdominal vertebrae…were made from radiographs and that the dorsal prongs of the basioccipital were mistaken for the first vertebra." (Coincidentally, nine abdominal vertebrae is the correct number if you count the vertebra that fuses into the basioccipital.) Here (Figs. 7-9), we count vertebra 1 as fused into the basioccipital. According to this method, *R. laevis* has nine abdominal and 10 caudal vertebrae (Fig. 7A; = 19 total vertebrae). The specimen of *M. lanceolatus* shown in Figure 8A has nine abdominal and eight caudal vertebrae (= 17 total vertebrae). The specimen of *M. mola* illustrated in Figure 9A, has nine abdominal vertebrae, and nine caudal vertebrae (= 18 total vertebrae).

Vertebrae of molids are simplified relative to those of other tetraodontiforms in that the centra of the abdominal vertebrae lack parapophyses and the articulating surfaces between the centra are smooth (Tyler 1980). As in all tetraodontiforms except triodontids, molids lack ribs (Gregory and Raven 1934, Tyler 1980; the elements in one species of monacanthid thought to possess ribs by Tyler 1980 were reinterpreted as intermuscular bones by Britz and Johnson 2012). The neural and haemal spines interdigitate with the dorsal- and anal-fin pterygiophores to form a stiffened body incapable of much lateral undulation. As noted by Raven (1939a: 7), the neural and haemal spines of *R. laevis* (Fig. 7A) are much more sharply inclined posteriorly than are those of *Masturus* (Fig. 8A) or

Mola (Fig. 9A). These angles of the neural and haemal spines relative to the vertebral centrum relate to the position of the dorsal and anal fins along the body, with the dorsal and anal fins of *R. laevis* positioned more posteriorly on the body (Fig. 7A) than in either *M. lanceolatus* (Fig. 8A) or *M. mola* (Fig. 9A). According to Raven (1939a: 7) "The most remarkable feature of the skeleton [of *R. laevis*] is the caudal inclination of the haemal and neural spines, indicating the posterior displacement of the dorsal-and anal-fins. This, in conjunction with the great development of the dorsal and anal fin musculature and the narrow high fins, suggests that *Ranzania*, contrary to earlier opinions, is a fast-swimming form."

Dorsal and anal fins, skeletal supports, and clavus

The number of dorsal- and anal-fin rays varies, although the intraspecific variation (and perhaps geographic variation) in meristic characters is not well documented for any molid. The posterior fin rays are greatly expanded towards their tips, with multiple bifurcations. In *Mola*, for example, each fin ray may have up to 50 tips (Tyler 1980). The tips of the more posterior fin rays in the dorsal and anal fins curve posteriorly, giving each fin ray a bent-broom appearance (Figs. 7A, 8A, and 9A).

The pterygiophores that support the dorsal and anal fins were interpreted differently by Tyler (1980) and Johnson and Britz (2005). Tyler (1980) recognized basal, median, and distal radials (labeled as basal, median, and distal pterygiophores in Tyler 1980, fig. 312) as three separate elements. In contrast, based on their ontogenetic study of fin development in *Monotrete leiurus* (Britz and Johnson, 2005b), Johnson and Britz (2005: figs. 3, 4) concluded that the elongate supporting element in the dorsal and anal fins of *Ranzania laevis* represent a proximal-middle radial and that the distal radials are

associated with the bases of the fin rays. The distal tips of the proximal middle radials are fused together (shown but not labeled in Tyler 1980: fig. 306; also see Johnson and Britz 2005: fig. 4). Further study is needed to resolve the arrangement of the supporting cartilages and their associated ossifications in molids. Aspects of the homologies of skeletal elements supporting the clavus were clarified in a pair of elegant studies by Johnson and Britz (2005) and Britz and Johnson (2005b), who compared the ontogeny of the axial skeleton of *Ranzania laevis* to that of a tetraodontid, *Monotrete leiurus*, which has typical hypurals supporting the caudal fin rays. Prior to their study, there had been two hypotheses to explain the structure of the clavus: 1) the clavus is a highly modified caudal fin (Goodsir 1841, Cleland 1862, Schmidt 1921a, Gudger 1937a, b, Winterbottom 1974a); or 2) highly modified components of the dorsal and anal fins take the place of the caudal fin (Ryder 1886, Boulenger 1904, Regan 1903, Raven 1939a, Fraser-Brunner 1951, Tyler 1970, 1980, Santini and Tyler 2002). Johnson and Britz (2005) noted that most authors favor the second option but that they did not explain or illustrate their reasoning. By examining the ontogeny from larval to juvenile stages of *Ranzania laevis*, Johnson and Britz (2005) showed that the clavus is not a modified caudal fin, but instead is formed by elements of the dorsal and anal fins. This interpretation is based on three observations: 1) the notochord (= chorda in Johnson and Britz 2005; also see Leis, 1977, 1984) never flexes during development; 2) the clavus is supported by a series of skeletal elements and fin rays that close the gap between them; and 3) the elongate cartilages that support the clavus are structurally equivalent to the dorsal- and anal-fin pterygiophores (Johnson and Britz 2005). Nakae and Sasaki (2006) showed that the innervation of the fin rays of the clavus in *Mola mola* resembles that of the dorsal and anal-fin rays of typical

teleosts, supporting the conclusion of Johnson and Britz (2005) that the clavus is formed by modified elements of the dorsal and anal fins.

The last centrum of molids ends in a cartilaginous cap that articulates with radial elements of the claval pterygiophores, a condition unknown in other tetraodontiforms or teleosts (Johnson and Britz 2005: 18). Whether there are two elements in series (the proximal-middle claval radials and claval distal radials as interpreted for *Ranzania laevis* by Johnson and Britz 2005: fig. 3) or three elements in series (separate proximal, middle, and distal claval radials as interpreted for *Mola mola* by Tyler 1980: fig. 312) remains unclear, and this question cannot be resoved without further detailed dissection and study of the fin supports throughout ontogeny in all three genera of molids.

The clavus is supported by a taxonomically variable number of fin rays. There are 19 claval fin rays in the specimen of *Ranzania laevis* shown in Figure 7A, 21 claval fin rays in the specimen of *Masturus lanceolatus* shown in Figure 8A, and 16 claval fin rays in the specimen of *Mola mola* shown in Figure 9A. Only in *M. lanceolatus,* however, are caudal fin rays putatively present (Fig. 8A; Fraser-Brunner 1951 and Tyler 1980). These caudal fin rays appear to be supported by the posteriormost vertebral centrum (Fig. 8A). Fraser Brunner (1951: 101) noted "It is admittedly hazardous to speak of caudal rays when the hypural bones are lost, since in normal fishes caudal rays are distinguishable only by their association with the hypurals. But I feel convinced that these central rays of the clavus in *Masturus* are homologous with the hypocaudal rays of the more generalized forms…" This interpretation was adopted by later authors (e.g., Tyler 1980) and is followed here (Fig. 8A), although the homology of these fin rays in *M. lanceolatus* warrants further study.

Pectoral girdle and fin

The pectoral girdle of all molids contains the same elements, but the positions, sizes, and shapes of these elements in *Ranzania laevis* (Fig. 7A) differ from *Masturus lanceolatus* (Fig. 8A) or *Mola mola* (Fig. 9A). All molids lack a posttemporal, and the supracleithrum articulates directly with the pterotic through a broad lap suture. The supracleithrum of *R. laevis* is more slender anteriorly than that of the other two genera. The cleithrum and coracoid are similar in all three genera. A single postcleithrum is found in all genera of Molidae, and is unique in having an anteroventral extension that lies lateral to the pectoral radials. The anterodorsal process of the postcleithrum extends anteriorly to contact the medial face of the supracleithrum. Posteriorly, the postcleithrum of *R. laevis* greatly expanded and plate-like whereas it is short and ventrally curved in *M. lanceolatus* and *Mola* (Figs. 7A, 8A, and 9A)

Ranzania laevis has 14 pectoral fin rays (Figs. 7A), whereas *Masturus lanceolatus* has 10 (Fig. 8A) and *Mola* has 12 (Fig. 9A; also see Tyler 1980). Intraspecific variation for pectoral-fin ray counts is unknown.

Pelvic girdle and fin

All molids, as well as all other tetraodontoids (except for the monotypic extant Triodontidae, *Triodon macropterus*), lack all evidence of a pelvis and pelvic fins (Tyler 1962).

Integument and hypodermis

In dissection (Fig. 15A, B), one of the most striking features of *Mola mola* is the thickness of the body wall, which in CUMV 98740, 1500 mm TL, is about 39 mm thick

(skin 1 mm + hypodermis 38 mm, Fig. 15B) near the posteroventral corner of the abdominal cavity. The body wall of *M. mola* has been reported to reach as much as 6 inches (=152 mm; Goodsir 1841). We confirmed that *Masturus lanceolatus* shares the greatly thickened body wall with *M. mola* and that the thickened body wall extends broadly over the body of the fish. The body wall of *Ranzania laevis* is much thinner over much of the body with the exception of the mid-ventral keel, but nowhere does it approach the thickness seen in *M. mola* or *M. lanceolatus*. Over the body surface of *M. mola* a mucus cuticle is evident in fresh as well as preserved material (Fig. 15C). Brimley (1939: 296) noted that the skin of *Mola mola* was slimy, but that the skin of *Masturus lanceolatus* was not slimy.

Composition of the body wall

Important questions about the body wall of molids include what are its constituent tissues, how are they organized, and how should they be compared with other vertebrates? A schematic of the body wall of *M. mola* (Fig.15D) offers a proposed terminology for these tissues to foster broad comparisons. At the surface of the body wall of *M. mola* is the mucus cuticle that presumably is produced by the very thin epidermal epithelium (blue, Fig. 15D). Critical epidermal features yet to be studied are the secretion, maintenance, and role of the mucus cuticle that covers the skin. In skin samples studied using a dissecting microscope (Fig. 15C), the mucus cuticle of *M. mola* appears to be carried on the finely branched tips of the scales (note, these finally branched tips of the scales are lost during most preparations, e.g., c&s and SEM). Deep to the epidermal epithelium are the bases of the scales and two layers of dermal tissues, termed by convention in other vertebrates, the stratum laxum and stratum compactum (Fig. 15D).

Together, the mucus cuticle, epidermal epithelium, scales, stratum laxum, and stratum compactum make up the skin.

Scales

Katayama and Matsuura (2016:96) studied scale morphology of extant Molidae, discovering that *Masturus* + *Mola* share a common pattern of intermixed rounded to elliptical large and small scales on the body. Both large and small scales have a single central spine, and are tightly interdigitated with each other (Fig. 16, Katayama and Matsuura 2016). The hexagonal body scales of *Ranzania laevis* are larger and thicker (Fig. 16A, Tyler 1980: 379) than those of either *Masturus* or *Mola*, whose scales are similar in size (Fig. 16B, C). They are interdigitated on their edges, but less so than in *Masturus* + *Mola*. Instead of a central spine, the scales of *R. laevis* bear a row of 1–4 short and blunt spines in the central region of each scale (Fig. 16, Katayama and Matsuura 2016). In his key, Fraser-Brunner (1951: 94) describes the skin of *R. laevis* as smooth in contrast to the rough skin of *Masturus lanceolatus* + *Mola*, a difference no doubt related to the large central spines illustrated by Katayama and Matsuura (2016). Sawai et al. (this book) show that scale morphology is also diagnostic at the species level with *Mola*.

Hypodermis

The skin is only about 1 mm thick in adult *Mola mola* (e.g., CUMV 98740, 1500 mm TL) but the layer of tissue deep to it is greatly thickened. Many names have been applied to this thick layer, which is not part of the skin by conventional definitions because it is deep to the dermis. The most descriptive term for it in the broader scheme of comparative vertebrate anatomy is hypodermis. Many other terms have been used for

molid hypodermis, including: “Tissue of a very peculiar kind” (Goodsir 1841: 189); “Subdermal connective tissue” (Green 1899: 321); “Collagenous material... rubber like armor” (Gregory and Raven 1934: 150); “Layer of subcutaneous tissue” (Roon and Pelkwijk 1939: 68); “Greatly thickened collagenous dermis” (incorrectly interpreted as the stratum compactum by Logan and Odense 1974: 1040); “Thick layer of collagenous connective tissue” (Tyler 1980: 379); “Subcutaneous gelatinous tissue” (Watanabe and Sato 2008); and “Capsule” (Davenport et al. 2018: 1). We propose that the simple term hypodermis is the best descriptor for this tissue because it clarifies its position in the body wall and facilitates comparisons with other vertebrates. There are histological differences between the hypodermis of *Mola mola* and the hypodermis of other teleosts. For example, *Phoxinus* and *Scomber* have fat cells in the hypodermis (Whitear, 1986: figs. 2,3), as do most mammals. We did not observe fat cells in the histological materials of the hypodermis of *M. mola* that we studied, nor are any reported in the literature (see Davenport et al. 2018 and this book for more on histology of the hypodermis). Nevertheless, the hypodermis of molids, scombrids, cyprinids, and mammals is in a similar position within the body wall and should share the common term hypodermis.

As more has been learned more about the diving behaviors of *M. mola*, new interpretations about the hypodermis have been proposed by Watanabe and Sato (2008) and Davenport et al. (2018 and this book). Specifically, the hypodermis may play a role in buoyancy because it has a density of 1.015 g ml^{-1}, rendering it positively buoyant in seawater. Given the volume of the hypodermis and its allometric changes in thickness as individuals grow larger (Davenport et al. this volume), the hypodermis functions to

decrease the overall density of the fish. Finally, Nakamura et al. (2015) proposed that the hypodermis reduces heat loss during deep dives into cold water.

Muscles

See Davenport et al. (this volume) for information on muscles and locomotion in molids.

Brain and sense organs

Harting (1865: plate 3, fig. 1) illustrated a specimen interpreted as *Mola mola* that showed an enlarged cranial cavity relative to the size of the brain. Our dissections of *M. mola* (VIMS 35803) do not show a particularly striking disparity in the size of the cranial cavity relative to the brain (Fig. 17A, B). The vestibular cavity, occupied by the membranous labyrinth, is continuous with the cranial cavity, which can give an artificial impression of a very large space in which the brain is housed (note that the vestibular system has been removed in Harting's illustration).

Brain

The brain and inner ears are suspended within the cranial cavity by a tissue that is, positionally at least, homologous to the arachnoid layer of other vertebrates (Fig. 17A, B). A tough layer of connective tissue, about 100 μm thick, lines the cranial cavity (VIMS 35803, 1180 mm TL). We interpret this tough layer as the outer meninx, or dura mater. The tissue that we interpret as arachnoid is directly beneath the dura mater and, on the dorsal side of the cavity, extends as much as 40 mm before reaching the brain (VIMS 35803). In dissection, the arachnoid layer appears spongy; its fibers would be surrounded by cerebrospinal fluid in life. It is surprisingly tough and cannot be easily removed as an intact tissue layer. If it is homologous to the arachnoid tissue of other vertebrates, then it

is a far thicker layer than, for example, in a typical mammal. Regardless of its homologues in other vertebrates, the arachnoid suspends the brain as a shock absorber.

Brains of molids have been illustrated in several accounts. Harting (1865: plate 3, figs. 1-3) shows a lateral view of the brain in the cranial cavity as well as dorsal and ventral aspects of the brain removed from the cavity showing the large optic nerves, large optic tectum, and relatively large hypophysis. Vignal (1881: 371) included an imprecise drawing of the dorsal and ventral surfaces. Burr (1928: fig. 1) labeled a line drawing showing major brain regions and roots of the cranial nerves (redrawn here as Fig. 17C, D). Contours of the brain surface in Burr's drawing appear a little angular compared to a macrophotograph of the dorsal aspect of the brain of *M. mola* in Uehara et al. (2015: fig. 2) and to our dissections (Fig. 17A, B). Burr (1928: figs. 40, 41) also provided a wax plate reconstruction of the brain and anterior portions of the spinal cord. These figures identified of the roots of the cranial nerves and we used Burr (1928: fig. 40) to prepare Figure 17E, updating his terminology.

Aspects of the external anatomy of the brain and the sizes of the roots of the cranial nerves correlate well with what we know about molid sensory systems. First, the olfactory nerve (I; Fig. 17C-E) and olfactory bulb are relatively small (Fig. 17E), as is the peripheral olfactory system of molids. Second, each optic tectum is large; correlated with this are the large eyes and optic nerves (II; Fig. 17B, E) as evidence of the importance of the visual system. Kappers et al. (1936: 168) noted that the optic decussation lies anterior to the diencephalon, a position different from that of most vertebrates. The prominent metencephalon relates to the large size of the vestibular system and coordination for swimming. The structure interpreted as the "lateral line lobe"

by Burr (1928; shown here in Fig. 17E) warrants more study because the lateral-line system is so reduced in molids yet the region appears large both in a dissected brain and in the wax plate model.

We were unable to trace fully the roots of the cranial nerves in our dissection of *Mola mola* (VIMS 35803) to confirm the findings of Burr (1928). It will be important to do this when better fixed material is available because there are aspects of Burr's (1928) figures that cannot be interpreted without new study. For example, he recognized two lateral-line nerves, which he termed anterior and posterior lateral-line nerves. Our context for thinking about the lateral-line nerves has changed in the decades since Burr (1928; for example, see Northcutt and Bemis 1993).

Nakae and Sasaki (2006) described and illustrated in detail the peripheral distributions of some of the cranial nerves using specimens prepared by a modified Sihler method (Nakae and Sasaki 2004). Nakae and Sasaki (2006: 244; fig. 8A) state: "The reduced number of foramina for emergence of the nerves from the cranium is a distinct feature of *M. mola*." For example, they noted that the glossopharyngeal and vagal nerves (IX and X) exit the cranial cavity via a foramen in the prootic, which we can confirm (Fig. 17B). The presence of the prootic foramen for these nerves differs from the arrangement they report for *Triacanthodes anomalus*, in which IX exits at the junction of the prootic, basioccipital, and exoccipital bones, and X exits through its own foramen in the exoccipital. They interpret that the different pattern in *Mola* is a result of alterations in the posterior part of the cranium related to fusion of the first vertebra with the basioccipital.

Spinal cord

Since the 19th century, molids have been recognized as having a short spinal cord (e.g., Owen 1866; see Chanet et al. 2013 for review). The spinal cord defies easy characterization because the only part of the CNS that enters the spinal canal in the vertebrae is the tiny filum terminale, which contains a central canal but little else (Uehara et al. 2015: fig. 2d). The filum terminale does not give rise to spinal nerves from within the spinal canal, and the spinal canal is occupied primarily by dorsal and ventral roots of the cauda equina. If we define a spinal cord by its location in the spinal canal, then molids lack a spinal cord (Uehara et al., 2015: 291). If we define the spinal cord by the location of the first spinal nerve, the definition preferred by Uehara et al. (2015) and that we agree with, then molids have a spinal cord even though it is contained within the cranium. In their material, vertebra 13 was the last to have a spinal canal.

It is tempting to correlate the shortened spinal cord of *Mola mola* with reductions in the caudal region. However, given that a similarly short spinal cord is reported in other tetraodontiforms that do not have a clavus and instead have typical caudal regions, Uehara et al. (1986: 333) suggested that it is more likely that all or most tetraodontiforms are characterized by an abbreviated spinal cord with a long filum terminale surrounded by the cauda equina.

Like other tetraodontiforms, molids lack Mauthner cells (Uehara et al. 2015: 299); these large neurons, which extend from the hindbrain into the spinal cord, mediate escape responses such as C-starts in other teleosts.

Lateral-line system

The lateral-line system of molids is reduced compared to that of other teleosts, and Tyler (1980: 368) and Santini and Tyler (2002) considered it to be absent or

extremely inconspicuous. This is because the lateral line of molids does not form canal structures but instead consists only of superficial neuromasts in specialized scales, as has been documented in the detailed study of the peripheral nerves of *Mola mola* by Nakae and Sasaki (2006: fig 1; reproduced here in Fig. 18). They report that there are relatively few neuromasts overall (e.g., 27 in the trunk line). The neuromasts are restricted to the anterior part of the body, i.e., they do not extend onto the clavus. Nakae and Sasaki (2006) showed that the lines of neuromasts in *M. mola* are innervated by the anterodorsal, anteroventral, and posterodorsal lateral-line nerves as in other gnathostomes (Fig. 18). They described the trunk line as extending in an abbreviated arch dorsal to the pectoral fin and terminating just anterior to the level of the insertions of the dorsal and anal fins (Fig. 18B). The trunk line is continuous with the lines on the head, connecting to the supratemporal line across the posterior dorsal surface of the head and a postotic line that continues anteriorly as the infraorbital line (Fig. 18B). Above the eye, Nakae and Sasaki identified a line of neuromasts forming the supraorbital commissure, which connects with the supraorbital line. The supraorbital and infraorbital lines do not connect anteriorly. A separate preopercular line continues ventrally in front of the gill opening, then loops dorsally toward the eye. This portion of the preopercular neuromast line may correspond to the mandibular line of other fishes because it is innervated by the mandibular ramus of the anteroventral lateral-line nerve; however, the neuromasts do not extend as far forward as the mandibular region of *M. mola*.

Using a dissecting scope, we confirmed the presence of neuromast lines in juvenile *Ranzania laevis*, *Masturus lanceolatus*, and *Mola* sp. These lines are difficult to identify because the neuromasts are often spaced far apart and only faint lines connect

them. Comparative anatomical review of the sensory lines of all genera of molids is warranted.

Olfactory system

The olfactory system of adult molids is greatly reduced (Fig. 3), and in Tyler's (1980: 368) diagnosis, he states that there are "two minute nostrils flush with the surface of the skin." The nares of *Masturus lanceolatus* (VIMS 8120) are smaller and much farther from the eye than in *Mola*. In *Ranzania laevis*, the nares are also very small but located more dorsally than in either *Masturus* or *Mola*. No histological studies are available for the reduced olfactory organ itself (e.g., Jinxiang and Wanduan 1982), but components of the olfactory system in the brain of *M. mola* include a corresponding small olfactory bulb (Olf; Fig. 17D). Together, the small superficial nares, which likely do not allow much water flow through the system, and the tiny olfactory bulb, suggest that olfaction is not an important sense for adult molids.

Eyes

Harting (1865: plate 2, fig. 1) observed left-right asymmetry of the eyes of *Mola mola*. In the specimen he illustrated, the bottom of the left eye is more ventral than the bottom of the right eye. It would be useful to restudy this in a large series of specimens because it has been little noted in the literature (but see Meek 1904, who corroborated this observation in a single specimen). Externally, in *M. mola*, the eye is protected by a strong ring of skin that is reflected to produce a deep conjunctival recess before continuing over the surface of the eye as its cornea. The conjunctival recess allows the eye to move and also provides space for the nictitating membrane to cover the eye's

surface. Cuvier (1805b: 434) wrote about the ability of *Mola mola* to fully cover the eye, noting that it was a peculiarity "not seen elsewhere." [*Le poisson - lune (Tetraodon mola) nous a présenté une particularité que nous n'avons point vue ailleurs*.] The function of the nictitating membrane was also noted by Brimley (1939), who stated: "A nictitating membrane enabled the creature to open and close its eyes. I saw this happen several times and the fisherman also called attention to this feature."

Like other molids, *Mola mola* has large eyes in proportion to its body length, although most measurements are from juveniles (Phillips et al. 2015). They also have good movement of their eyes, particularly in the ventral plane (Kino et al. 2009: fig. 4). There are several, not mutually exclusive, interpretations for how *M. mola* uses its eyes during prey capture. Acceleration towards prey items in shallow water during diurnal foraging and feeding suggests that *M. mola* visually searches for prey (Nakamura et al. 2015). Phillips et al. (2015) interpreted that molids also visually forage at depth, and that *M. mola* may approach gelatinous prey from below highlighting them against the water above. In their study of visual acuity, Kino et al. (2009: fig. 3c) documented blind spots directly above and below the body. They interpreted that the large eyes are used to find prey during the downward portion of a dive because of the high density of photoreceptors in the dorsotemporal portion of the retina, which serves the lower frontal portion of the visual field.

Ear

Cuvier (1805b: 469) described the membranous labyrinth and three semicircular canals of *Mola*. However, Cleland (1862) incorrectly stated that *Mola* has only two semicircular canals, an error corrected by Harting (1865), Thompson (1889), and Meek

(1904) based on materials from specimens that are junior synonyms of *Mola mola*. The descriptions and figures by Thompson (1889) describe a pillar passing through the arc of the posterior vertical canal. Meek (1904) corrected this to show that the pillar passed not through the space enclosed by the anterior vertical canal, but through the arc of the posterior canal. Harting's (1865) illustrations and our study of the right side of VIMS 35803 agree with Meek's (1904) description.

The membranous labyrinth is not surrounded closely by a skeletal labyrinth, but is instead suspended by the arachnoid layer in a cavity continuous with the cranial cavity. The membranous labyrinth has the regions found in other teleosts, including a utriculus with its superior sinus; a utricular recess; the anterior, posterior, and horizontal semicircular ducts; the sacculus; and the lagena (Fig. 19). In our specimen, these last two chambers are very closely associated with each other and with the utriculus. The sacculus and lagena are reduced in size compared to other teleosts because the otoliths are small. Thompson (1889: 2) observed six maculae in the specimen he studied: one in each of the three ampullae for each of the three semicircular ducts and one each in the utricular recess, sacculus, and lagena.

The poorly consolidated otoliths of *Mola* have been variously interpreted in the literature. Cuvier (1805b: 456-457) described the otoliths as gelatinous. Cleland (1862) incorrectly stated that *Mola* lacks otoliths (his error was subsequently corrected by others; see Tyler 1980: 29), but it is easy to understand Cleland's mistake because the mineralized portions of the sagittal otolith are tiny (Fig. 19). Nolf (1985) illustrated an unconsolidated otolith from *M. mola* that was later termed "chalk dust" by Nolf and Tyler (2006). Gauldie (1990: fig. 3b) illustrated the asteriscus and sagitta *in situ* in the

endolymphatic sac. SEMs presented by Gauldie (1990: fig. 4) show individual disc-shaped otoconia in the sagitta of *M. mola* and *M. alexandrini* (*M. ramsayi* in Gauldie's 1990 study). The otoconia range from 50–100 μm in length, and the separations between individual otoconia explain why dried otoliths of *Mola* fall apart and appear as chalk-like calcareous granules. As to the mineral composition of the granules, there are different interpretations. For example, Carlström (1963) interpreted the mineral of the otoconia of teleosts generally as aragonite, a morph of calcium carbonate; however, Gauldie (1990) interpreted the mineral in Molidae as vaterite, another morph of calcium carbonate. More recently, Pracheil et al. (2019) reviewed the phylogenetic distribution of vaterite morphs in actinopterygians, coelacanths, and lungfishes. They found that vaterite morphs are more common within actinopterygians than previously suggested by authors including Carlström (1963) and Gauldie (1990). Vaterite otoliths have been associated with reduced ability to perceive sound (Oxman et al. 2007, Reimer et al. 2016), which combined with the small size of the otoliths, suggests that hearing is not an important sense in *Mola*.

The small otolith of *Ranzania laevis* was described by Nolf and Tyler (2006:155, plate 18, figs. 10a, b). In contrast to *Mola*, it has spine-like crystal extrusions and an "elongate ventral portion, a strong but structureless crista inferior accentuated by a deep ventral portion of the sulcus, and a very narrow, strongly salient dorsal area." They noted that this otolith morphology is most similar to that of diodontids among tetraodontiforms. The mineral composition of the otoliths of *R. laevis* is unknown. However, Smith et al. (2010) reported that no otoliths were present in the three specimens of *R. laevis* examined, and instead, "microscopic calcareous granules" which they considered like the

otoconia of *M. mola*. We could not evaluate the condition of the otoliths in our specimens of *R. laevis*.

Taste, pain, temperature, and touch

We did not find literature relevant to interpreting the sense of taste in molids. Similarly, apart from the cutaneous branches of the nerves identified by Nakae and Sasaki (2006), we found no information on the senses of pain, temperature, and touch.

Digestive system and swim bladder

A comparative study of multiple specimens of all three genera side-by-side has never been conducted, but aspects of the anatomy of the digestive system of molids are included in many accounts (e.g., Agassiz 1857, Gregory and Raven 1934, Raven 1939 a, b, Suyehiro 1942, Chanet et al. 2012). The viscera of *Ranzania laevis*, *Masturus lanceolatus*, and *Mola* exhibit different organizations (Fig. 20). For example, the gut of *R. laevis* is relatively short, and its stomach is preceded by an esophageal sphincter (not shown but observed in ANSP 103501; Raven 1939a: fig 2). In contrast, the elongate digestive system of *M. lanceolatus* and *Mola* has as many as 15 intestinal loops (Suyehiro 1942) and no esophageal or pyloric sphincters. In both *M. lanceolatus* and *Mola*, the loops of the intestine are surrounded by a mesenteric sac that originates from a broad connection of the mesentery along the posterodorsal wall of the peritoneal cavity. This sac is particularly evident in fresh dissections (e.g., Fig. 21). The presence or absence of a mesenteric sac needs to be confirmed in better preserved material of *R. laevis* than was available to us. The peritoneum of molids is unpigmented and the peritoneal cavity is well separated from the pericardial cavity by the transverse septum.

We identified two problems with earlier accounts: (1) Viscera were rarely saved after dissection and this makes it difficult to confirm that descriptions of the viscera relate to specific taxa, e.g., whether the dissection was made of *Masturus* or *Mola*; and (2) Terms for the portions of the gut tube and associated organs vary between published accounts. Additional comparative work, particularly new histological studies, like the methods of Carlucci et al. (2019), need to be conducted. Here, we comment on our original observations and summarize the literature.

Esophagus, stomach, and intestine

Agassiz (1857: 319) described the unusual digestive tract of *Mola* long ago as: "The stomach [is] directly continuous with the intestine, without any indication of difference, either in form, or structure of the mucous membrane; the whole tract resembling a long hose from one orifice to the other." There has been confusion about the presence of a "stomach" in molids, some of which comes from differing definitions of stomach loss. Wilson and Castro (2011: 8) used a three part classification for gross anatomical shapes of fish stomachs: straight (I-shaped), siphonal (U or J shaped) or cecal (Y shaped); *Mola mola* has the straight or I-shaped form. Straight stomachs are relatively rare among teleosts, and are often associated with an aglandular stomach and little specialization of the mucosa; to some, this is adequate evidence of stomach loss. Another possible definition for stomach loss is the absence of valves at the esophageal and pyloric ends of the region. Cuvier (1805c: 525-526) identified a stomach in *Mola*, but noted that it did not have esophageal or pyloric valves. Gregory and Raven (1934: fig 1) and Raven (1939a: fig. 2) label a stomach in their illustrations. According to Steenstrup and Lütken (1898), the small stomach of *Orthagoriscus* is not easily distinguished from the intestine.

Suyehiro (1942: 192) appears to have been the first author to state that the stomach is absent in *M. mola*. *Ranzania laevis* has a distinct esophageal sphincter according to Raven (1939a: fig. 2); he does not describe a pyloric sphincter in his text or figure.

We investigated the condition of the "stomach" in *Masturus lanceolatus* (VIMS 8021). The esophagus is relatively thick-walled and has six longitudinal folds (Fig. 22A). In contrast to the condition reported for *Ranzania laevis*, the esophageal-stomach junction in *M. lanceolatus* is not marked by a sphincter but instead by a change in the walls (Fig. 22B). In VIMS 8021, the "stomach" has a series of 8-9 longitudinal folds, and it merges directly with the intestine, i.e., there is no pyloric sphincter. The bile duct, which is thick-walled, opens directly into the "stomach" (Fig. 22B). We were not able to study this region of the gut in *Mola mola*, but Gregory and Raven (1934) do not illustrate or mention either esophageal or pyloric sphincters.

In both *Masturus* and *Mola*, the intestine is long, coiled, and occupies much of the abdominal cavity (Figs. 20B, C and Fig. 21, Chanet et al. 2012: figs. 3, 5, and 6). The intestine is relatively shorter in *Ranzania laevis* (Fig. 20A).

Liver and gallbladder

The liver of the specimen of *Ranzania laevis* that we dissected had two lobes and many lobules (we were unable to make an exact count because of the frailty of the liver in this specimen). In *Masturus lanceolatus* (Fig. 20B; VIMS 8120), the liver consists of a single, large lobe, but in *Mola mola* both left and right liver lobes were present (Fig. 21A); the left lobe is larger than the right. We observed a large, spherical gallbladder in *M. mola* on the right side of the abdominal cavity between the two liver lobes (Fig. 21A, B; Chanet et al. 2012; fig. 7).

Swim bladder

We confirmed presence of the swim bladder in a dissection of a juvenile *Masturus lanceolatus* (Fig. 23A, B, 57 mm TL, MCZ 24875). We also used a micro-CT dataset to demonstrate for the first time presence of a swim bladder in a larval *Mola mola* (Fig. 23C, D; 7 mm TL, MCZ 61454). The swim bladder in this specimen is a large outpocketing from the esophagus, with very thin walls at this stage. In this larva, the intestine loops dorsally on the right side of the abdomen, and the swim bladder is positioned to the left of the intestine; it is slightly collapsed. We cannot be certain about the position of the swim bladder in life because the size and location in this specimen may be an artifact of fixation; in life it could have expanded across the body cavity. We did not study conditions of the swim bladder in larval or juvenile *Ranzania laevis*. We did not find a swim bladder in any of the adult specimens of the three genera of molids, nor did we study a developmental series that would have been sufficient to determine when the swim bladder is lost.

Heart and gill arch circulation

Molid hearts and circulation patterns are unusual compared to those of other teleosts and need to be considered from the new perspective of molids as active, fast swimming, fishes.

Heart

Based on our dissections of specimens of *Ranzania laevis* (ANSP 103501), *Masturus lanceolatus* (VIMS 8120) and *Mola mola* (VIMS 35803), the heart of molids is large relative to body size, with thick walls (Fig. 24A, B). The atrium is shaped like a tall pyramid; it receives blood from large hepatic and cardinal veins via a thin-walled sinus

venosus with internal trabeculations (not visible in Fig. 24). From the sinus venosus, the atrium extends ventrally along the inner face of the pericardial cavity, against the transverse septum (Fig. 24A). The walls of the atrium are trabeculated and many pockets are defined by these trabeculae (Fig. 24B), which suggests the heart has a great capacity to receive venous blood.

Ventral to the atrium is the thick-walled and strongly trabeculated ventricle (Fig. 24A, B). Blood passes from the atrium through the atrioventricular valve, which has four leaflets in the specimen of *Masturus lanceolatus* we dissected (VIMS 8120; indicated in Fig. 24B by the numbers 1-4). The leaflets are yellow and stiffer compared to the surrounding cardiac musculature and endothelium (Fig. 24B). We confirmed presence of four atrioventricular leaflets in a specimen of *Mola mola* (VIMS 35803), and tested their function in this specimen by compressing the ventricle filled with fluid. Compression caused all four leaflets to close the atrioventricular opening. Rosén (1912: 7) reported that the number of atrioventricular leaflets ranged from 3-5 based on the literature. Not having a specimen to dissect, he concluded that there are four because this was the most commonly reported number. Rosén also noted that no other living tetraodontiform has as many atrioventricular leaflets. Valves make the contracting chambers of the heart into pumps – without them, blood would flow in both directions upon contraction of a chamber. More leaflets likely result in more complete closure of the orifice between chambers, and because of this, we interpret that the chambers of the hearts of molids function as high pressure pumps.

In contrast to the ventricle, the walls of the bulbus arteriosus are not trabeculated, but they are unusually thick and muscular for a teleost. We confirmed that the well-

developed ventriculo-bulbar valve has four leaflets in *Masturus lanceolatus* (Fig. 24B: indicated i-iv; VIMS 8120) as noted by Harting (1865: plate 3, fig. 6). Rosén (1912) noted that the number of leaflets in the ventriculo-bulbar valve of *Mola* is greater than in other tetraodontiforms. The muscular walls and well-developed leaflets separating the ventricle from the bulbus arteriosus suggest that the bulbus arteriosus plays an important role in pressurizing blood to pass through the large arrays of gill filaments.

Gill arch circulation

The stout ventral aorta gives rise to four large afferent branchial arteries on each side of the body. The afferent branchial arteries serve gills 1-4. An unusual feature of molid circulation concerns the pattern of branching of afferent branchial arteries serving gills 3 and 4 (Fig. 24C, D, Fig. 25A, B). As shown in ventral view with the ventral aorta in position (Fig. 24C), the three larger gills receive correspondingly large afferent branchial arteries (ABA 1-3); the afferent branchial artery for the fourth gill (ABA 4) is about half the diameter of the other three arteries. When the ventral aorta is reflected (Fig. 24D), the origin of ABA 4 can be seen in its position anterior to the origin of ABA 3. This branching pattern was described by Milne-Edwards (1858) and Parker (1900) for specimens that were presumably *Mola mola*, and is shown schematically in Figure 25A, B.

According to Milne-Edwards (1858) and confirmed by Parker (1900), the heart of their specimens had three coronary arteries. We confirmed this in *M. mola* (VIMS 35803) and used information in Parker (1900: fig. 1) to produce a schematic diagram of the coronary arteries (Fig. 25A, B). On the ventral side (Fig. 25A), efferent branchial arteries 1, 2, and 3 give rise to a vessel termed the lateral hypobranchial artery, which, in turn,

merges with the lateral hypobranchial artery from the contralateral side to form the median hypobranchial artery (Fig. 25A). Posteriorly, the median hypobranchial artery gives off a small epigastric artery to supply the pericardial wall. The remaining branch continues posteriorly as the ventral coronary artery to supply the ventral surface of the ventricle. On the dorsal side, each of the paired efferent branchial arteries 4 (serving gill 4) gives rise to vessels that become the right and left dorsal coronary arteries (Fig. 25B).

Adeney and Hughes (1977: fig. 4) described the double afferent system of vessels serving the gills in *Mola mola* (Fig. 25C). For example, upon entering gill 1, afferent branchial artery 1 divides into two vessels termed the lower and upper afferent branchial arteries (Fig. 25C). Blood passes from these vessels through afferent filament arteries and the secondary lamellae of the gill before reaching the efferent filament arteries (Fig. 25C). Each efferent filament artery joins the dorsal or ventral efferent branchial arteries in a manifold like arrangement, eventually leading to the efferent branchial artery proper (EBA, Fig. 25C).

Upon exiting the gills, the efferent branchial arteries join to form the major arterial trunks in a circulus cephalicus (Fig. 25D) that Ridewood (1899) illustrated based on a specimen of *Ranzania laevis* (= *Orthagoriscus truncatus* in his text, a junior synonym of *R. laevis*). There is a striking difference in the position of origin of the coeliaco-mesenteric artery, which does not have a paired origin from right and left EBA 3 + EBA 4 in any of the other tetraodontiform or other teleosts he studied. Both the extent of variation within molids and the functional significance of this unusual circulatory pattern are unknown. Our dissection of *Mola mola* (VIMS 35803) suggests that it may

have a still different pattern in which the coeliaco-mesenteric arteries originate only from EBA 4. More work is needed to confirm this pattern.

Respiration

The unusual anatomy and circulation of molid gills received attention more than 150 years ago in a paper by Alessandrini (1839) that was beautifully illustrated in color. In the intervening years, only the account by Adeney and Hughes (1977) stands out as contributing significant new information, for example the first estimate of gill surface area (see Hughes 1984, which provides a review of gill surface area). Although Adeney and Hughes (1977) did not cite Alessandrini's (1839) account, the two papers have similar basic findings and we base our account on both of them as well as new observations of *Mola mola*.

Molids have restricted gill openings just anterior to the pectoral base that are covered by a valve (Figs. 2, 3). The gills of *Mola mola* are within paired structures that we term gill sacs; these sacs define the opercular chambers (Fig. 26A). Within each gill sac is the pseudobranch and four large gills partially supported by ceratobranchials 1-4; ceratobranchial 5 does not bear a gill. The epibranchials and ceratobranchials of *M. mola* are surprisingly small relative to the large gills (Fig. 7, 8, 9), and they do not directly support most of the gill tissue, serving instead to define the internal gill openings through which water passes from the pharynx into the gill sac. Adeney and Hughes (1977) divided the gills into ventral, middle, and dorsal regions, indicated by dashed lines in Figure 26D. The gill-arch skeleton proper (e.g., ceratobranchials) is limited to the middle region. The expansion of the gills both dorsally and anteriorly to the supporting skeletal

elements of the gill arch can be most easily appreciated if the gill sac is cut open and the pseudobranch reflected (Fig. 26D).

The great expansion of the gills relative to the skeletal elements of the arch is possible for two reasons. First, the gill filaments (primary lamellae) are heavily mineralized, and because the gill rays of each hemibranch fuse at their bases and form a strong structural support for the primary gill lamellae (Adeney and Hughes 1977:828). Second, a series of novel elements, termed upper and lower cartilage blocks by Adeney and Hughes (1977: fig. 2a), also support the gills. Adeney and Hughes (1977:828) state: "This structure supports the hemibranch and replaces the gill arch." Only connective tissue attaches the skeletal elements of the arch and the gill lamellae even in the middle of the gill, closest to the gill arch skeleton.

In *Mola mola*, the internal gill openings that allow water flow from the pharynx into the gill sac are restricted (Fig. 26B, C); this is in part because the small epibranchials and ceratobranchials define these internal openings. Each internal gill opening has a series of soft, short gill rakers (Fig. 26B, C, E). As water passes through the internal gill opening to the gill sac, it is directed over the primary gill lamellae. In Figure 26E for example, which shows the medial surface of right gill 1, there are approximately 200 primary lamellae. The hemibranchs are offset from each other on opposite sides of a gill (Fig. 26G). In the cross section of primary lamellae shown in Figure 27G, the I-shaped structure of each lamellum can be seen, with the side closest to the septum supported by the mineralized gill ray. Channels between adjacent primary lamellae are about 0.5 mm wide in a 1180 mm TL specimen. In contrast to Adeney and Hughes (1977), we consider that the secondary lamellae are closely packed and numerous. One consideration not

addressed by Adeney and Hughes (1977) is the role of the gills in ionic regulation, specifically, the elimination of excess monovalent ions such as Na+ and Cl-. This is an important aspect of gill physiology that should be addressed given the diet of adult molids (gelatinous prey is isotonic with seawater). Although we were unable to estimate either total gill surface area based on the materials at hand or potential for salt excretion, these are important future goals for studies of molid biology.

Urinary system

The kidneys are large, rounded, independent, paired retroperitoneal structures that extend anteriorly as far as the occipital region of the neurocranium (Fig. 27A). Each is served by a large renal portal vein carrying blood from the posterior part of the body to the kidney (Fig. 27B). The kidney tissue is divided into several lobes that can be easily separated, and in our specimen of *Mola mola* (VIMS 35803) there are three lobes in the right kidney. Chanet et al. (2012: table 1) noted the independence of the left and right kidneys, and considered this as a possible synapomorphy of tetraodontiforms and lophiiforms. The condition in tetraodontiforms and lophiiforms contrasts with typical teleosts in which the elongate kidneys are joined between the haemal arches dorsal to the abdominal cavity (Chanet et al. 2013).

Ureters extend posteriorly to reach the large, median, urinary bladder which lies along the posterior wall of the abdominal cavity (Owen 1866: 536, Gregory and Raven 1934: fig. 1). The urinary bladder empties into the urogenital sinus which also receives gametes from the gonads. The urogenital sinus of *Mola mola* has a separate opening to the exterior, immediately posterior to the anus (Gregory and Raven 1934: fig. 1; we confirmed this in *Ranzania laevis* and *Masturus lanceolatus*).

Reproductive system

Mola mola is recognized as the most fecund extant vertebrate based on a single paper by (Schmidt 1921b), who reported that the ovary of a 1.5 m specimen contained an estimated 300,000,000 eggs. This claim, however, has never been verified. Our specimens of *Masturus lanceolatus* (VIMS 8120) and *Mola mola* (VIMS 35803) each had a single small ovary, 80-100 mm long; the specimens were not much smaller than the one studied by Schmidt (1921b). For reproductive anatomy and biology of molids, refer to the chapter in this volume by McBride et al.

Endocrine organs

Little is known about the endocrine organs of molids probably because it is challenging to conduct physiological observations and experiments. Available interpretations are based on anatomy, and even these are limited.

Hypophysis

Harting (1865: plate 3, fig. 1) showed a large hypophysis lying beneath the brain. Burr (1928: fig. 13) illustrated a section through the hypophysis, but it only shows components of the neurohypophysis. Here, we reproduce Burr's wax plate reconstruction of the brain and hypophysis of *Mola mola* (Fig. 17E). The adenohypohysis has not been studied, but we can predict that the hypophyseal portal system is not present because it was lost in the evolutionary history of teleosts (see Liem et al. 2001 fig. 15-5).

The epiphysis and paraphysis of *Mola mola* were illustrated in the wax-plate reconstruction of the brain by Burr (1928: fig. 40; Fig. 17E). Nothing is known about their potential role in endocrine functions.

Thyroid and related tissues

Chanet et al. (2012, 2013: fig. 8) report that the compact thyroid gland is in a blood lacuna dorsal to the ventral aorta. They interpret this condition as a synapomorphy of tetraodontiforms and lophiiforms (Chanet and Meunier 2014). No published information about c-cells, parathyroid tissue, or the ultimobranchial body is available as of June 2019.

Chromaffin cells and cortical tissues

The chromaffin cells and islets of cortical tissues (for a phylogenetic overview on the evolution of the adrenal gland, see Liem et al. 2001: fig. 15.9) are not known in molids but should be a target of future research.

Urophysis

Hamana (1962) reported that molids lack a urophysis (caudal neurosecretory system), which is unusual for a teleost. This reduction is probably related to the reduced spinal cord and extensive cauda equina of molids. Fridberg and Bern (1968:178) note that this conclusion is based on light-microscopy and that re-examination using electron microscopy is needed.

Discussion

Information about systematics, locomotion, and behavior published since the turn of the 21st century (e.g., Britz and Johnson, 2005a, b, Johnson and Britz, 2005, Nakae and Sasaki 2006, 2010, Dewar et al. 2010, Nakamura et al. 2015, Watanabe and Sato 2008, Nyegaard et al. 2018a, b) is powering new interest in molid anatomy. In particular, we can begin to view molid anatomy in light of new behavioral studies.

Early accounts (e.g., Binney 1842: 93) describe *Mola mola* as “very sluggish” and that “their slow movements and inefficient jaws prevent them from pursuing a more

active prey." Nearly 100 years later, Burr (1928: 35) stated: "Its habits are described as being lethargic, slow-moving, not infrequently found apparently asleep on the surface of the water." Data from tagging studies (e.g., Watanabe and Sato 2008, Houghton et al. 2009, Dewar et al. 2010, Nakamura et al. 2015, Thys et al. 2015) provide a different view, showing that molids are well-adapted and efficient swimmers that make deep foraging dives. For example, when not basking, *Mola mola* swim at speeds of 0.4–0.7 m s^{-1}, even accelerating to 6 m s^2, which is comparable to other large fishes such as marlins and pelagic sharks (Watanabe and Sato 2008, Nakamura et al. 2015, Thys et al. 2015). These findings cause us to reframe interpretations of molid anatomy, including, for example, the osteodentine beak (Fig. 10), elongate pharyngeal teeth (Fig. 12), greatly thickened hypodermis (Fig. 15), enlarged vestibular ducts with minute otoconia (Fig. 19), ontogenetic loss of the swim bladder (Fig. 23), large heart and coronary circulation from multiple vessels (Figs. 24, 25), and large gills (Fig. 26). There are also many specializations of body musculature and tendons related to moliform locomotion (Webb 1994, Watanabe and Sato 2008, Davenport et al. 2018; see Davenport et al. this volume).

Dentition and diet

The beaks of molids differ from the beaks of even closely related tetraodontoids. For example, Hilgendorf (1893:3-4) briefly compared molids, tetraodontids, and diodontids. He reported that the beak of *Mola* is not covered with enameloid, and that this is unlike the condition in *Tetraodon* and *Diodon*. Instead, as subsequently shown by Andreucci et al. (1982), the beak is solely composed of osteodentine. Our results confirm that the beak is osteodentine and that it lacks enameloid (Fig. 11C). Molids also lack tooth germs entering the base of the beak. This contrasts with the condition in other

tetraodontoids, in which tooth germs enter the dentigerous bone at the base of the beak and develop intraosseously into hypermineralized elements within the beak (e.g., Thiery et al. 2017: fig. 5). Beaks of other fishes, like other tetraodontiforms including diodontids, triodontids, and tetraodontids (Thiery et al. 2017), as well scarids and oplegnathids, develop from individual tooth germs. In these groups, the tooth germs develop into more densly mineralized portions of the tooth. These fishes also feed on relatively hard prey. Although there is no direct evidence for this, perhaps the simplification of the beak of molids (loss of enameloid and loss of tooth germs) is related to a diet of gelatinous prey.

Finally, although we illustrate an ontogenetic series of triturating teeth (Fig. 12), we still have much to learn about triturating teeth in molids. For example, it remains unknown if the well-developed triturating teeth in larvae and juvenile *Mola mola* (Fig. 12) are either lost (i.e., simply not replaced with new teeth) or if they are progressively incorporated into the posteroventral edge of the beak during ontogeny. Presumably these changes in dentition are associated with ontogenetic changes in diet and the diversity of dietary items. Although molids feed on gelatinous prey, and Nakamura et al. (2015) showed that *M. mola* specifically target such prey, other studies document a wide diversity of prey based on stomach contents (Bakenhaster and Knight-Gray 2016, also see review in Pope et al. 2010). For example, Syväranta et al. (2012) and Harrod et al. (2013) used stable isotope analysis, suggesting that *M. mola* <1 m TL eat a broad range of prey; this interpretation has been further supported by DNA barcoding of stomach contents by Sousa et al. (2016), who documented ontogenetic changes in diet composition in a series of 57 individuals ranging from 370 mm to 1110 mm TL. They

grouped these individuals into four size classes (Sousa et al. 2016: fig. 3) and showed that small *M. mola* eat harder prey than do large individuals, which had higher percentages of geleatinous oraganisms in their diet.

As adults, *Mola mola* feed on soft bodied prey such as jellyfishes, typically during deep dives (Nakamura et al. 2015). When feeding on the gonads and oral arms of jellyfishes, *M. mola* leaves the bell intact (Nakamura et al. 2015: 595). This suggests that they bite off portions of a jellyfish with the beak. Brimley (1939) noted the resemblance of molid beaks to those of sea turtles, a resemblance close enough that beaks of some fossil molids were initially misidentified as those of sea turtles (Weems 1985). Suyehiro (1942) interpreted that the long, recurved pharyngeal teeth are related to the diet of jellyfishes. *Dermochelys coriacea*, the leatherback sea turtle, also feeds on jellyfishes, and, like *M. mola*, has long, recurved tooth-like keratinized papillae in the anterior parts of the esophagus (see Magalhães et al. 2012: fig. 1).

Other anatomical features may relate to the diet of *Mola mola*. For example, leatherback sea turtles (*Dermochelys coriacea*; Hays et al. 2018) rely on lachrymal salt glands to excrete salt ingested from their diet of jellyfishes. No special salt excretory gland has been reported in molids, but *M. mola* has a greatly enlarged urinary bladder, kidneys, and gills which might play a role in salt elimination.

Ontogenetic loss of swim bladder

Most literature suggests that molids do not have a swim bladder (e.g., Fraser-Brunner 1943, Breder and Clark 1947, McCune and Carlson 2004, Watanabe and Sato 2008, Chanet et al. 2012). However, subsequently, Fraser-Brunner (1951:151, fig. 9B) illustrated and labeled an “air bladder” in a 21 mm specimen of *Masturus lanceolatus* (=

Masturus oxyuropterus in Fraser-Brunner 1951) He described the structure he labeled as: "a very delicate, bubble-like structure at the center of mass, which unfortunately collapsed while I was examining it." It is not surprising that juvenile molids have a swim bladder because all other tetraodontiforms have one (Chanet et al. 2014). No one has reported the presence of a swim bladder in adult molids with the sole exception of Suyehiro (1942: 194), who stated: "Air-bladder large, wall rather thick." Based on our dissections, we suggest that Suyehiro (1942) mistakenly interpreted the large urinary bladder as a swim bladder.

Fraser-Brunner (1951: 151) not only described the swim bladder in *Masturus lanceolatus*, but also interpreted that the swim bladder is present in larvae and small juveniles, and later lost during ontogeny. Our observations support his finding (Fig. 23), but it remains unknown at what body size the swim bladder is lost. The swim bladder is likely important in the biology of larval molids, helping them maintain buoyancy during early lifestages when they are essentially spherical (Fig. 4, 5). Swim bladder loss in adult molids may relate to diving and foraging behaviors. For example, McCune and Carlson (2004) interpreted that the absence of a swim bladder in molids relates directly to frequent diving to depths of 1000 m or more (see Dewar et al. 2010; Thys et al. 2017). Watanabe and Sato (2008) proposed that adult *Mola mola* achieve neutral buoyancy by means of the thick, low-density hypodermis (see Fig. 15). Because the hypodermis is incompressible, it is superior to a gas-filled swim bladder because it allows for faster diving (Watanabe and Sato 2008).

The condition of the swim bladder has been used as a phylogenetic character. For example, Santini and Tyler (2002: Character 43) stated, "Air bladder: present and well

developed (0); absent, at least in adults (1)" with only the Molidae being scored as state 1. We agree with this as an important diagnostic character for the family.

Heart, circulation, and gills

In light of recent reports on the activity of *Mola mola*, we can offer a new perspective on the heart and circulatory system. The large heart of molids has abundant trabeculae in both the atrium and ventricle, thick muscular walls of the ventricle and bulbus arteriosus, and complex valves between the chambers. In both *Masturus lanceolatus* and *M. mola,* we confirmed the presence of an atrioventricular valve with four leaflets and a ventriculo-bulbar valve with four leaflets. The presence of these well-developed leaflets suggest that they are there to accommodate large pressures generated by the ventricle and bulbus arteriosus. (We are skeptical about older reports (reviewed in Rosén 1912) of fewer than four or more than four leaflets in the atrioventricular valve because this feature can be difficult to evaluate in poorly fixed specimens; also, we would not expect this level of variation in heart structure between specimens.) There are two unusual aspects of molid coronary circulation that may also relate to high heart function and activity levels. First, in most teleosts, only a single vessel on each side of the body, typically a branch of efferent branchial artery 2, contributes to formation of the coronary arteries (Rosén 1912). In contrast, the coronary arteries of molids take blood from efferent brachial arteries 1-4 on both sides of the body (Fig. 25). Second, the presence of three distinct coronary arteries in *Mola mola* is atypical for teleosts, which usually have only two coronary arteries. Together, the multiple sources of oxygenated blood from the gills and the multiple vessels supplying the thick walls of the ventricle suggest that molids have a powerful circulatory system. It would be interesting to measure heart rate

and other physiological parameters to better understand the overall activity metabolism of molids.

Based on cardiovascular and gill anatomy, we interpret that molids pump large volumes of blood over large arrays of gill filaments. The great expansion of the gills is only possible because of the heavily mineralized gill rays and the novel cartilaginous blocks that effectively replace the conventional skeletal elements supporting the gills of other teleosts (e.g., ceratobranchials and epibranchials). Adeney and Hughes (1977:826-827) interpreted that the position of the buccal cavity relative to the restricted gill opening means that the main stream of water flow moves across the region of greatest filament area; this should be checked in live specimens. Adeney and Hughes also concluded (1977:836) that "The gill area of *Mola* falls within the range of Gray's (1954) intermediate activity group of fishes and this correlates reasonably well with its known habits." At the time that they suggested this, molids were thought to be sluggish. It would be interesting to reexamine gill surface area using SEM and micro-vascular studies because the secondary lamellae appear to us to be very thin and very closely packed.

Next steps

Material for the study of molid anatomy remains the biggest obstacle to detailed analyses. Well-fixed specimens are essential to answer many of the outstanding anatomical questions about molids, such as the arrangement of the roots of the cranial nerves and their central connections in the brain. For detailed understanding of circulation, micro-vascular studies will be necessary, and these require fresh material. Questions about the lining of the "stomach" or anatomical organization of the kidneys can be best answered histologically. To address the paucity of information on sensory

systems, such as taste, well-fixed materials for SEM imaging are needed. For many of these questions, it would also be useful to study larvae and large adults to document the development of structures.

Summary

Hallmarks of the evolutionary and anatomical diversification of molids include the simplification, reduction, and loss of many structures, combined with specializations and innovative elaborations of other organ systems. Compared to other tetraodontoids (triodontids, diodontids, and tetraodontids), molids have reduced, eliminated, or modified many structures including: loss of the caudal peduncle and caudal fin and modifications of the dorsal and anal fins to form the clavus; decrease in vertebral numbers from 20 (Triodontidae) to 16-18 (Molidae); loss of teeth and enameloid in the beak; reduction of pectoral radials to three rather than four elements; loss of the coronomeckelian; reduction of the interopercle to a simple slender rod of bone (*Ranzania* and *Mola*) or lost completely (*Masturus*); reduction of the lateral-line system; minute nostrils, which are flush with the skin; ontogenetic loss of the swim bladder, which is present in early life history stages; spinal cord contained completely within the braincase, presumably because the first vertebra is incorporated into the neurocranium; and reduced otoliths relative to body size.

Anatomical specializations of molids relative to other tetraodontoids are perhaps even more impressive than the losses and reductions. These include: an unusually thick hypodermis (especially thickened in *Masturus lanceolatus* and *Mola*); four gills greatly expanded dorsally and ventrally beyond their supporting skeletal arches, made possible by novel cartilages at the bases of calcified gill rays; long, slender teeth on

pharyngobranchials 2–4; new arrangements of bony elements, muscles, nerves, and fin rays in the clavus that replace the caudal peduncle and caudal fin; the postcleithrum with its anteriorly directed process toward or over the pectoral radials; the high dome or ribbon-like posterodorsal prolongation of the epioccipital; the greatly prolonged pterotic; dorsal-and anal-fin rays widely separated from their pterygial supports by a large block of cartilage; large heart with thick walls and many trabeculae; four valves separating the atrium from the ventricle and four valves separating the ventricle from the bulbus arteriosus; three coronary arteries; enlarged kidneys; and the enormous sizes of adults in the *Masturus lanceolatus* + *Mola* clade.

Knowledge of molid anatomy has developed over several hundred years, yet it is far from complete as shown by our new interpretations that begin to link molid anatomy to their active existence as pelagic divers. Much remains to be learned through the study of new materials.

Specimens Examined

All specimens examined are single specimen lots stored in alcohol unless otherwise indicated. Total lengths (TL) are listed, when available. Institutional abbreviations follow Sabaj (2016).

Masturus lanceolatus

AUS I.25362-019, 7.5 mm TL

AUS I.43072-003, 32 mm TL (length includes claval extension)

MCZ 24875, 57 mm TL

UF 136518, 164 mm TL (length includes claval extension)

UF 234607, n = 11, 5-20 mm TL

VIMS 40709, 690 mm TL

VIMS 8120, 1175 mm TL

***Mola* sp.**

AUS IA.2423 *Mola* sp., 32 mm TL

AUS I.27082-001 *Mola* sp., 74 mm TL

Mola mola

ANSP 153731, 2 of 3 specimens examined, 223 mm TL, 245 mm TL

ANSP 109090, est. 400 mm TL, dry skeleton

CAS 13244, est. 466 mm TL

CAS 25828, est. 406 mm (=16 inches), dry skeleton, jaws only

CAS 53080, 390 mm TL

CUMV 98740, est. 1500 mm TL

MCZ 61454, 7.4 mm TL

MCZ 41675, 13.6 mm TL

MCZ 87065, 19 mm TL

MCZ 41503, 55 mm TL

MCZ 154682, length unknown, dry skeletal

USNM 102086, length unknown, jaws only

SU 16438, 306 mm SL, c&s

SU 16441, 310 mm SL, c&s

VIMS 35803, 1180 mm TL

VIMS 40046, 400 mm TL, jaws only

VIMS 40047, 390 mm TL, jaws only

VIMS 40710, 22 mm TL

Ranzania laevis

ANSP 103501, 492 mm TL

CAS 99414, 3 of 4 specimens examined, 125 mm TL, 128 mm TL, 135 mm TL

OS 1432, n = 4, 90 mm TL, 89 mm TL, est. 88 mm TL, 89 mm TL

USNM 385363, 2 of 500+ specimens examined, 6 mm TL, 11 mm TL

VIMS 40705, n = 2, 80 mm TL, 85 mm TL

VIMS 40706, 99 mm TL, CT scanned

VIMS 40707

VIMS 40708, 83 mm TL

Acknowledgments

We are especially grateful to John Galbraith, Heath Cook, and Jakub Kircun, Northeast Fisheries Science Center, and Phoebe Woodworth-Jefcoats, Pacific Island Fisheries Science Center, who collected fresh material that we studied and accessioned in the Nunnally Ichthyology Collection, Virginia Institute of Marine Science. We thank Sarah Huber, Nunnally Ichthyology Collection; Karsten Hartel, Andrew Williston, Harvard Museum of Comparative Zoology; Robert Robins, Larry Page, David Boyd, Florida Museum of Natural History; Mariangeles Arce-H., Mark Sabaj, Academy of Natural Sciences, David Catania, California Academy of Science; Charles Dardia, Casey Dillman, Cornell University Museum of Vertebrates; Kris Murphy, Diane Pitassy, Sandra Raredon, Dave Johnson, Ai Nonaka, Smithsonian Institution; and Mark McGrouther, Amanda Hay, Australian Museum, who provided loans of specimens in their care to us for study. Krill Carson, New England Coastal Wildlife Alliance, hosted KEB for a visit, and shared her knowledge as well as materials of *Mola mola*. Jan Factor took photographs used in Figure 15A and B. Keichii Matsuura, National Museum of Nature and Science, provided SEM images used in Figure 16. Masanori Nakae, National Museum of Nature and Science, and Ichthyological Society of Japan provided permission to use the photograph in Figure 18. Kim Smith, Department of Primary Industries and Regional Development, Western Australia, provided useful comments and photographs about the mouth and gonads of fresh specimens of *Ranzania laevis*. Teresa Porri, Cornell University Multiscale Imaging Facility CT scanned specimens used in this study and helped us to visualize molid anatomy. O. Damaj, R. Pasiak, and M. Slade, Cornell Veterinary College Diagnostic Laboratory prepared histological materials. VIMS Hargis

Library, William & Mary Library, and Biodiversity Heritage Library provided many references. B. McGuire, B. Collette, and M. Vecchione provided comments on the manuscript. Support for this project was provided by a National Science Foundation GRFP, John E. Olney Sr. Ichthyology Award, Virginia Institute of Marine Science Office of Academic Studies, Clyde D. & Lois W. Marlatt, Jr. Fellowship, and the Tontogany Creek Fund. Support for CT scanners used provided by NIH S10OD012287 for the ZEISS/Xradia Versa 520 X-ray Microscope and from NIH S10OD025049 for the SkyScan 1276. We thank Tierney Thys, Jonathan Houghton, and Graeme Hays for inviting us to contribute this chapter, which is contribution No. 3853 of the Virginia Institute of Marine Science, William & Mary.

Literature Cited

Adeney, R.J. and G.M. Hughes. 1977. Some observations on gills of oceanic sunfish, *Mola mola*. J. Mar. Biol. Assoc. U.K. 57: 825–837.

Agassiz, A. 1857. *Orthragoriscus mola*, on grounds of internal anatomy, does not belong in the same family with *Diodon* and *Tetraodon*, but is the type of a distinct family. Untitled paper, Proc. Am. Acad. Arts Sci. 3: 319.

Alessandrini, A. 1839. De piscium apparatu respirationis tum speciatim Orthragorisci = *Orthragoriscus alexandrini* Ranzani. Nuovi Coram. Acad. Sci. Inst. Bonon. (Accad. Sci. Istit. Bologna) 3: 359–382.

Alfaro, M.E., F. Santini and C.D. Brock. 2007. Do reefs drive diversification in marine teleosts? Evidence from the pufferfish and their allies (order Tetraodontiformes). Evolution 61: 2104–2126.

Andreucci, R.D., H.A. Britski, and J. Carneiro. 1982. Structure and evolution of tetraodontoid teeth - An autoradiographic study (Pisces, Tetraodontiformes). J. Morph. 171: 283–292.

Arcila, D. and J.C. Tyler. 2017. Mass extinction in tetraodontiform fishes linked to the Palaeocene–Eocene thermal maximum. Proc. R. Soc. B. 284: 1-8.

Bakenhaster, M.D. and J.S. Knight-Gray. 2016. New diet data for *Mola mola* and *Masturus lanceolatus* (Tetraodontiformes: Molidae) off Florida's Atlantic coast with discussion of historical context. Bull. Mar. Sci. 92: 497–511.

Bass, A.L., H. Dewar, T. Thys, J.T. Streelman, and S.A. Karl. 2005. Evolutionary divergence among lineages of the ocean sunfish family, Molidae (Tetraodontiformes). Mar. Biol. 148: 405–414.

Beauregard, M. 1893. Contribution à l'étude de *Orthagoriscus truncatus* (Flem.). Bull. Soc. Sci. Nat. Ouest. Fr. 3: 229–246.

Bemis, K.E., J.C. Tyler, W.E. Bemis, K. Kumar, R.S. Rana, and T. Smith. 2017. A gymnodont fish jaw with remarkable molariform teeth from the early Eocene of Gujarat, India (Teleostei, Tetraodontiformes). Journal of Vertebrate Paleontology 37(6): 10 pages.

Berkovitz, B. and P. Shellis, P. 2017. The teeth of non-mammalian vertebrates. Amsterdam, the Netherlands: Elsevier.

Betancur-R, R., E.O. Wiley, G. Arratia, A. Acero, N. Bailly, M. Miya, G. Lecointre and G. Orti. 2017. Phylogenetic classification of bony fishes. BMC Evolutionary Biology. 17: 1–40.

Binney, A. 1842. Observations made during two successive summers at Nahant, on the habits of the *Orthogariscus mola* or short sunfish. Proc. Boston Soc. Nat. Hist. 1: 93.

Boulenger, G.A. 1904. Teleostei. pp 539–727. *In*: S.F Harmer and A. E. Shipley [eds]. The Cambridge natural history, vol. VII. Hemichordata, Ascidians and Amphioxus, Fishes. London: Macmillan.

Breder, C.M. and E. Clark. 1947. A contribution to the visceral anatomy, development and relationships of the Plectognathi. Bull. Amer. Mus. Nat. Hist. 88: 287–319.

Brimley, H.H. 1939. The ocean sun-fishes on the North Carolina coast: The Pointed-Tailed *Masturus lanceolatus* and the Round-Tailed *Mola mola.* J. Elisha Mitchell Soc. 55: 295–303.

Britz, R. and G.D. Johnson. 2005a. Occipito-vertebral fusion in ocean sunfishes (Teleostei: Tetraodontiformes: Molidae) and its phylogenetic implications. J. Morph. 266: 74–79.

Britz, R. and G.D. Johnson. 2005b. Leis' conundrum: Homology of the clavus of the ocean sunfishes. 1. Ontogeny of the median fins and axial skeleton of *Monotrete leiurus* (Teleostei, Tetraodontiformes, Tetraodontidae). J. Morph. 266: 1–10.

Britz, R. and G.D. Johnson. 2012. The caudal skeleton of a 20 mm *Triodon* and homology of its components. Proc. Biol. Soc. Wash. 125: 66–73.

Burr, H.S. 1928. The central nervous system of *Orthagoriscus mola*. J. Comp. Neuro. 45: 33–128.

Carlucci, R., D. Mentino, D. Semeraro, P. Ricci, L. Sion and G. Scillitani. 2019. Comparative histochemical analysis of intestinal glycoconjugates in the blunthead pufferfish *Sphoeroides pachygaster* and grey triggerfish *Balistes capriscus* (Teleostei: Tetraodontiformes). J. Fish Biol. 94: 122–131.

Carnevale, G. and F. Santini. 2007. Record of the slender mola, genus *Ranzania* (Teleostei, Tetraodontiformes), in the Miocene of the Chelif Basin, Algeria. Systematic Paleontology. 6(2007): 321–326.

Carnevale, G., L. Pellegrino and J.C. Tyler. Evolution and fossil record of the ocean sunfishes. This volume.

Carlström, D. 1963. A crystallographic study of vertebrate otoliths. Biol. Bull. Marine Biological Laboratory, Woods Hole, Mass. 125: 441–463.

Chanet, B. and F.J. Meunier. 2014. The anatomy of the thyroid gland among "fishes": Phylogenetic implications for the Vertebrata. Cybium. 38: 89–116.

Chanet, B., C. Guintard and G. Lecointre. 2014. The gas bladder of puffers and porcupinefishes (Acanthomorpha: Tetraodontiformes): Phylogenetic interpretations. J. Morph. 275: 894–901.

Chanet, B., C. Guintard, E. Betti, C. Gallut, A. Dettai and G. Lecointre. 2013. Evidence for a close phylogenetic relationship between the teleost orders Tetraodontiformes and Lophiiformes based on an analysis of soft anatomy. Cybium. 37: 179–198.

Chanet, B., C. Guintard, T. Boisgard, M. Fusellier, C. Tavernier, E. Betti, S. Madec, Y. Richaudeau, C. Raphael, A. Dettai and G. Lecointre. 2012. Visceral anatomy of Ocean Sunfish (*Mola mola* (L., 1758), Molidae, Tetraodontiformes) and Angler (*Lophius piscatorius* (L., 1758), Lophiidae, Lophiiformes) investigated by non-invasive imaging techniques. Comptes Rendus Biologies 335: 744–752.

Cleland, J. 1862. On the anatomy of the Short Sunfish (*Orthagoriscus mola*). Nat. Hist. Rev. 170–185.

Cuvier, G. 1805. Leçons d'anatomie comparée, tome III. La première partie des organes de la digestion, Baudouin, Paris. ~~558 p.~~

Cuvier, G. 1805. Leçons d'anatomie comparée. 5 vol. Paris. [Vol I, 518 p.; Vol. II, 697 p.; Vol. III, 558 p.; Vol. IV, 539 p.; Vol. V, 368 p.]

Davenport, J., N.D. Phillips, E. Cotter, L.E. Eagling and J.D.R. Houghton. 2018. The locomotor system of the Ocean Sunfish *Mola mola* (L.): Role of gelatinous exoskeleton, horizontal septum, muscles and tendons. J. Anat. 233: 347–357.

Dewar, H., T. Thys, S.L.H. Teo, C. Farwell, J. O'Sullivan, T. Tobayama, M. Soichi, T. Nakatsubo, Y. Kondo, Y. Okada, D.J. Lindsay, G.C. Hays, A. Walli, K. Weng, J.T. Streelman and S.A. Karl. 2010. Satellite tracking the world's largest jelly

predator, the Ocean Sunfish, *Mola mola*, in the Western Pacific. J. Exp. Mar. Biol. Ecol. 393: 32–42.

Ebenezer I.P. and J.J. Joel. 1984. On a large Sunfish *Ranzania typus* from the southwest coast. Indian J. Fisheries. 31: 360–361.

Fitch, J.E. 1969. A second record of the Slender Sunfish *Ranzania laevis* (Pennant), from California. Bull. Southern Californian Academy of Sciences. 68: 115–118.

Fraser-Brunner, A. 1943. Notes on the plectognath fishes. VIII. The classification of the suborder Tetraodontoidea, with a synopsis of the genera. Ann. Mag. Nat. Hist. Ser. 11. 10: 1–18.

Fraser-Brunner, A. 1951. The ocean sunfishes (family Molidae). Bull. Br. Mus. (Nat. Hist.) Zool. 1: 89–121.

Fricke, R., W.N. Eschmeyer and R. Van der Laan (eds.). 2019. Eschmeyer's Catalog of Fishes: Genera, species, references. (http://researcharchive.calacademy.org/research/ichthyology/catalog/fishcatmain.asp). Electronic version accessed 15 October 2019.

Fridberg, G. and H.A. Bern. 1968. The urophysis and the caudal neurosecretory system of fishes. Biol. Rev. 43: 175–199.

Gauldie, R.W. 1990. Vaterite otoliths from the Opah, *Lampris immaculatus* and two species of Sunfish, *Mola mola* and *M. ramsayi*. Acta Zoologica (Stockholm). 71: 193-199.

Gesner, K. 1558. Historiae animalium, Liber IV. Qui est de piscium and aquatilium animantium natura. Tigurum (Zurich).

Gill, T.N. 1884. Synopsis of the plectognath fishes. Proc. U.S. Nat. Mus. v. 7 (nos 26-27) (art. 448): 411–427.

Gill, T.N. 1897. The distinctive characters of the Molinae and Ranzaniinae. Science. 156: 966–967.

Goodsir, J. 1841. On certain peculiarities in the structure of the Short Sun-fish (*Orthagoriscus mola*). Edinburgh New Philos. J. 30:188–194.

Goette, A. 1879. Beiträge zur vergleichenden Morphologie des Skeletsystems der Wirbelthiere. II. Die Wirbelsaule und ihre Anhänge. 5. Die Teleostier. Arch. Mikrosk. Anat. (Bonn) 16:117–142.

Grande, L. and W.E. Bemis. 1998. A comprehensive phylogenetic study of amiid fishes (Amiidae) based on comparative skeletal anatomy. An empirical search for interconnected patterns of natural history. J. Vertebr. Paleontol. (Memoir 4, supplement) 18.

Gray, I.E. 1954. Comparative study of the gill area of marine fishes. Biol. Bull. Marine Biological Laboratory, Woods Hole, Mass. 107: 219-225.

Green, E.H. 1899. The chemical composition of the sub-dermal connective tissue of the Ocean Sunfish. Bull. U.S. Fish Comm. 19: 321–324.

Gregory, W.K. 1933. Fish skulls: A study of the evolution of natural mechanisms. Trans. Am. Philos. Soc. 23: 75–481.

Gregory, W.K. and H.C. Raven. 1934. Notes on the anatomy and relationships of the ocean sunfish (*Mola mola*). Copeia 1934 (4): 145–151.

Gudger, E.W. 1935. Some undescribed young of the Pointed-tailed Ocean Sunfish, *Masturus lanceolatus*. Copeia. 1935 (1): 35–38.

Gudger, E.W. 1937a. The natural history and geographical distribution of the Pointed-tailed Ocean Sunfish (*Masturus lanceolatus*), with notes on the shape of the tail. Proc. Zool. Soc. London, Ser. A, p. 363–396.

Gudger, E.W. 1937b. The structure and development of the pointed tail of the ocean sunfish, *Masturus lanceolatus*. Ann. Mag. Nat. Hist. Ser. 10, 19: 1–46.

Gudger, E.W. 1939. Three six-inch Pointed-tailed Ocean Sunfish, *Masturus lanceolatus*, the largest post-larva on record. J. Elisha Mitchell Sci. Soc. 55: 305–313.

Hamana, A.K., 1962. Über die Neurophysis spinalis caudalis bei Fischen. 3. Kyoto Pref. Med. Univ. 71: 478–490.

Harrod, C.J. Syväranta, L. Kubicek, V. Cappanera, and J.D.R. Houghton. 2013. Reply to Logan and Dodge: 'Stable isotopes challenge the perception of Ocean Sunfish *Mola mola* as obligate jellyfish predators.' J. Fish. Bio. 82: 10–16.

Harting, P. 1865. Notices zoologiques, anatomiques et histiologiques, sur 1'*Orthragoriscus Ozodura*; suivies de considérations sur l'ostéogénèse des téléostiens en général. Verb. K. Akad. Wet. (Amsterdam) ll (2): 1–48.

Hays, G.C., T.K. Doyle and J.D.R. Houghton. 2018. A paradigm shift in the trophic importance of jellyfish? Trends Ecol. Evol. 33: 874–884.

Hilgendorf, F.M. 1893. Ueber die Bezahnung der Gattung *Mola* (*Orthagoriscus*). Sitzungsber. Gesamten Naturforscher. Freunde Berl. 1893: 3–4.

Hilton, E.J. 2002. Osteology of the extant North American fishes of the genus *Hiodon* Lesueur, 1818 (Teleostei: Osteoglossomorpha: Hiodontiformes). Fieldiana (Zoology) new series 100: 1–142.

Hilton, E.J. 2011. Bony Fish Skeleton. pp. 434–448. *In*: A.P. Farrell [ed.]. Encyclopedia of Fish Physiology: From Genome to Environment, volume 1. Academic Press, San Diego, CA, USA.

Houghton, D.R., N. Liebsch, T.K. Doyle, A.C. Gleiss, M.K.S. Lilley, R.P. Wilson, and G.C. Hays. 2009. Harnessing the sun: Testing a novel attachment method to record fine scale movements in Ocean Sunfish (*Mola mola*). Tagging and Tracking of Marine Animals with Electronic Devices, Reviews: Methods and Technologies in Fish Biology and Fisheries 9, DOI 10.1007/978-1-4020-9640-2 14.

Hughes, G.M. 1984. General anatomy of the gills. *Fish Physiology* 10: 1–72.

Hughes, G.M. and M. Morgan. 1973. The structure of fish gills in relation to their respiratory function. Biol. Revs. 48: 419–475.

Jinxiang, S. and L. Wanduan. 1982. A study of patterns of the olfactory organ of tetraodontiform fishes in China. Acta Zoologica Sinica 28: 389–98.

Johnson, G.D. and R. Britz. 2005. Leis' conundrum: Homology of the clavus of the ocean sunfishes. 2. Ontogeny of the median fins and axial skeleton of *Ranzania laevis* (Teleostei, Tetraodontiformes, Molidae). J. Morph. 266: 11–21.

Kappers, C.U., G.C. Huber and E.C. Crosby. 1936. *The Comparative Anatomy of the Nervous System of Vertebrates, Including Man*, Vol. 1. Hafner, New York.

Kaschkaroff, D.N. 1914a. Materialien zur vergleichenden Morphologic der Fische. Vergleichendes Studium der Organisation von Plecjognathi. Bull. Soc. Imp. Nat. (Moscow), New Ser., 27: 263–370.

Kaschkaroff, D.N. 1914b. Zur Kenntnis des feineren Baues und der Entwickelung des Knochens bei Teleostiem. I. Die Knochenentwickelung bei *Orthagoriscus mola*. Anat. Anz. 47: 113–138.

Katayama, E. and K. Matsuura. 2016. Fine structures of scales of ocean sunfishes (Actinopterygii, Tetraodontiformes, Molidae): Another morphological character supporting phylogenetic relationships of the molid genera. Bull. Natl. Mus. Nat. Sci., Ser. A, 42: 95–98.

Kaschkaroff, D.N. 1916. La structure et le developpement de I'os d' *Orthagoriscus mola*. Zool. Zh. (Rev. Zool. Russe, Moscow) 1:136–138.

Kino, M., T. Miayzaki, T. Iwami and J. Kohbara. 2009. Retinal topography of ganglion cells in immature Ocean Sunfish, *Mola mola*. Environmental Biology of Fishes 85: 33–38.

Koelreuter, I.T. 1766. Piscium rariorum e museo Petropolitano exceptorum descriptiones continuatae. Novi Commentarii Academiae Scientiarum Imperialis Petropolitanae v. 10 (for 1764): 329–351, Pl. 8.

Kölliker, R.A. 1859. On the different types in the microscopic structure of the skeleton of osseous fishes. Ann. Mag. Nat. Hist., Ser. 3, 4: 67–77.

Kölliker, R.A. 1860. Ueber die Knochen von Orthagoriscus. Sitzungber. Phys.-Med. Ges. (Wtirtzburg), 1859: 38.

Konstantinidis, P. and G.D. Johnson. 2012. Ontogeny of the jaw apparatus and suspensorium of the Tetraodontiformes. Acta Zool. 93: 351–366.

Lacepedè, B.G. 1836. Histoire naturelle des poissons, tome 2, Duménil, Paris, 1836.

Leis, J.M. 1977. Development of eggs and larvae of Slender Mola, *Ranzania laevis* (Pisces, Molidae). Bull. Mar. Sci. 27: 448–466.

Leis J.M. 1984. Tetraodontiformes: Relationships. pp. 459–463. *In*: H.G. Moser, W.J. Richards, D.M. Cohen, M.P. Fahay, A.W. Kendall, and S.L. Richardson [eds]. *Ontogeny and Systematics of Fishes*. Allen Press, Lawrence, KS, USA.

Leydig, F. 1857. Lehrbuch der Histologie des Menschen und der Thiere. Frankfurt.

Liénard, E. 1840. Description d'une nouvelle espèce du genre mole (*Orthagoriscus*, Schn.) découverte à l'île Maurice. Revue Zoologique par la Société Cuvierienne (Paris) v. 3: 291–292.

Liem, K.F., W.E. Bemis, W.F. Walker, L. Grande. 2001. Functional anatomy of the vertebrates: an evolutionary perspective. Orlando, FL: Harcourt College Publishers.

Linnaeus, C. 1758. Systema naturae per regna tria naturae, secundum classes, ordinus, genera, species, cum characteribus, differentiis, synonymis, locis. Tomus I. Editio decima, reformata. Impensis Direct. Laurentii Salvii, Holmiae.

Logan, V.H. and P.H. Odense. 1974. Integument of ocean Sunfish (*Mola mola* L) (Plectognathi) with observations on lesions from 2 ectoparasites, *Capsala martinieri* (Trematoda) and *Philorthagoriscus serrates* (Copepoda). Can. J. Zool. 52(8):1039–1045.

Lyczkowski-Shultz, J. 2005. Molidae: Molas, ocean sunfishes. *In*: W.J Richards [ed]. Early Stages of Atlantic Fishes: An Identification Guide for the Western Central North Atlantic. CRC Press, Boca Raton, FL, USA.

Magalhães, M. dos. S., A.J. Barsante Santos, N.B. da Silva, and C.E.B. de Moura. 2012. Anatomy of the digestive tube of sea turtles (Reptilia: Testudines). Zoologia. 29: 70–76.

McCune, A.R. and R.L. Carlson. 2004. Twenty ways to lose your bladder: Common natural mutants in zebrafish and widespread convergence of swim bladder loss among teleost fishes. Evol. Dev. 6: 246–259.

Meek, A. 1904. Notes on the auditory organ and the orbit of *Orthagoriscus mola*. Anat. Anz. 25:217–219.

Milne-Edwards, H. 1858. Leçons sur la physiologie et l'anatomie compare de l'homme et des animaux. Tome 3. Paris.

Nakae, M. and K. Sasaki. 2004. Homologies of the adductor mandibulae muscles in Tetraodontiformes as indicated by nerve branching patterns. Ichthyol. Res. 51: 327–336.

Nakae, M. and K. Sasaki. 2006. Peripheral nervous system of the Ocean Sunfish *Mola mola* (Tetraodontiformes: Molidae). Ichthyol. Res. 53: 233–246.

Nakae, M. and K. Sasaki. 2007. Review of spino-occipital and spinal nerves in Tetraodontiformes, with special reference to pectoral and pelvic fin muscle innervation. Ichthyol. Res. 54: 333–349.

Nakae, M. and K. Sasaki. 2010. Lateral line system and its innervation in Tetraodontiformes with outgroup comparisons: Descriptions and phylogenetic implications. J. Morph. 271: 559–579.

Nakamura, I., Y. Goto and K. Sato 2015. Ocean Sunfish rewarm at the surface after deep excursions to forage for siphonophores. J. Ani. Ecol. 84: 590–603.

Nardo, G.D. 1840. Considerazioni sulla famiglia dei pesci *Mola*, e sui caratteri che li distinguono. Annali delle Scienze del Regno Lombardo-Veneto, Padova 10: 105–112.

Nolf, D. 1985. Otolithi Piscium. *In*: H. P. Schultze (ed.). Handbook of Paleoichthyloyy. 10. Fischer, Stuttgart and New York. 1–145.

Nolf, D. and J.C. Tyler. 2006. Otolith evidence concerning interrelationships of caproid, zeiform and tetraodontiform fishes. Bulletin de L'Institut Royal des Sciences Naturelles de Belgique, Biologie 76: 147–189.

Northcutt, R.G. and W.E. Bemis. 1993. Cranial nerves of the coelacanth, *Latimeria chalumnae* [Osteichthyes, Sarcopterygii, Actinistia] and comparisons with other Craniata. Brain Behav. Evol. Supplement to vol. 42: 1–76.

Nowikoff, M. 1910. Ueber den Bau des Knochens von *Orthagoriscus mola*. Anat. Anz. 37:97–106.

Nyegaard, M., E. Sawai, N. Gemmell, J. Gillum, N.R Loneragan, Y. Yamanoue and A.L. Stewart. 2018a. Hiding in broad daylight: molecular and morphological data reveal a new ocean sunfish species (Tetraodontiformes: Molidae) that has eluded recognition. Zool. J. Linnean Soc. 182: 631–658. [First published online on 19 July 2017].

Nyegaard, M. and E. Sawai. 2018b. Species identification of sunfish specimens (Genera *Mola* and *Masturus*, Family Molidae) from Australian and New Zealand natural history museum collections and other local sources. Data Brief. 19: 2404–2415.

Nyegaard, M., N. Loneragan and M.B. Santos. 2017. Squid predation by Slender Sunfish *Ranzania laevis* (Molidae). J. Fish Biol. 90(6):2480–2487.

Owen, R. 1839. Sur la structure microscopique et le developpement des dents des poissons Gymnodontes. Ann. Sci. Nat. Zool. Ser. 2, 12: 347–352.

Owen, R. 1840, 1845. Odontography; or, a treatise on the comparative anatomy of the teeth. 2 vols. London. [Vol 1 (1840), 655 p.; Vol 2 (1845), 37 p. + 1–150 plates.)

Owen, R. 1846. Lectures on the comparative anatomy and physiology of the vertebrate animals. Part I. Fishes. London.

Owen, R. 1853. Descriptive catalogue of the osteological series contained in the Museum of the Royal College of Surgeons of England. Vol. I: Pisces, Reptilia, Aves, Marsupialia. London.

Owen, R. 1866. On the anatomy of vertebrates. Vol. 1. Fishes and reptiles. Longmans, Green and Company, London.

Oxman, D.S., R. Barnett-Johnson, M.E. Smith, A. Coffin, D.L. Miller, R. Josephson, A.N. Popper. 2007. The effect of vaterite deposition on sound reception, otolith morphology, and inner ear sensory epithelia in hatchery-reared Chinook salmon (*Oncorhynchus tshawytscha*). Can. J. Fish. Aquat. Sci. 64:1469–1478.

Parker, G.H. 1900. Note on the blood vessels of the heart in the Sun-fish (*Orthagoriscus mola* Linn.). Anatomischer Anzeiger 17: 313–316.

Pellegrin, J. 1912. Sur la presence d'un banc de *Ranzania truncate* Retzius A la Martinique. Bull. Soc. Zool. Fr. 37:228–231.

Pennant, T. 1776. British Zoology. 4th Edition. London. Vol. 3: Class III. Reptiles. Class IV. Fish. Benjamin White, London. v. 3: 1–425, Pls/. 1–73. [Fishes, p. 41–46, 75–409, pls 8–73.]

Phillips, N.D., C. Harrod, A.R. Gates, T.M. Thys, and J.D.R. Houghton. 2015. Seeking the sun in deep, dark places: mesopelagic sightings of ocean sunfishes (Molidae). J. Fish. Bio. 87: 1118–1126.

Politis, P.J., J.K. Galbraith, P. Kostovick, and R.W. Brown. 2014. Northeast Fisheries Science Center bottom trawl survey protocols for the NOAA Ship Henry B. Bigelow. US Department of Commerce, Northeast Fish Sciences Center Reference Document 14-06; 138 p. Retrieved from http://nefsc.noaa.gov/publications/.

Pope, E.C., G.C. Hays, T.M Thys, T.K. Doyle, D.W. Sims, N. Queiroz, V.J. Hobson, L. Kubicek and J.D.R. Houghton. 2010. The biology and ecology of the Ocean Sunfish *Mola mola*: A review of current knowledge and future research perspectives. Rev. Fish. Biol. Fisher. 20: 471–487.

Pracheil, B.M., R. George and B.C. Chakoumakos. 2019. Significance of otolith calcium carbonate crystal structure diversity to microchemistry studies. Rev. Fish. Biol. Fisher. 29: 569–588.

Putnam, F.W. 1871. On the young of *Orthagoriscus mola*. Proc. Amer. Soc. Adv. Sci. for 1870, 19: 255–260.

Ranzani, C. 1839. Dispositio familiae Molarum in genera et in species. Novi Commentarii Academiae Scientiarum Instituti Bononiensis v. 3: 63–82, Pl. 6 + foldout table.

Raven, H.C. 1939a. Notes on the anatomy of *Ranzania truncata*. Amer. Mus. Novitates 1038: 1–7.

Raven, H.C. 1939b. On the anatomy and evolution of the locomotor apparatus of the Nipple-tailed Ocean Sunfish (*Masturus lanceolatus*). Bull. Amer. Mus. Nat. Hist. 76: 143–150.

Regan, C.T. 1903. On the classification of the fishes of the suborder Plectognathi; with notes and descriptions of new species from specimens in the British Museum collection. Proc. Zool. Soc. Lond. 1902: 284–303.

Reimer T., T. Dempster, F. Warren-Myers, A.J. Jensen, S.E. Swearer. 2016. High prevalence of vaterite in sagittal otoliths causes hearing impairment in farmed fish. Sci. Rep. 6: 25249.

Ridewood, W.G. 1899. On the relations of the efferent branchial blood vessels to the circulus cephalicus in teleostean fishes. Proc. Zool. Soc. London. 1899: 939-956, pl. LXIII–LXV.

Robinson, B.H. 1975. Observations on living juvenile specimens of the Slender Mola, *Ranzania laevis* (Pisces, Molidae). Pacific Sci. 29: 27-29.

Rondelet, G. 1554. Libri de piscibus marinis, in quibus verae piscium effigiens expressae sunt. Quae in tota piscium historia contineantur, indicat elenchus pagina nona et decima. Postremo accesserunt indices necessarii. Lugdunum (Lyon): Matthias Bonhomme.

Roon, J.M. van, and J.J. ter Pelkwijk. 1939. Mechanism of the jaw and body muscles of *Orthagoriscus mola* L. Zool. Meded. (Leiden) 22: 66–75.

Rosén, N. 1912. Studies on the plectognaths. 1. The blood-vascular system. Ark. Zool. 7: l–24.

Rosén, N. 1913a. Studies on the plectognaths. 2. The air-sac, with notes on other parts of the intestines. Ark. Zool. 7: l–23.

Rosén, N. 1913b. Studies on the plectognaths. 3. The integument. Ark. Zool. 8: l–29.

Rosén, N. 1913c. Studies on the plectognaths. 4. The body-muscles. Ark. Zool. 8: 1–14.

Rosén, N. 1916a. Studies on the plectognaths. 5. The skeleton. Ark. Zool. 10: l–28.

Rosén, N. 1916b. Ueber die Homologie der Fischschuppen. Ark. Zool. 10: 1–36.

Ryder, J.A. 1886. On the origin of heterocercy and the evolution of the fins and fin-rays of fishes. Rep. U.S. Fish Comm. 1884: 981–1085.

Sabaj, M.H. 2019. Standard symbolic codes for institutional resource collections in herpetology and ichthyology: An Online Reference. Version 7.1 (21 March 2019). Electronically accessible at http://www.asih.org, American Society of Ichthyologists and Herpetologists, Washington, DC.

Santini, F. and J.C. Tyler. 2002. Phylogeny of the ocean sunfishes (Molidae, Tetraodontiformes), a highly derived group of teleost fishes. Ital. J. Zool. 69: 37–43.

Santini, F. and J.C. Tyler. 2003. A phylogeny of the families of fossil and extant tetraodontiform fishes (Acanthomorpha, Tetraodontiformes), Upper Cretaceous to recent. Zool. J. Linnean Soc. 139: 565–617.

Sawai, E., Y. Yamanoue, M. Nyegaard and Y. Sakai. 2018. Redescription of the Bump-head Sunfish *Mola alexandrini* (Ranzani 1839), senior synonym of *Mola ramsayi* (Giglioli 1883), with designation of a neotype for *Mola mola* (Linnaeus 1758) (Tetraodontiformes: Molidae). Ichthyol. Res. 65: 142–160

Schmidt, J. 1921a. Contributions to the knowledge of the young of the sunfishes (*Mola* and *Ranzania*). Meddel. Komm. Havunders. Ser. Fiskeri, 6: 1–16.

Schmidt, J. 1921b. New studies of sunfishes made during the "Dana" Expedition, 1920. Nature 107: 76–79.

Smith, K.A., M. Hammon and P.G. Close. 2010. Aggregation and stranding of Elongate Sunfish (*Ranzania laevis*) (Pisces: Molidae) (Pennant, 1776) on the southern coast of Western Australia. J. Royal Soc. Western Australia 93: 181–188.

Sousa, L.L., R. Xavier, V. Costa, N.E. Humphries, C. Trueman, R. Rose, D.W. Sims, and N. Quieroz. 2016. DNA barcoding identifies a cosmopolitan diet in the ocean sunfish. Sci. Rep. 6: 1–9.

Steenstrup, J. and C. Lütken. 1863. Oversigt over det kgl. danske Vidensk Selsk Forhandl. Copenhagen.

Steenstrup. J. and C. Lütken. 1898. Spolia Atlantica. Bidrag til kundskab om klump-eller maanefiskene (Molidae). Dan. Vidensk. Selsk. Skr. 6te Raek. Naturvidensk. Math. Afd. Copenhagen. 9: 1–102.

Stephan, P. 1900. Recherches histologiques sur la structure du tissus osseux des poissons. Bull. Biol. Sci. Fr. Belg. Paris. Ser. 5, 2: 281–429.

Studnicka, F.K. 1916. Ueber den knochen von Orthagoriscus. Anat. Anz. 49: 151–169, 177–194.

Supino, F. 1904. Contributo allo studio del tessuto osseo dell'*Orthagoriscus*. Atti R. Accad. Lincei, Rend., CI. Sci. Fis., Mat. Nat., Ser. 5, 13: 118-121.

Suyehiro, Y. 1942. A study on the digestive system and feeding habits of fish. Jap. J. Zool. 10: 1–303.

Syväranta, J., C. Harrod, L. Kubicek, V. Caooanera, and J.D. Houghton. 2012. Stable isotopes challenge the perception of Ocean Sunfish *Mola mola* as obligtate jellyfish predators. J. Fish. Bio. 80: 225–231.

Thiery, A.P., T. Shono, D. Kurokawa, R. Britz, Z. Johanson, and G. Fraser. 2017. Spatially restricted dental regeneration drives pufferfish beak development. PNAS 114: E4425-E4434.

Thompson, D'A.W. 1888. On the auditory labyrinth of *Orthagoriscus mola* L. Anat. Anz. 3: 93–96.

Thys, T.M., J. P. Ryan, H. Dewar, C.R. Perle, K. Lyons, J. O'Sullivan, et al. 2015. Ecology of the Ocean Sunfish, *Mola mola*, in the southern California current system. J. Exp. Mar. Biol. Ecol. 471: 64–76.

Thys, T.M., A.R. Hearn, K.C. Weng, J.P. Ryan, and C. Peñaherrera-Palma. 2017. Satellite Tracking and Site Fidelity of Short Ocean Sunfish, *Mola ramsayi*, in the Galapagos Islands. J. Mar. Bio. 2017: 1–10.

Trois, E.F. 1884-1884. Ricerche sulla struttura della *Ranzania truncata*. Parts I, II. Atti del R. Istituto Veneto, Tom. II, (6), Part I, pp. 1269–1306; Part II, pp. 1543–1559.

Tyler, J.C. 1962. The pelvis and pelvic fin of plectognath fishes; a study in reduction. Proc. Acad. Nat. Sci. Phila. 114: 207-250.

Tyler, J.C. 1970. The progressive reduction in number of elements supporting the caudal fin of fishes of the order Plectognathi. Proc. Acad. Nat. Sci. Philadelphia. 122: 1–85.

Tyler, J.C. 1980. Osteology, phylogeny, and higher classification of the fishes of the order Plectognathi (Tetraodontiformes). NOAA Technical Report NMFS Circular 434: 1–422.

Tyler, J.C. and A.F. Bannikov. 1992. New genus of primitive ocean sunfish with separate premaxillae from the Eocene of southwest Russia (Molidae, Tetraodontiformes). Copeia, 1992: 1014–1023.

Uehara, M. and T. Ueshima. 1986. Morphological studies of the spinal cord in Tetraodontiformes fishes, J. Morph. 190: 325–333.

Uehara, M., Y.Z. Hosaka, H. Doi, and H. Sakai. 2015. The shortened spinal cord in tetraodontiform fishes. J. Morph. 276: 290–300.

Vignal, W. 1881. Note sur l'anatomie des centres nerveux du mole, *Orthagoriscus mola*. Arch. Zool. Exp. Gen. 9: 369–386.

Watanabe, Y. and K. Sato. 2008. Functional dorsoventral symmetry in relation to lift-based swimming in the Ocean Sunfish *Mola mola*. Plos One 3(10): e3446.

Webb, P.W. 1994. The Biology of Fish Swimming. pp. 45–62. *In*: The Mechanics and Physiology of Animal Swimming. L., Maddock, Q. Bone and J.M.V Rayner [eds]. Cambridge University Press, Cambridge.

Weems, R.E. 1985. Miocene and Pliocene Molidae (*Ranzania, Mola*) from Maryland, Virginia, and North Carolina (Pisces, Tetraodontiformes). Proc. Biol. Soc. of Wash. 98: 422–438.

Whitear, M. 1986. Dermis. Chapter 3. pp. 39–64. *In:* Biology of the Integument, Volume 2. J. Berieter-Hahn, A.G. Matolsty, and K.S. Richards [eds.] Springer Verlag, Berlin.

Winterbottom, R. 1974. The familial phylogeny of the Tetraodontiformes (Acanthopterygii: Pisces) as evidenced by their comparative myology. Smithson. Contrib. Zool. 155: 1–201.

Wilson, J.M. and L.F.C. Castro. 2011. Morphological diversity of the gastrointestinal tract in fishes. pp. 1–55. *In:* M. Grosell, A.P. Farrell, C.J. Brauner [eds.]. Fish Physiology 30: The multifunctional gut of fish. Elsevier Inc., London.

Yamanoue, Y., M. Miya, K. Matsuura, M. Katoh, H. Sakai and M. Nishida. 2004. Mitochondrial genomes and phylogeny of the ocean sunfishes (Tetraodontiformes: Molidae). Ichthyol. Res. 51(3):269–273.

Yamanoue, Y., M. Miya, K. Matsuura, M. Katoh, H. Sakai and M. Nishida. 2008. A new perspective on phylogeny and evolution of tetraodontiform fishes (Pisces: Acanthopterygii) based on whole mitochondrial genome sequences: Basal ecological diversification? BMC Evolutionary Biology 8.

Yoshita, Y., Y. Yamanoue, K. Sagara, M. Nishibori, H. Kuniyoshi, T. Umino, Y. Sakai, H. Hashimoto and K. Gushima. 2009. Phylogenetic relationship of two *Mola* sunfishes (Tetraodontiformes: Molidae) occurring around the coast of Japan, with notes on their geographical distribution and morphological characteristics. Ichthyol. Res. 56: 232–244.

Figure Captions

Figure 1. Phylogeny of the five extant species of Molidae recognized by Sawai, Nyegaard, and Yamanoue, this volume. The three species of *Mola* form a clade with *Masturus lanceolatus*; this clade is sister to *Ranzania laevis*.

Figure 2. External anatomy of adult specimens. **A.** *Ranzania laevis,* ANSP 103501, 492 mm TL. **B.** *Masturus lanceolatus*, VIMS 8120, 1175 mm TL. **C.** *Mola mola*, VIMS 35803, 1180 mm TL.

Figure 3. Adult molid specimens showing mouth, lips, and minute nares. **A, B.** *Ranzania laevis* ANSP 103501, 492 mm TL. The inflexible lips form a tube that extends beyond the beak. **C, D.** *Masturus lanceolatus*, VIMS 8120, 1175 mm TL. The lips form a horizontal, inflexible opening. **E, F.** *Mola mola*, VIMS 35803, 1180 mm TL. Lips are more flexible than in either *R. laevis* or *M. lanceolatus* and follow the contour of the beak.

Figure 4. External anatomy of larval molid specimens. **A.** *Ranzania laevis* VIMS 32389, 2.3 mm TL, **B.** *Ranzania laevis* USNM 385363, 6.1 mm TL, **C.** *Ranzania laevis* USNM 385363, 12.4 mm TL. **D.** *Masturus lanceolatus*, UF 234607, 9.3 mm TL (not including claval extension). **E**. *Masturus lanceolatus*, UF 234607, 13.9 mm TL (not including claval extension). **F.** *Masturus lanceolatus*, AMS I-43072-003, 23.0 mm TL (not including claval extension; 32 mm TL with claval extension).

G. *Mola mola*, MCZ 61454, 7.4 mm TL. **H.** *Mola mola*, MCZ 41675, 13.6 mm TL. **I.** *Mola mola*, VIMS 40710, 22.0 mm TL.

Figure 5. Micro-CT scans of larval *Mola mola* to show larval scales. **A-D.** MCZ 61454 *Mola mola*, 7.4 mm TL. **A.** Lateral, anterior left. **B.** Anterior. **C.** Dorsal, anterior left. **D.** Ventral, anterior left. **E-H**. MCZ 41675 *Mola mola*, 13.6 mm. **E.** Lateral, anterior left. **F.** Anterior. **G.** Dorsal, anterior left. **H.** Ventral, anterior left.

Figure 6. External anatomy of juvenile molid specimens. **A.** *Ranzania laevis,* CAS 99414, 130 mm TL. **B.** *Masturus lanceolatus*, UF 136518, 164 mm TL (length includes claval extension). **C.** *Mola* sp., AUS I.27082-001, 74 mm TL.

Figure 7. Skeleton of *Ranzania laevis*, ANSP 109435, 65.1 mm SL, anterior to left. Redrawn based on Tyler (1980: figs. 316, 320, and 321). **A.** Left lateral view. **B.** Gill arch. **C.** Branchiostegals in relation to hyoid arch. Abbreviations: afr, anal fin rays; ang-ar, anguloarticular; bb, basibranchial; bh, basihyal; boc, basioccipital; br, branchiostegal; bsp, basisphenoid; cha, anterior ceratohyal; cb, ceratobranchial; chp, posterior certatohyal; cl, cleithrum; clo, claval ossicles; co, coracoid; cfr, caudal fin rays; d, dentary; dfr, dorsal fin rays; eb, epibranchial; ecp, ectopterygoid; enp, endopterygoid; epo, epioccipital; exo, ecoccipital; fr, frontal; gr, gill raker; h, hyomandibula; hb, hypobranchial; hhd, dorsal hypohyal; hhv, venrtral hypohyal; ih, interhyal; iop, interopercle; let, lateral ethmoid; met, mesethmoid; mpt, metapterygoid; mx, maxilla; op, opercle; pal, palatine; pas,

parasphenoid; pb, pharyngobranchial; pcl, postcleithrum; pmr, proximal-middle radials; pmx, premaxilla; pop, preopercle; pro, prootic; pt, posttemporal; pto, pterotic; pts, pterosphenoid; q, quadrate; rar, retroarticular; scl, supracleithrum; soc, supraoccipital; sop, subopercle; spo, sphenotic, sym, symplectic.

Figure 8. Skeleton of *Masturus lanceolatus*, USNM 117330, 127 mm SL, anterior to left. Redrawn based on Tyler (1980: figs. 315, 319, and 321). **A.** Left lateral view. **B.** Gill arch. **C.** Branchiostegals in relation to hyoid arch. Abbreviations: afr, anal fin rays; ang-ar, anguloarticular; bb, basibranchial; bh, basihyal; boc, basioccipital; br, branchiostegal; bsp, basisphenoid; cha, anterior ceratohyal; cb, ceratobranchial; chp, posterior certatohyal; cl, cleithrum; clo, claval ossicles; co, coracoid; cfr, caudal fin rays; d, dentary; dfr, dorsal fin rays; eb, epibranchial; ecp, ectopterygoid; enp, endopterygoid; epo, epioccipital; exo, ecoccipital; fr, frontal; gr, gill raker; h, hyomandibula; hb, hypobranchial; hhd, dorsal hypohyal; hhv, venrtral hypohyal; ih, interhyal; iop, interopercle; let, lateral ethmoid; met, mesethmoid; mpt, metapterygoid; mx, maxilla; op, opercle; pal, palatine; pas, parasphenoid; pb, pharyngobranchial; pcl, postcleithrum; pmr, proximal-middle radials; pmx, premaxilla; pop, preopercle; pro, prootic; pt, posttemporal; pto, pterotic; pts, pterosphenoid; q, quadrate; rar, retroarticular; scl, supracleithrum; soc, supraoccipital; sop, subopercle; spo, sphenotic, sym, symplectic.

Figure 9. Skeleton of *Mola mola*, composite based on two specimens, SU 16438, 306 mm SL and SU 16441, 310 mm SL, anterior to left. Redrawn based on Tyler

(1980: figs. 306, 307, 310, 311, and 312). **A.** Left lateral view. **B.** Gill arch **C.** Branchiostegals in relation to hyoid arch. Abbreviations: afr, anal fin rays; ang-ar, anguloarticular; bb, basibranchial; bh, basihyal; boc, basioccipital; br, branchiostegal; bsp, basisphenoid; cha, anterior ceratohyal; cb, ceratobranchial; chp, posterior certatohyal; cl, cleithrum; clo, claval ossicles; co, coracoid; cfr, caudal fin rays; d, dentary; dfr, dorsal fin rays; eb, epibranchial; ecp, ectopterygoid; enp, endopterygoid; epo, epioccipital; exo, ecoccipital; fr, frontal; gr, gill raker; h, hyomandibula; hb, hypobranchial; hhd, dorsal hypohyal; hhv, venrtral hypohyal; ih, interhyal; iop, interopercle; let, lateral ethmoid; met, mesethmoid; mpt, metapterygoid; mx, maxilla; op, opercle; pal, palatine; pas, parasphenoid; pb, pharyngobranchial; pcl, postcleithrum; pmr, proximal-middle radials; pmx, premaxilla; pop, preopercle; pro, prootic; pt, posttemporal; pto, pterotic; pts, pterosphenoid; q, quadrate; rar, retroarticular; scl, supracleithrum; soc, supraoccipital; sop, subopercle; spo, sphenotic, sym, symplectic.

Figure 10. Overview of jaws fused across the midline and beak in *Mola mola* based on micro-CT scans. Light colors indicate higher density, darker colors indicates lower density. **A.** Anterior view of beak and fused jaws of MCZ 41503, 55 mm TL. **B.** Posterior view of beak and fused jaws of MCZ 41503, 55 mm. **C.** Anterior view of dentary and beak of M. mola CUMV 98740, 1500 mm TL showing the relatively more dense tissue of the beak in comparison to the bone of the dentary. Note the paired foramina that mandibular ramus V (mdr V) passes through. **D.** Left lateral view of dentary of CUMV 98740, 1500 mm TL. **E.** Digital sagittal

section of dentary of CUMV 98740, 1500 mm TL showing a large pulp cavity beneath the beak.

Figure 11. Three views of *Mola mola* CAS 13244, 466 mm TL to demonstrate the relationship between mineralized dental tissues and surrounding soft tissues. Circles indicate triturating teeth. **A.** Photograph of alcohol preserved specimen. Note the large oral pads of soft tissue that occur between the triturating teeth. White dashed line indicates the plane of section for the histological view shown in part C. **B.** Micro-CT scan of the same specimen shown in Part A, showing mineralized tissues of the beak and triturating surface. Note that the most anterior triturating teeth are integrated with the beak, and that there are smaller triturating teeth toward the posterior of the jaw that are covered by tissues of the oral pad. **C.** Sagittal histological section stained with hematoxylin and eosin through the beak and triturating teeth of the same specimen shown in Parts A and B. The beak consists of columns of osteodentine; the osteodentine is flanked by bone. Four triturating teeth lie posterior to the beak; the triturating teeth are continuous with the beak and are also made of osteodentine. Between the triturating teeth are soft tissues that form the pads of the oral epithelium. There is no evidence of tooth germs entering on the labial side of the beak as in other tetraodontoids (see Thiery et al. 2017: fig. 5).

Figure 12. Micro-CT scans of fused dentaries of *Mola mola* to show changes in triturating surfaces across ontogeny. **A.** MCZ 61454, 7.4 mm TL, the beak is

present and the dentaries are fused across the midline but there are no triturating teeth. **B.** MCZ 41675, 13.6 mm TL, 4-5 rows of similarly sized paired triturating teeth are present posterior to the beak. **C.** MCZ 41503, 55 mm TL, three slightly staggered rows of triturating teeth are located posterior to the beak. **D.** ANSP 109090, estimated 400 mm TL, irregularly sized and shaped triturating teeth are in three to four rows posterior to the beak; the teeth are spread out along most of the jaw. **E.** CAS 13244, 466 mm TL, four rows of triturating teeth are located posterior to the beak; some of these teeth are incorporated into the beak. **F.** CUMV 98740, 1500 mm TL, the region posterior to the beak does not have distinct triturating teeth.

Figure 13. Long recurved pharyngeal teeth of *Mola mola,* VIMS 35803, 1180 mm TL. **A.** Lateral view of pharyngeal teeth, anterior to left. **B.** Ventral view of pharyngeal teeth, anterior to left. Abbreviations: pb2, pharyngobranchial 2; pb3, pharyngobranchial 3; pb4, pharyngobranchial 4.

Figure 14. Cranial dissection of a fresh specimen of *Mola mola*, VIMS 35803, 1180 mm TL. Anterior to right. Abbreviations: br, branchiostegal.

Figure 15. Epidermis, dermis, and hypodermis of *Mola mola* CUMV 98740, 1500 mm TL. **A.** Extensive, thick layer of white hypodermis. **B.** Thickness of the body wall shown in a fresh specimen. **C.** Hair-like processes of the scales support a mucus cuticle. **D.** Schematic interpretation of layers of the body wall.

Figure 16. SEM photographs of scales on right lateral side of the body in three genera of molids. **A.** *Ranzania laevis*, NSMT-P 92686, 220 mm TL. **B.** *Masturus lanceolatus*, NSMT-P 63168, 480 mm TL. **C.** *Mola mola*, NSMT-P 75065, 292 mm TL. SEM images reprinted with permission from Eri Katayama and Keiichi Matsuura (2016), "Fine Structures of Scales of Ocean Sunfishes (Actinopterygii, Tetraodontiformes, Molidae): Another Morphological Character Supporting Phylogenetic Relationships of the Molid Genera," Bull. Natl. Mus. Nat. Sci., Ser. A, 42(2), pp. 95–98.

Figure 17. Brain of *Mola mola.* **A.** Cranial cavity of *M. mola*, VIMS 35803, 1180 mm TL. Anterior to right. Note the thick layer of arachnoid tissue. **B.** Closer, oblique view of brain with covering tissues removed; same specimen as in A. The optic tecta form the largest brain region. **C.** Lateral view, anterior to right, of brain of a specimen identified as *M. mola*, redrawn from Burr (1928: fig. 1) to show roots of cranial nerves and brain regions. Length of specimen unknown. **D.** Dorsal view, anterior to right of brain of same specimen in C. **E.** Wax-plate reconstruction of brain and cranial nerves adapted from Burr (1928: 66, fig. 40). Some abbreviations updated from the orginal. AL, Anterior lateral line nerve; C, Cerebellar lobes; Ch, cerebral hemisphere; Ep, Epiphysis; Hyp, Hypophysis; L, Lateral line lobe; Olf, Olfactory bulb; OT, Optic tectum; OV, Optic ventricle; Pa, Paraphysis; Pro, Preoptic recess; Sp, Spinal nerve; Sp1, First spinal nerve; Sp2, Second spinal nerve; T, Tela choroidea. The numbered cranial nerves are as

follows: I, Olfactory nerve; II, Optic nerve; III, Oculomotor nerve; PL, Posterior lateral line nerve; IV, Trochlear nerve; V, Trigeminal nerve; Vm, Motor root of trigeminal nerve; Vprof, Profundal branch of trigeminal nerve; Vs, Sensory root of trigeminal nerve; IXs, Sensory root of glossopharyngeal nerve; IXm, Motor root of glossopharyngeal nerve; VI, Abducent nerve; VIIm, Motor root of facial nerve; VIIs, Motor root of facial nerve; VIII, Octaval nerve; XS, Sensory root of vagal nerve; XM, Motor root of vagal nerve.

Figure 18. Lateral line of *Mola mola* **A.** Anterior part of the trunk line in *Mola mola* showing two lateral line scales indicated by circles. **B.** Lateral line system of *Mola mola*. Photograph reprinted and lineart redrawn with permission from the Ichthyological Society of Japan and Masanori Nakae and Kunio Sasaki (2006) "Peripheral nervous system of the ocean sunfish *Mola mola* (Tetraodontiformes: Molidae)," Ichthyol. Res. 53(3):233-246.

Figure 19. Large semicircular ducts and small poorly consolidated sagittal otoliths of *Mola mola*, VIMS 35803, 1180 mm TL. **A.** Dorsal view. **B.** Lateral view. Abbreviations: AVSD, anterior vertical semicircular duct; HSD, horizontal semicircular duct; PVSD, posterior vertical semicircular duct.

Figure 20. Overview of viscera of adult molids specimens. Anterior to right. **A.** *Ranzania laevis* ANSP 103501, 492 mm TL. **B.** *Masturus lanceolatus*, VIMS 8120, 1175 mm TL. **C.** *Mola mola*, VIMS 35803, 1180 mm TL.

Figure 21. Details of viscera of *Mola mola*. Anterior to right. **A.** CUMV 98740, 1500 mm TL. **B.** VIMS 35803, 1180 mm TL.

Figure 22. Structure of the esophagus and "stomach" of *Masturus lanceolatus*, VIMS 8120, 1175 mm TL. **A.** View of the esophagus from the anterior showing six longitudinal folds. **B.** Junction of esophagus with "stomach" in *Masturus lanceolatus.*

Figure 23. Swim bladder of larval molids. **A, B.** *Masturus lanceolatus* MCZ 24875, 57 mm TL. **A.** Illustration from Gudger (1935: fig. 1) by H. Ziska. **B.** Dissection of swim bladder in specimen shown in part A. Anterior to left (image reflected). **C, D.** *Mola mola* MCZ 61454, 7 mm TL. The swim bladder is an outpocket from the esophagus and is located near the midline of the body (green), to the left of the intestine (yellow). **C.** Lateral view. **D.** Anterior view.

Figure 24. Heart of *Masturus lanceolatus* and afferent branchial arteries of *Mola mola*. **A.** Heart of *M. lanceolatus*, showing its position in the pericardial cavity. VIMS 8120, 1175 mm TL, anterior to right. **B.** Detail of the heart of *M. lanceolatus* to show walls of the atrium, leaflets of the atrio-ventricular valve (1-4), the thick walls of the ventricle, and the four leaflets of the ventriculo-bulbar valve (i-iv). VIMS 8120, 1175 mm TL, anterior to right. **C.** Ventral aorta and afferent branchial arteries (ABA) of *M. mola*. VIMS 35803, 1180 mm TL, anterior to left.

D. Ventral aorta and afferent branchial arteries (ABA) of *M. mola* with the ventral aorta reflected to show origin of ABA 4 anterior to the origin of ABA 3. VIMS 35803, 1180 mm TL, anterior to left

Figure 25. Schematic diagrams of coronary arteries, aortic arches, and formation of the dorsal aorta. Based on Milne-Edwards (1858), Parker (1900), Ridewood (1899), and Adeney and Hughes (1977). **A.** Ventral coronary artery and its origins from arches 1, 2, and 3. **B.** Origin of paired dorsal coronary arteries from efferent branchial artery (EBA) 4. **C.** Gill 1 circulation showing branching of afferent branchial artery (ABA) 1 to form upper and lower branches, each of which has a dorsal and ventral branch. Afferent filament arteries arise from the upper and lower branches, pass through secondary gill lamellae (not shown), and deliver oxygenated blood via efferent filament arteries to efferent branchial artery (EBA) 1. **D.** Circulus cephalicus showing the formation of dorsal aorta and coeliaco-mesenteric artery in *Ranzania laevis*. All efferent branchial arteries (EBA) contribute to the dorsal aorta but only efferent branchial arteries (EBA) 3 and 4 contribute to the coeliaco-mesenteric artery.

Figure 26. Dissection of the gill arches of *Mola mola*, VIMS 35803, 1180 mm TL. Stars indicate unidentified parasites on the gills. **A.** Dorsal view, anterior to left, showing the gills still partially enclosed in the gill sac. **B.** View from the dissected oral cavity into the pharynx showing position of gill rakers, internal gill openings, and pharyngeal teeth. **C.** Ventral view of left gills removed from their gill sac to

show position of internal gill opening, location of gill rakers, and position of the four gills with respect to each other. **D.** Lateral view of left gill 1 showing the ventral, middle, and dorsal regions in relation to the gill arch skeleton. **E.** Medial view of right gill 1 dissected from specimen to show position of ceratobranchial 1, location of afferent and efferent branchial arteries (ABA and EBA, respectively), and the locations of materials shown in more detail in Parts F and G. **F.** Dissected inner and outer hemibranchs showing position of ceratobranchial 1 and locations of major vessels. **G.** Transected portion of inner and outer hemibranchs to show general organization of gill tissues. The primary lamellae on opposite sides of the gill septum are staggered.

Figure 27. Dissection of kidney of *Mola mola*, VIMS 35803, 1180 mm TL. **A.** Lateral view, anterior to right; gill arches have been removed and head has been sagittally sectioned. The kidney extends forward to the occipital region of the neurocranium. Dashed line demarcates cranial-vertebral junction; note that the kidney extends anteriorly to this point. **B.** Lateral view, anterior to right. Large renal portal veins serving kidneys.

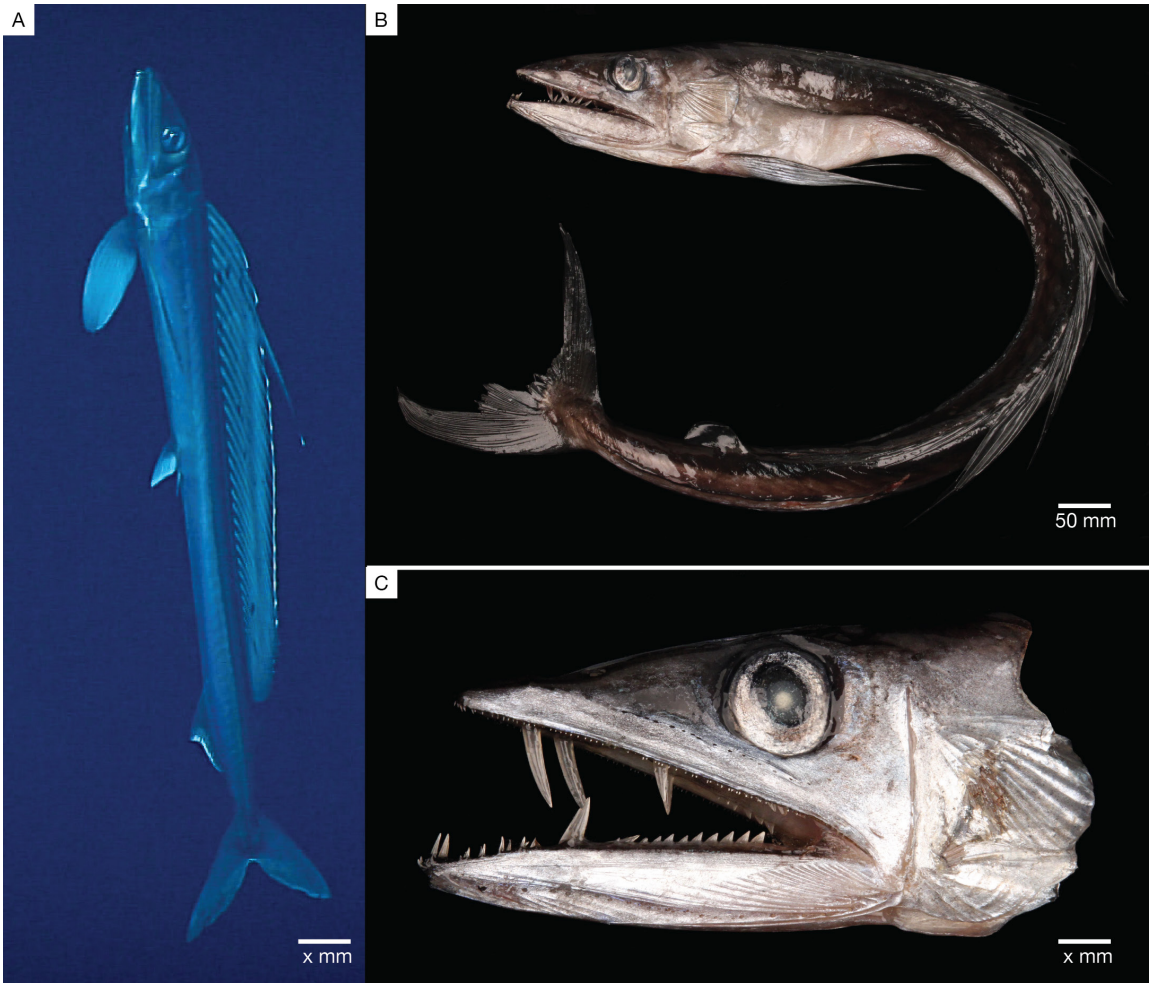

Chapter 1 Figure 1

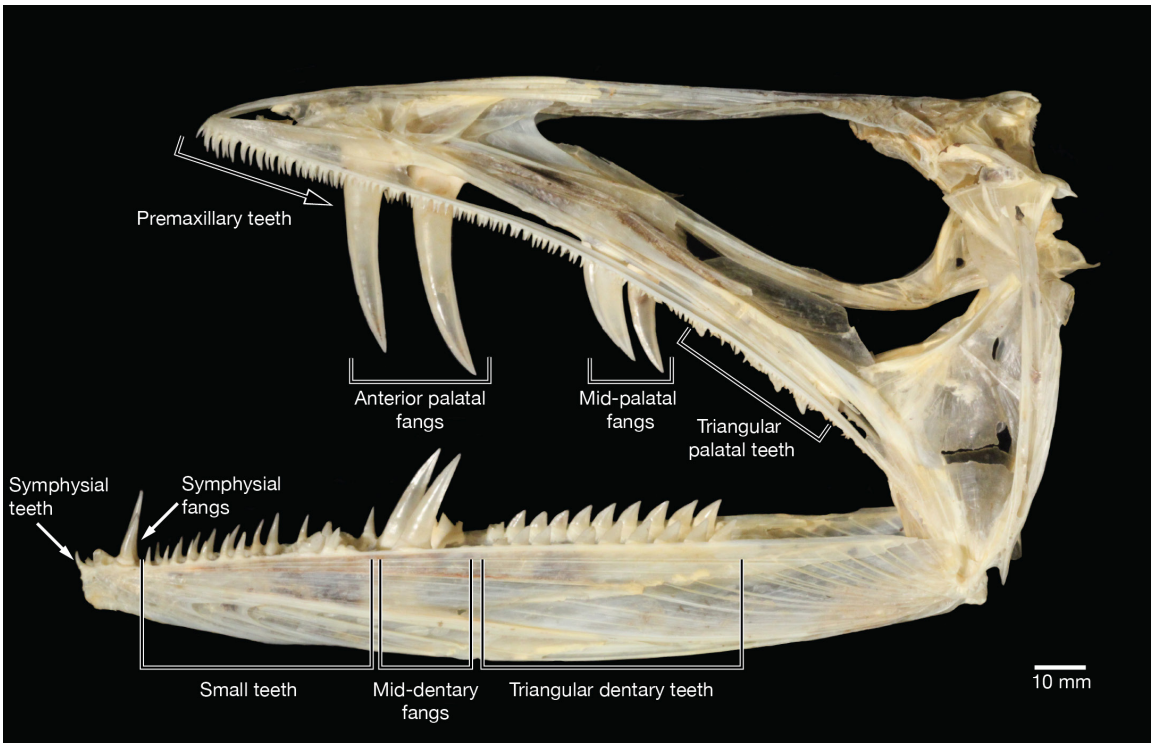

Chapter 1 Figure 2

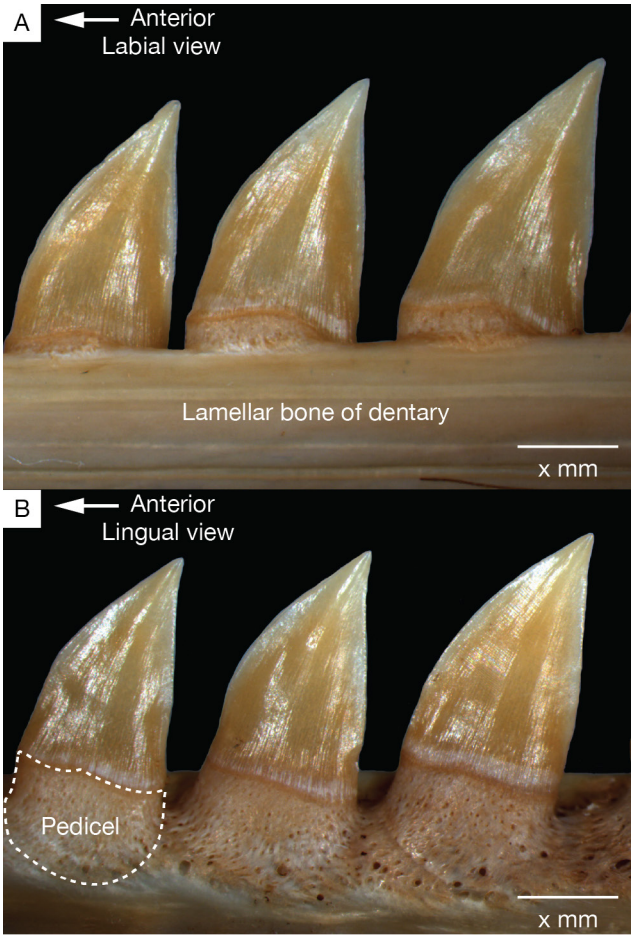

Chapter 1 Figure 3

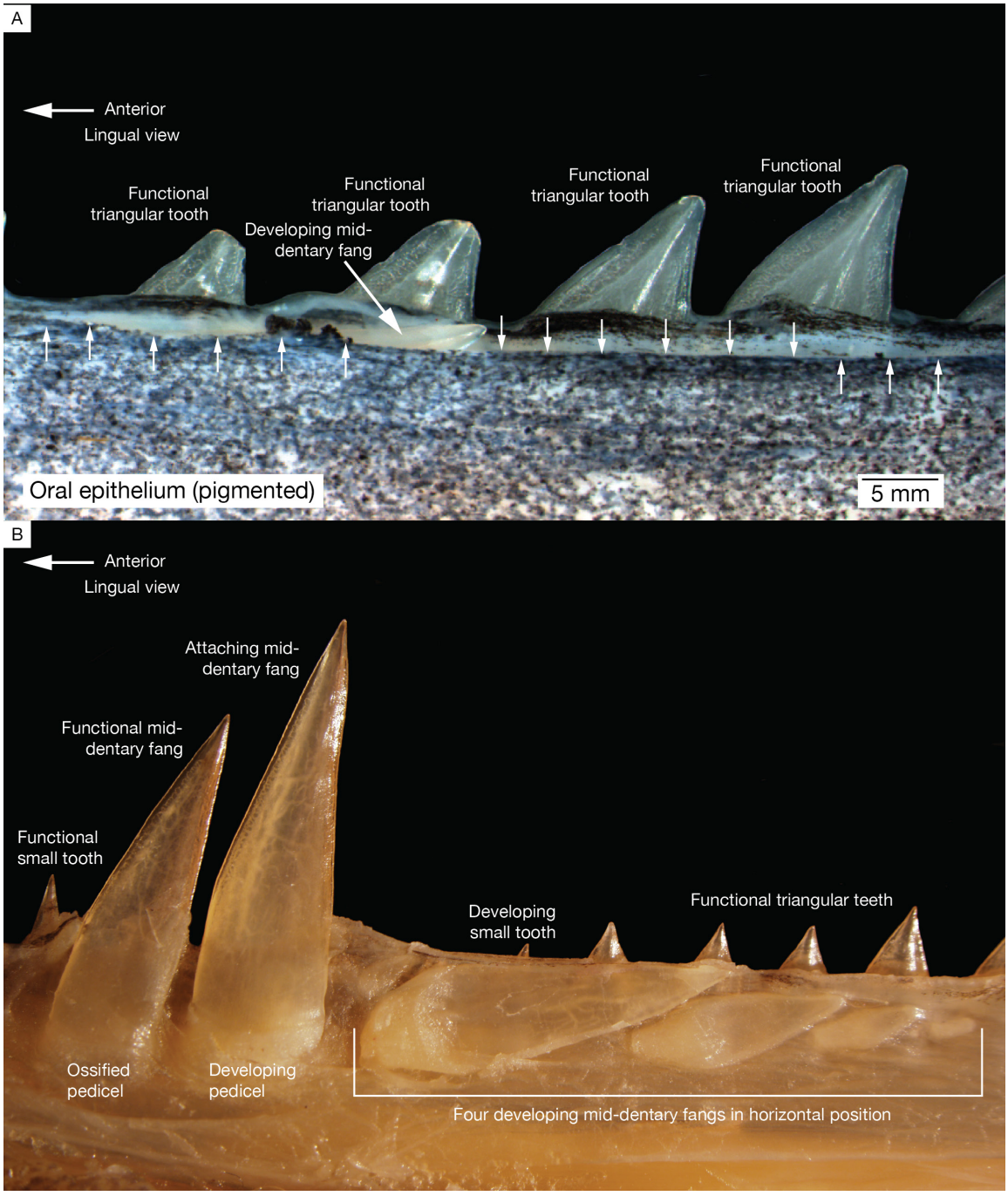

Chapter 1 Figure 4

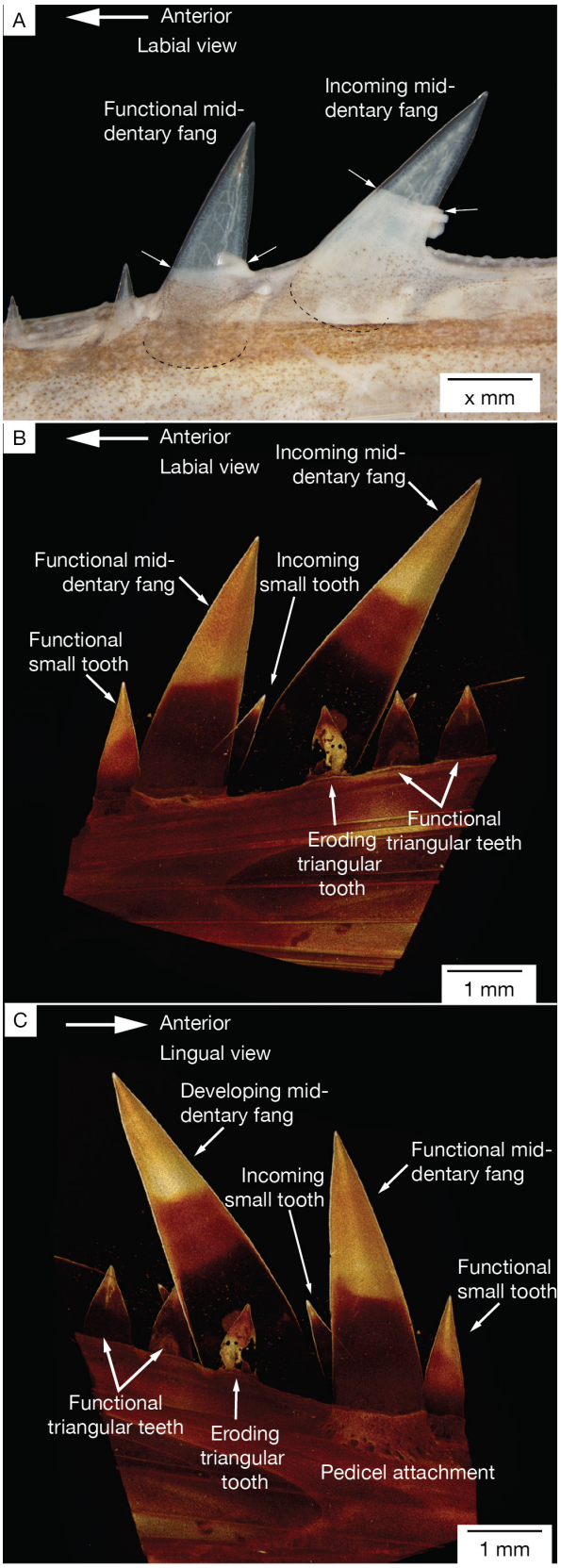

Chapter 1 Figure 5

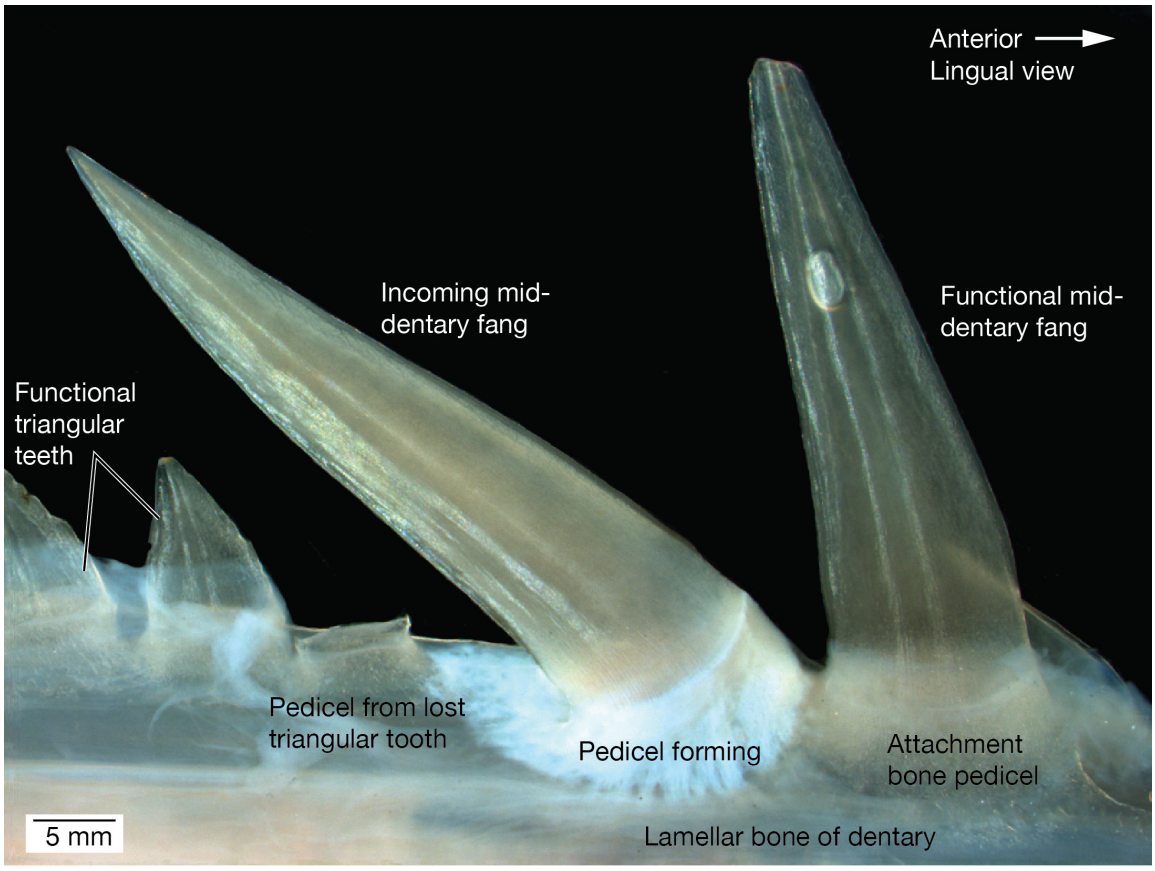

Chapter 1 Figure 6

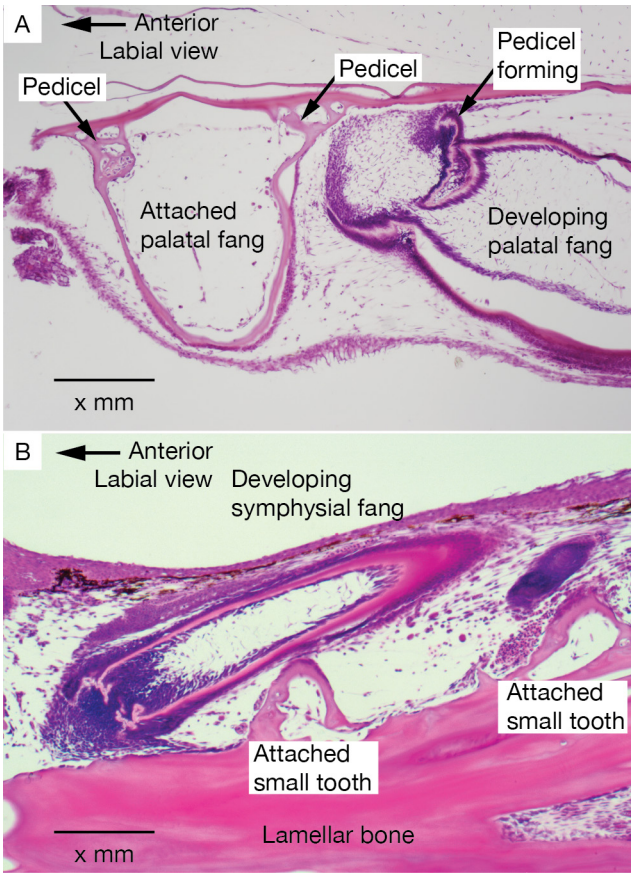

Chapter 1 Figure 7

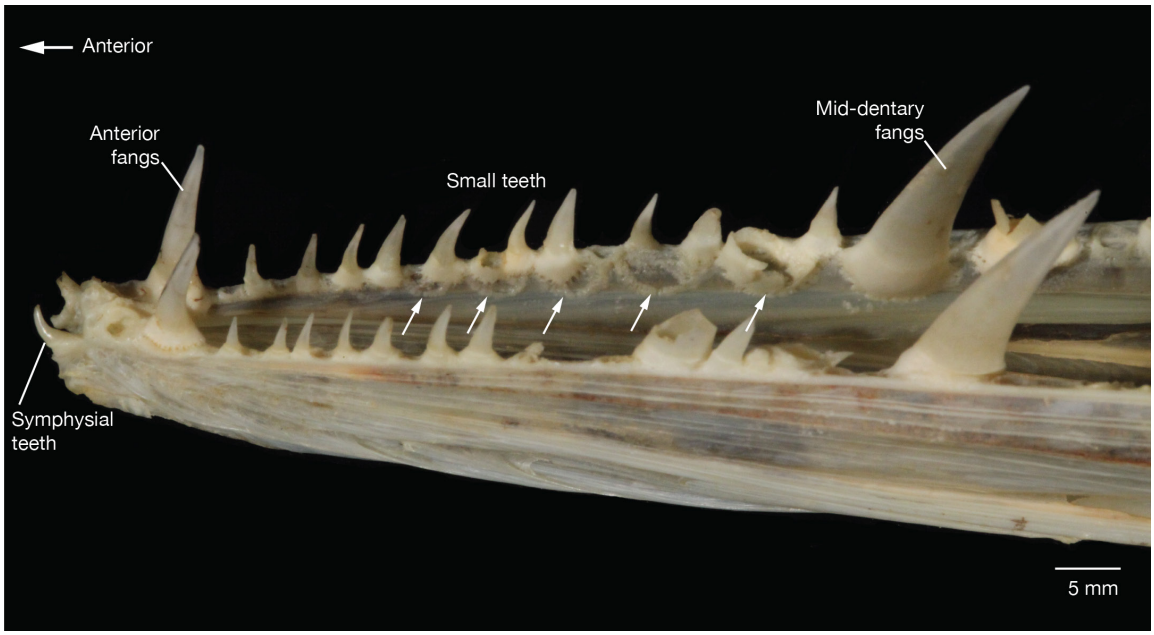

Chapter 1 Figure 8

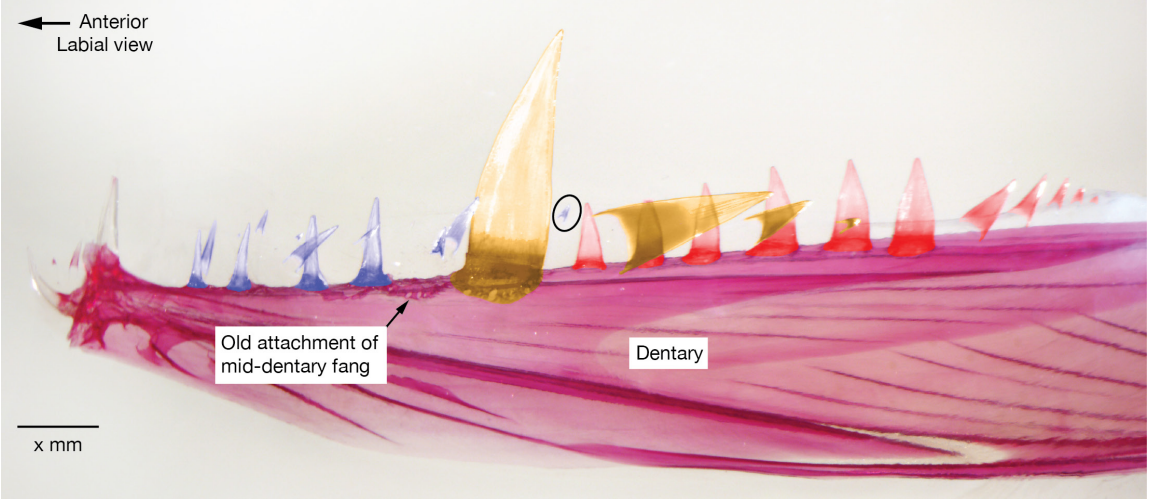

Chapter 1 Figure 9

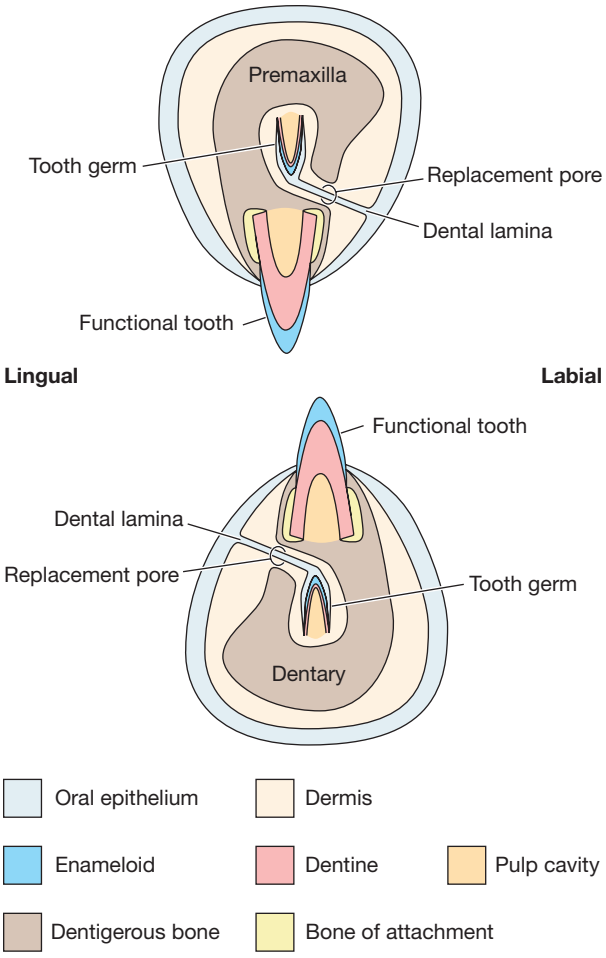

Chapter 2 Figure 1

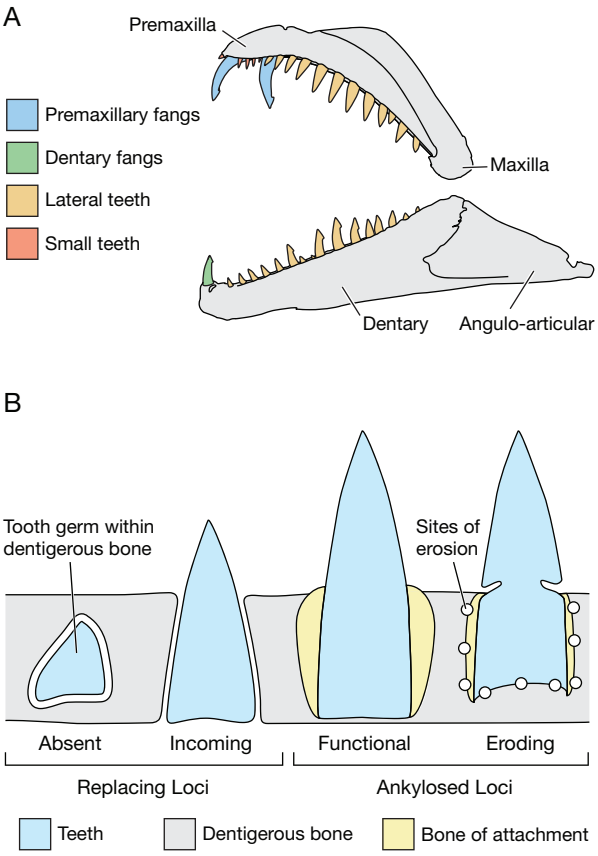

Chapter 2 Figure 2

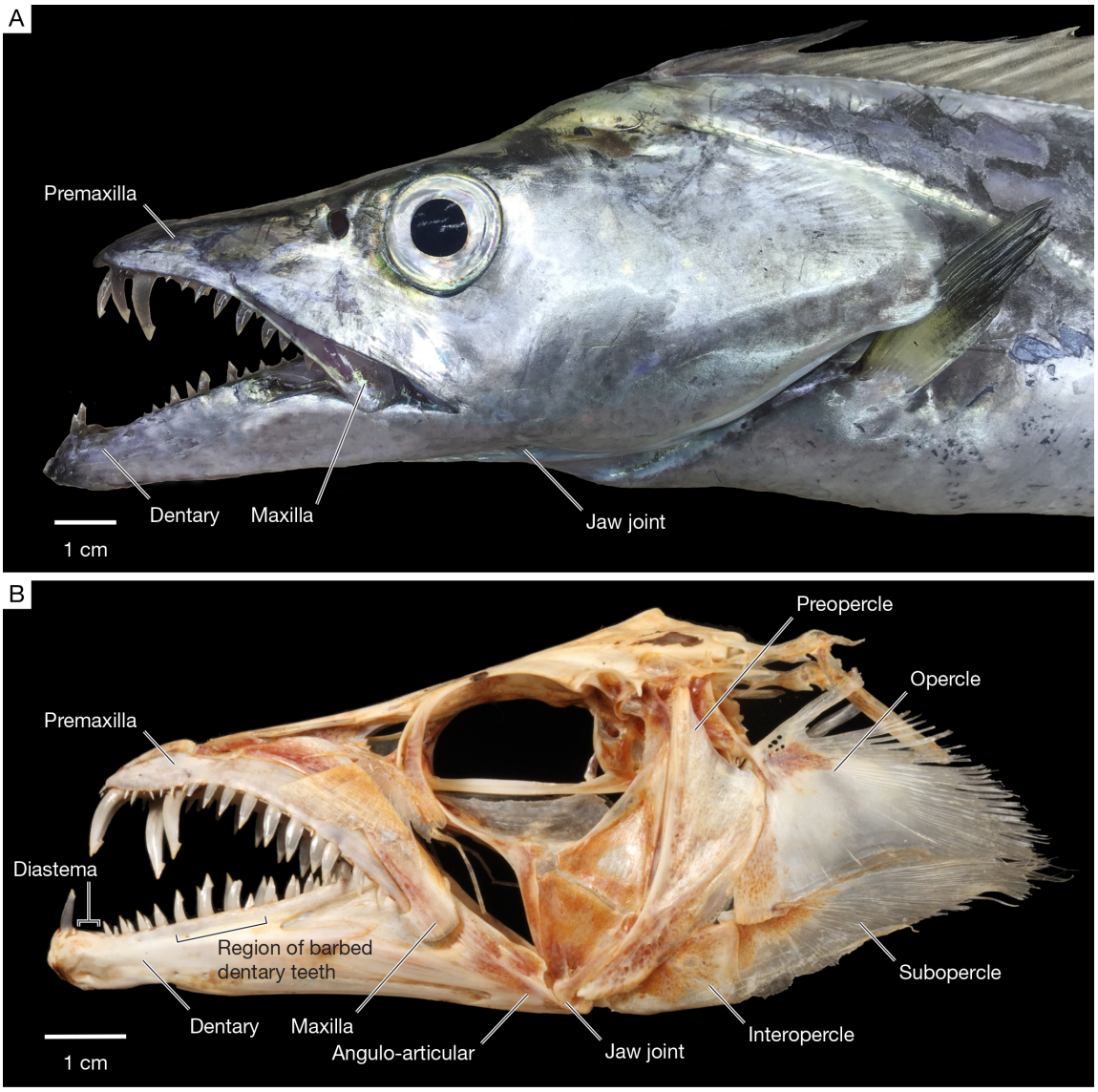

Chapter 2 Figure 3

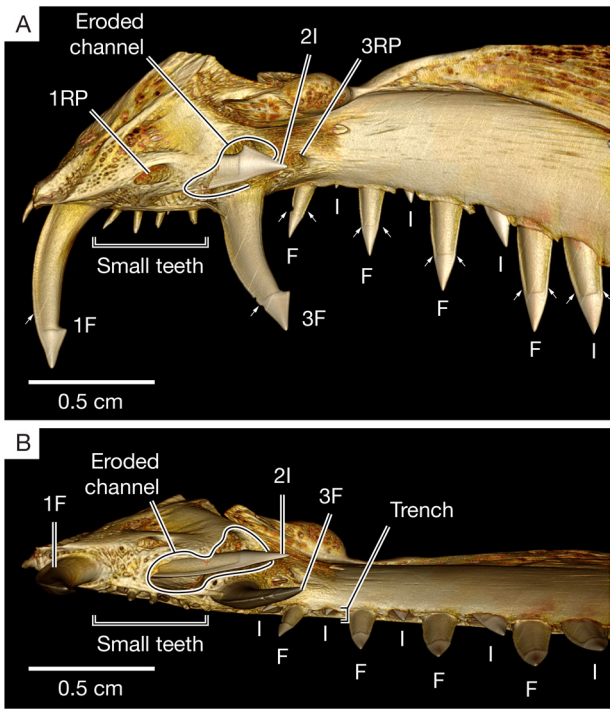

Chapter 2 Figure 4

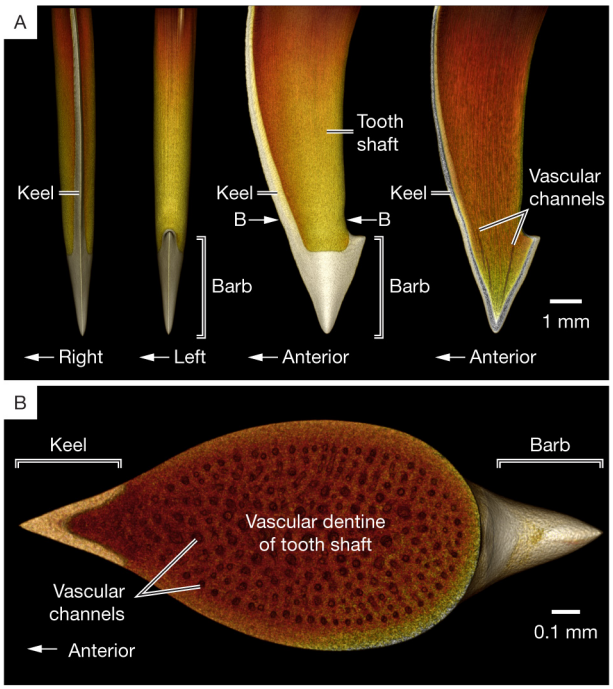

Chapter 2 Figure 5

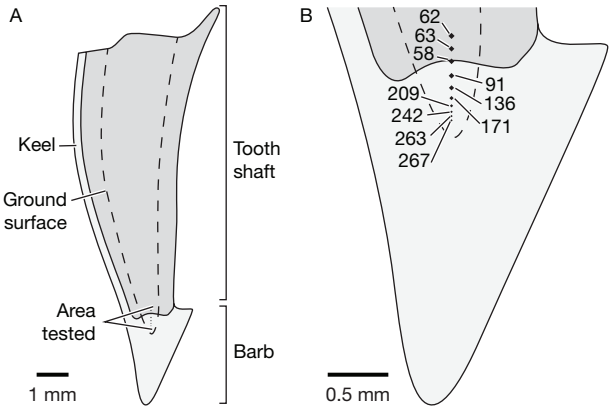

Chapter 2 Figure 6

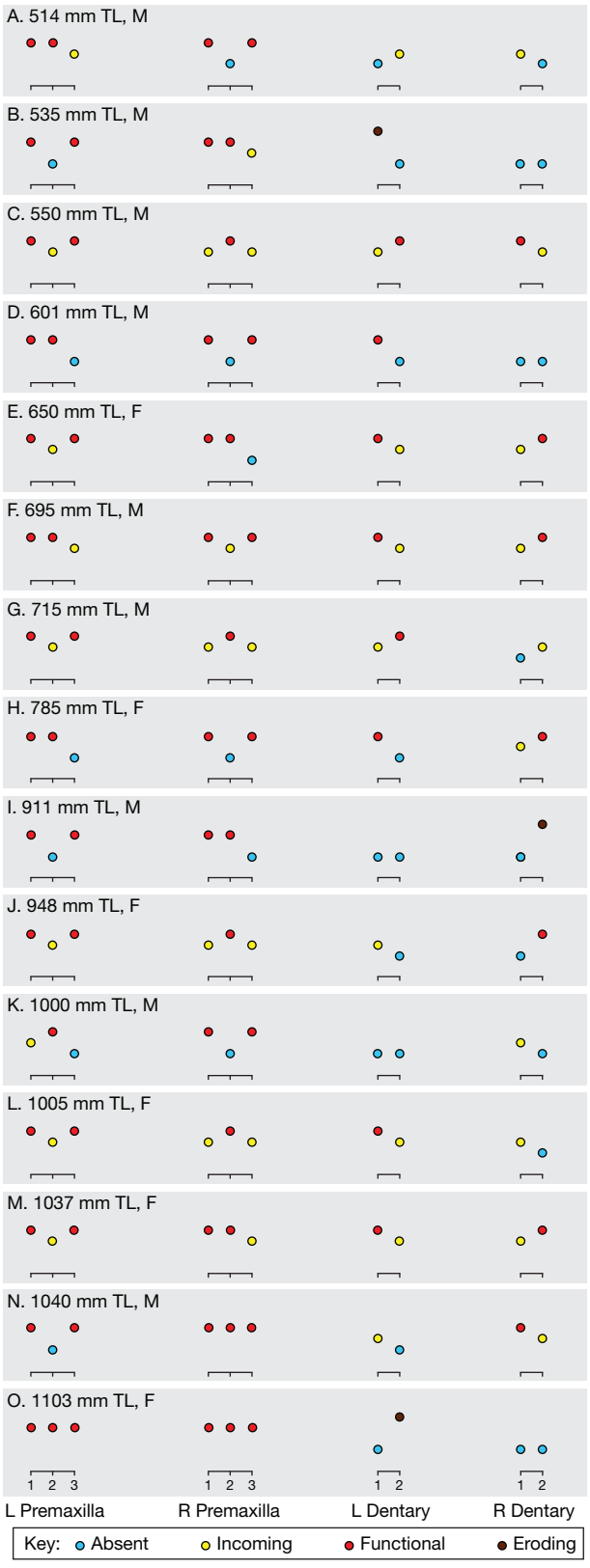

Chapter 2 Figure 7

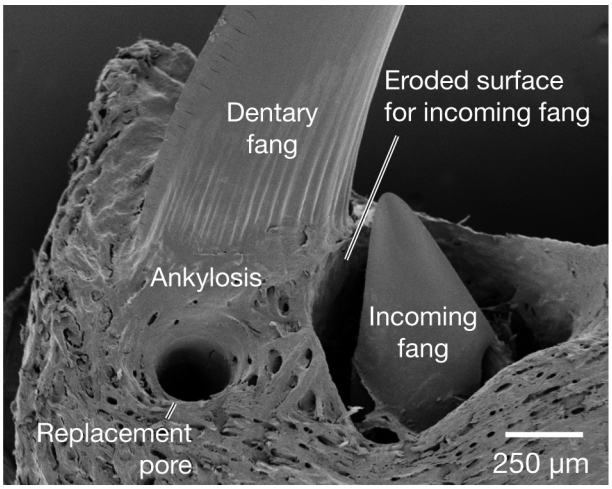

Chapter 2 Figure 8

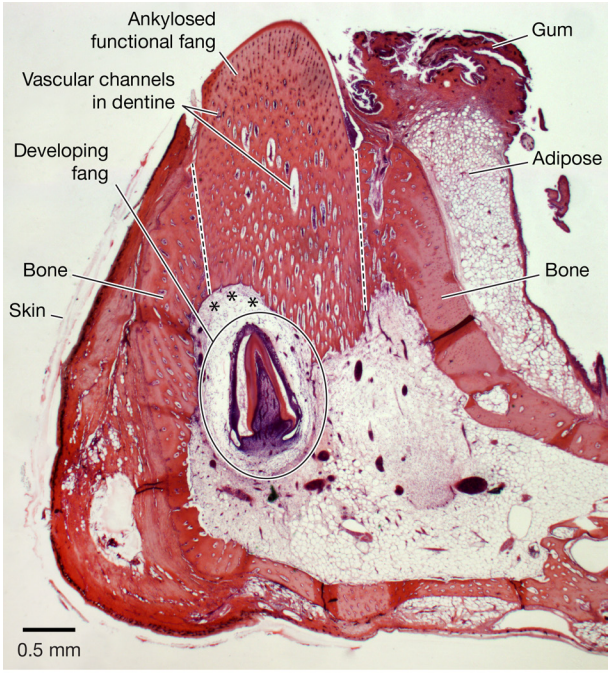

Chapter 2 Figure 9

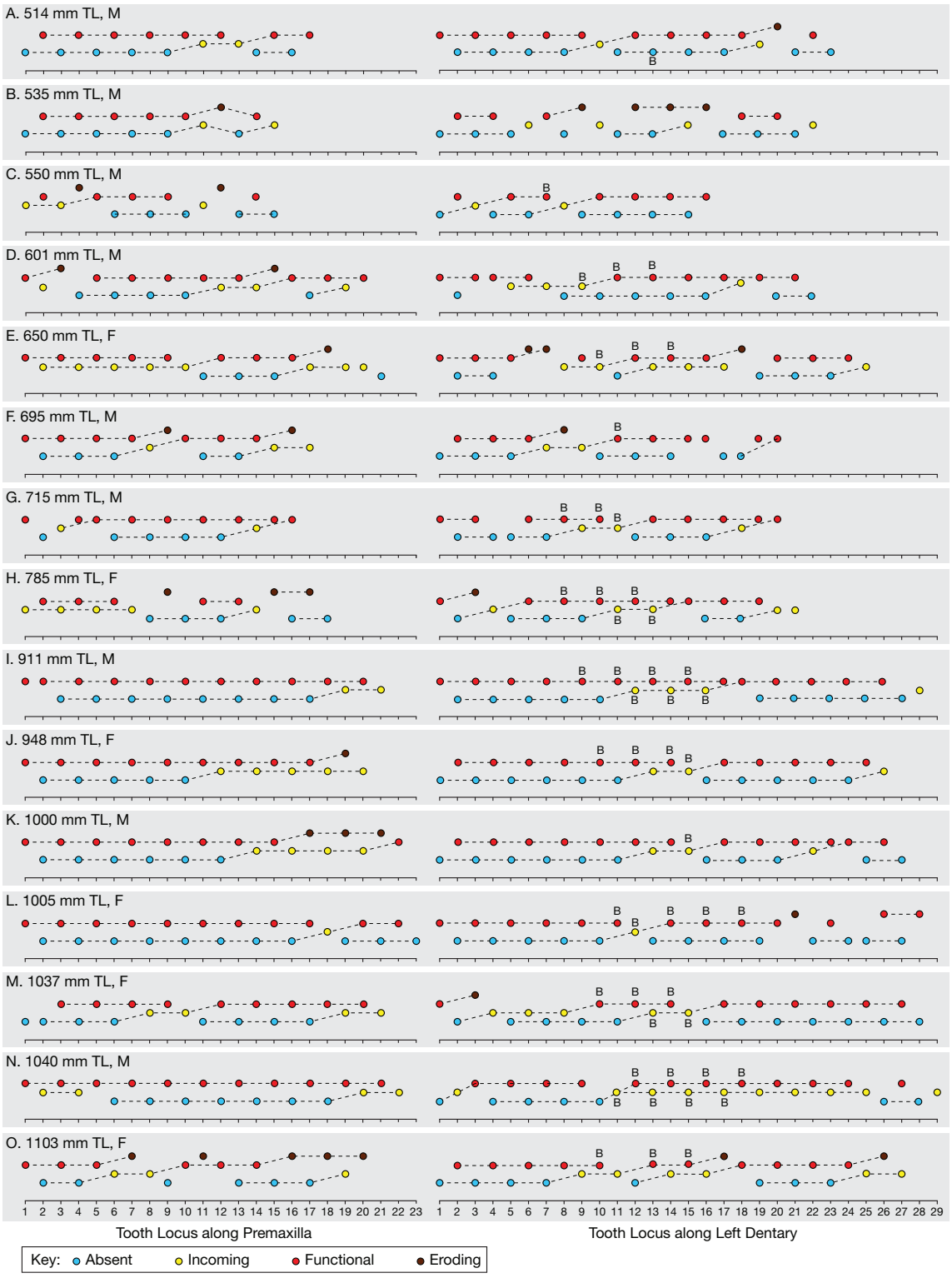

Chapter 2 Figure 10

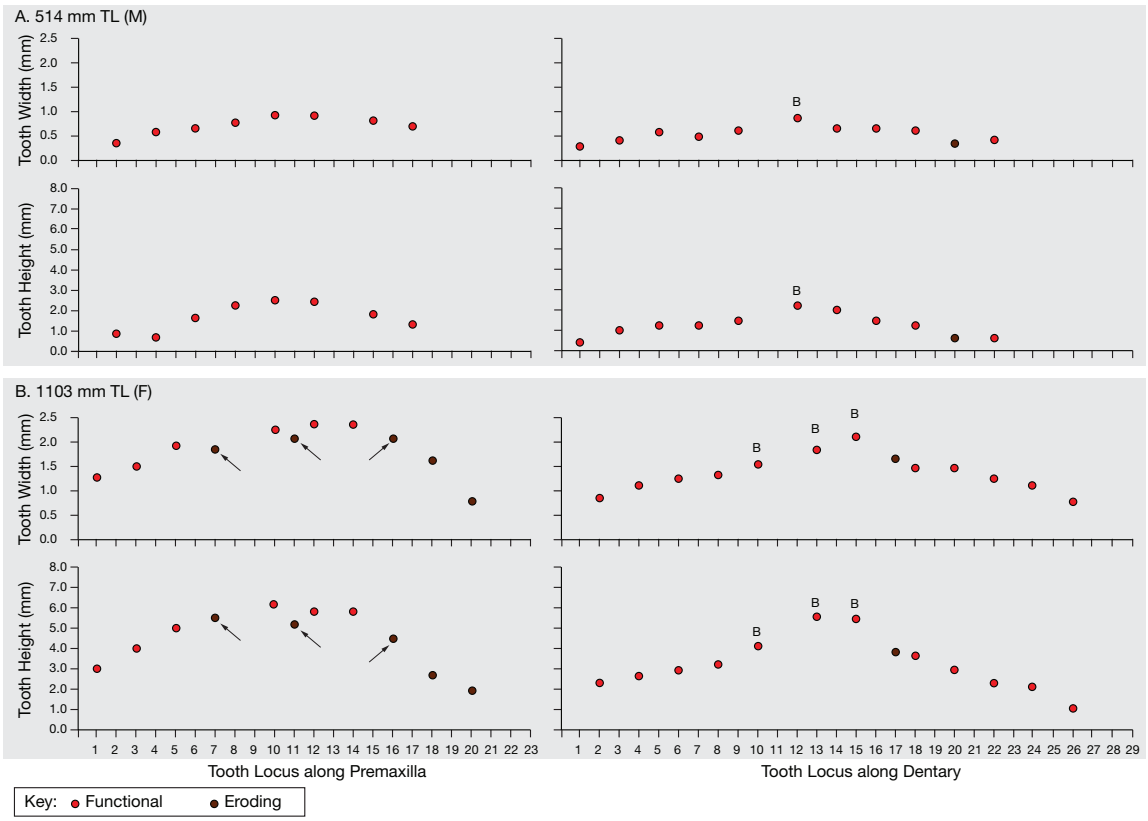

Chapter 2 Figure 11

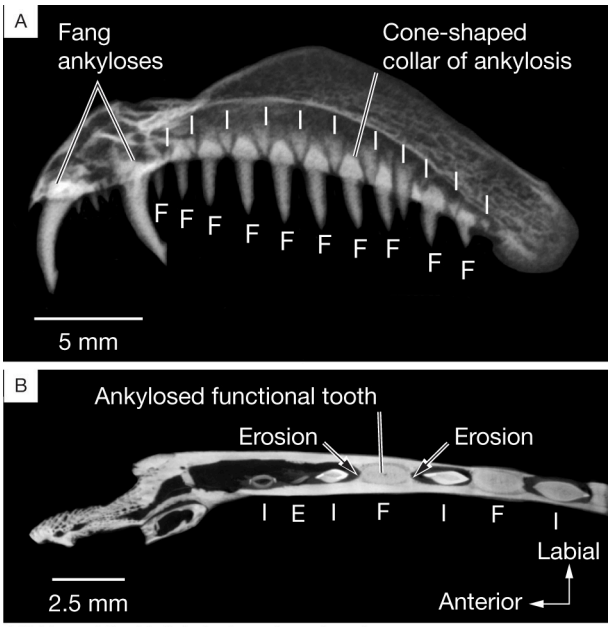

Chapter 2 Figure 12

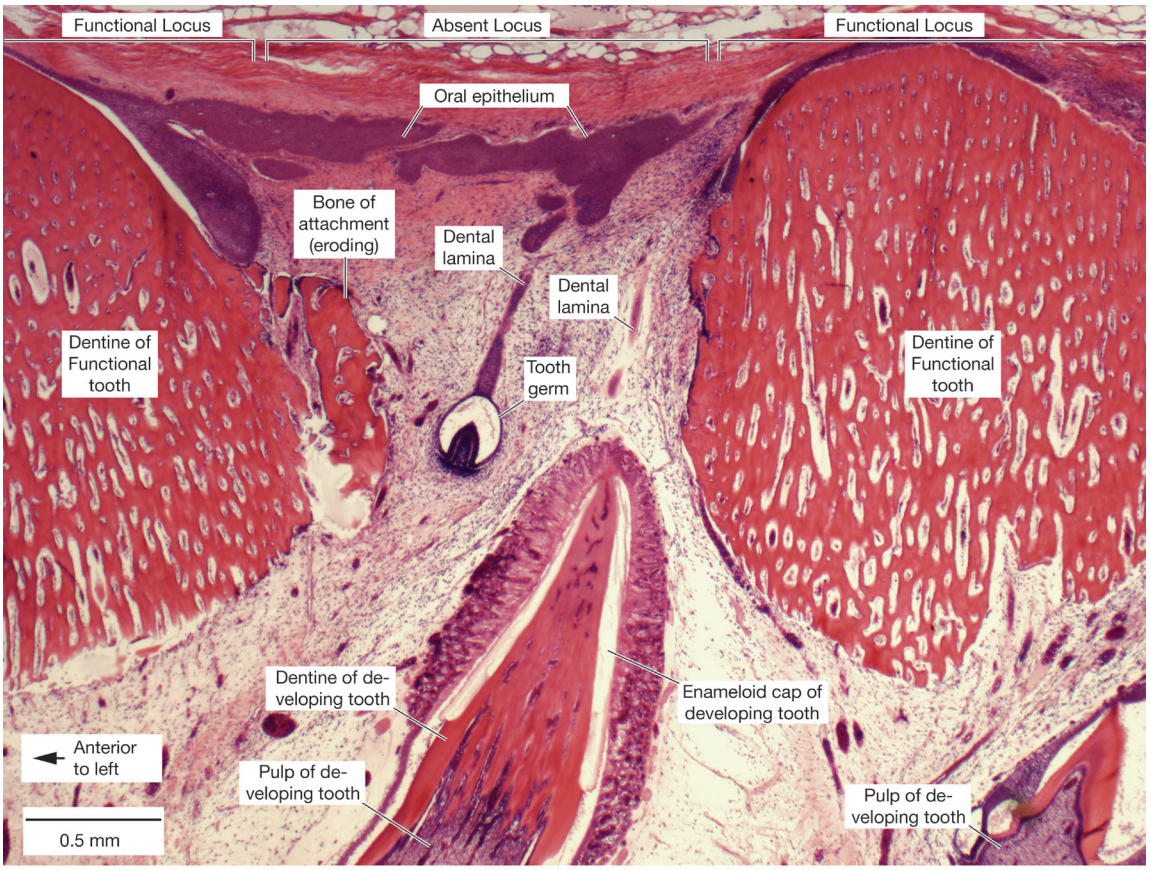

Chapter 2 Figure 13

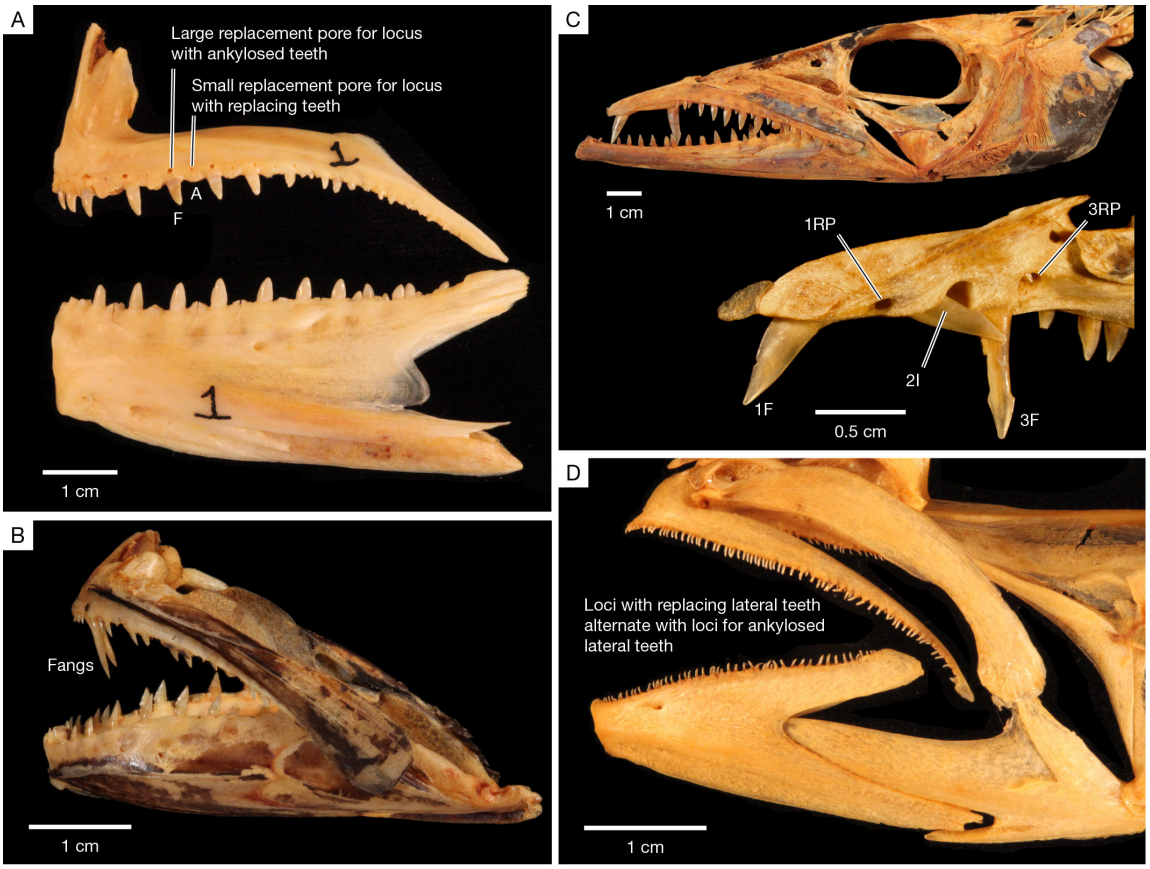

Chapter 2 Figure 14

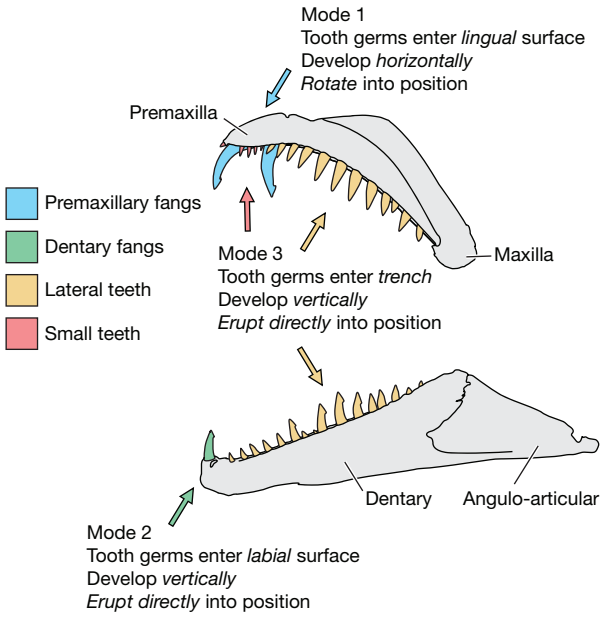

Chapter 2 Figure 15

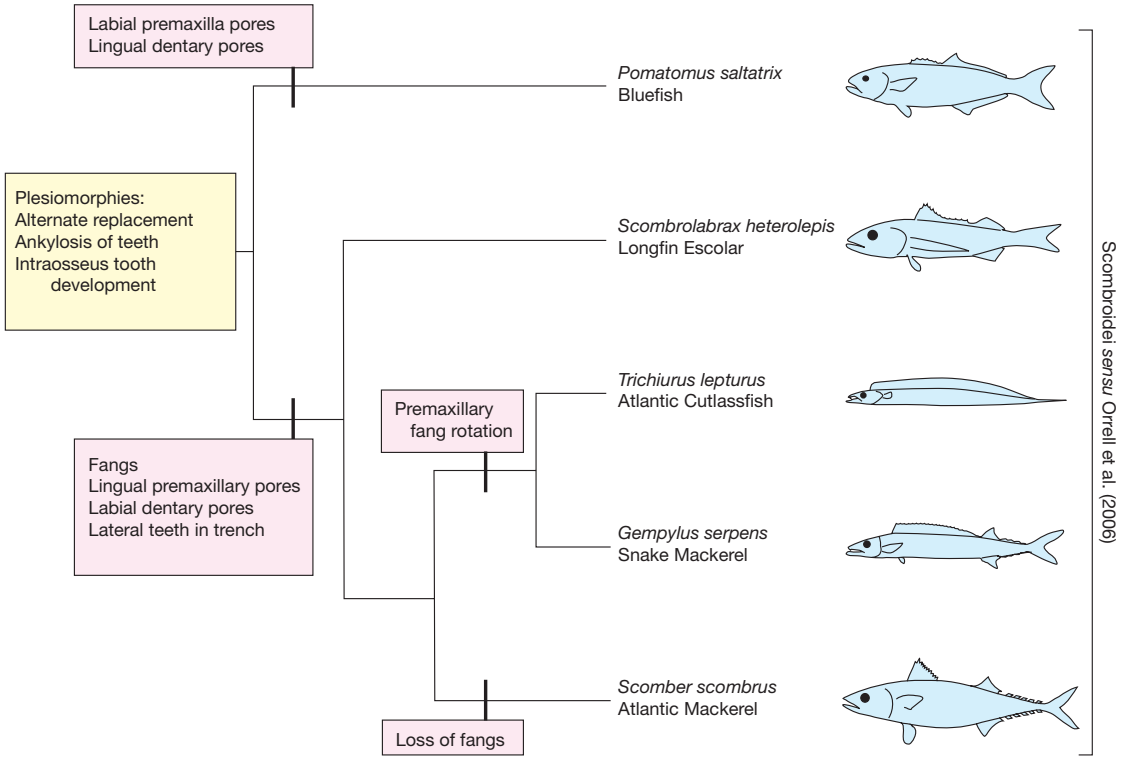

Chapter 2 Figure 16

A. Bluefish Type (*Pomatomus saltatrix*)

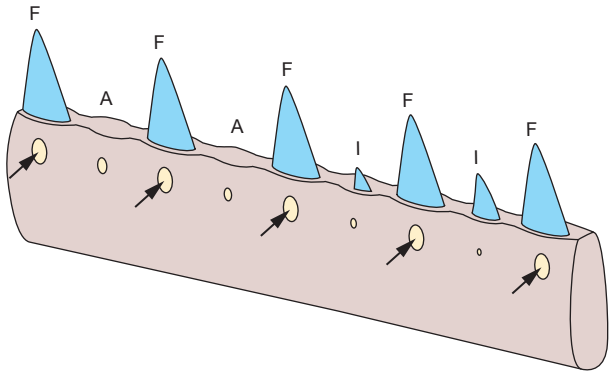

B. Cutlassfish Type (*Trichiurus lepturus*)

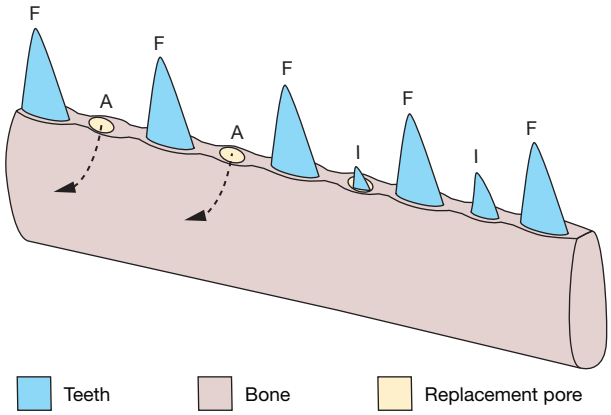

Chapter 2 Figure 17

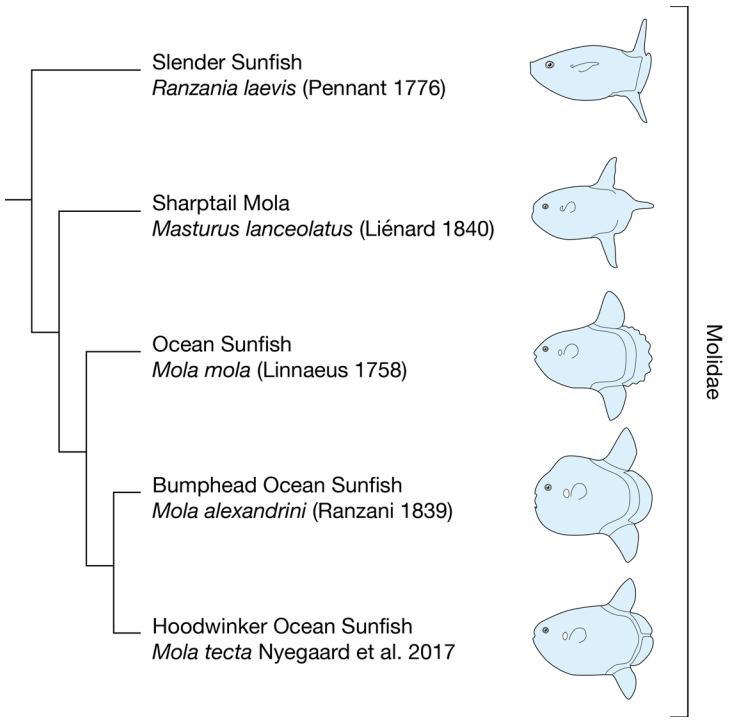

Chapter 3 Figure 1

Chapter 3 Figure 2

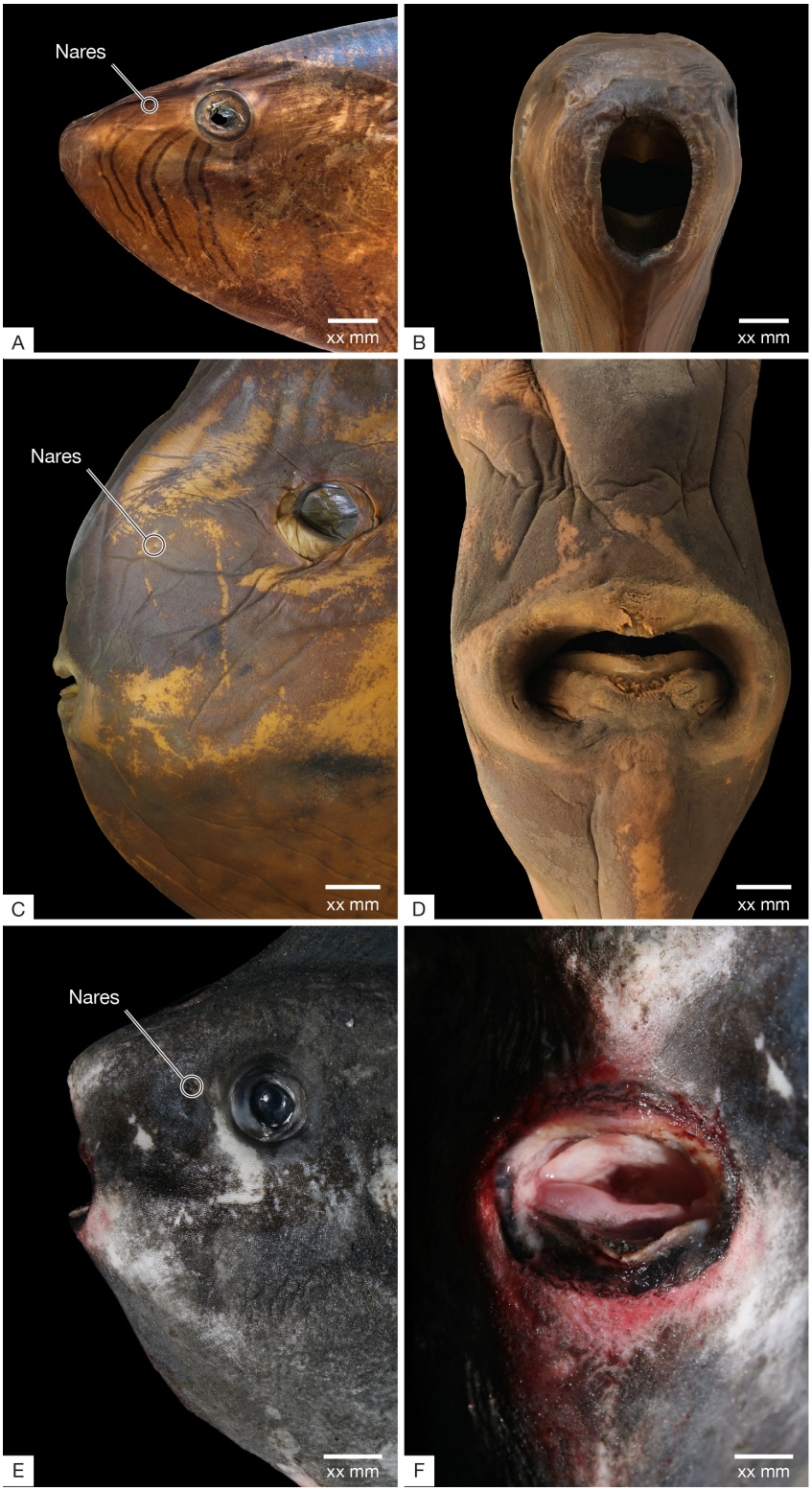

Chapter 3 Figure 3

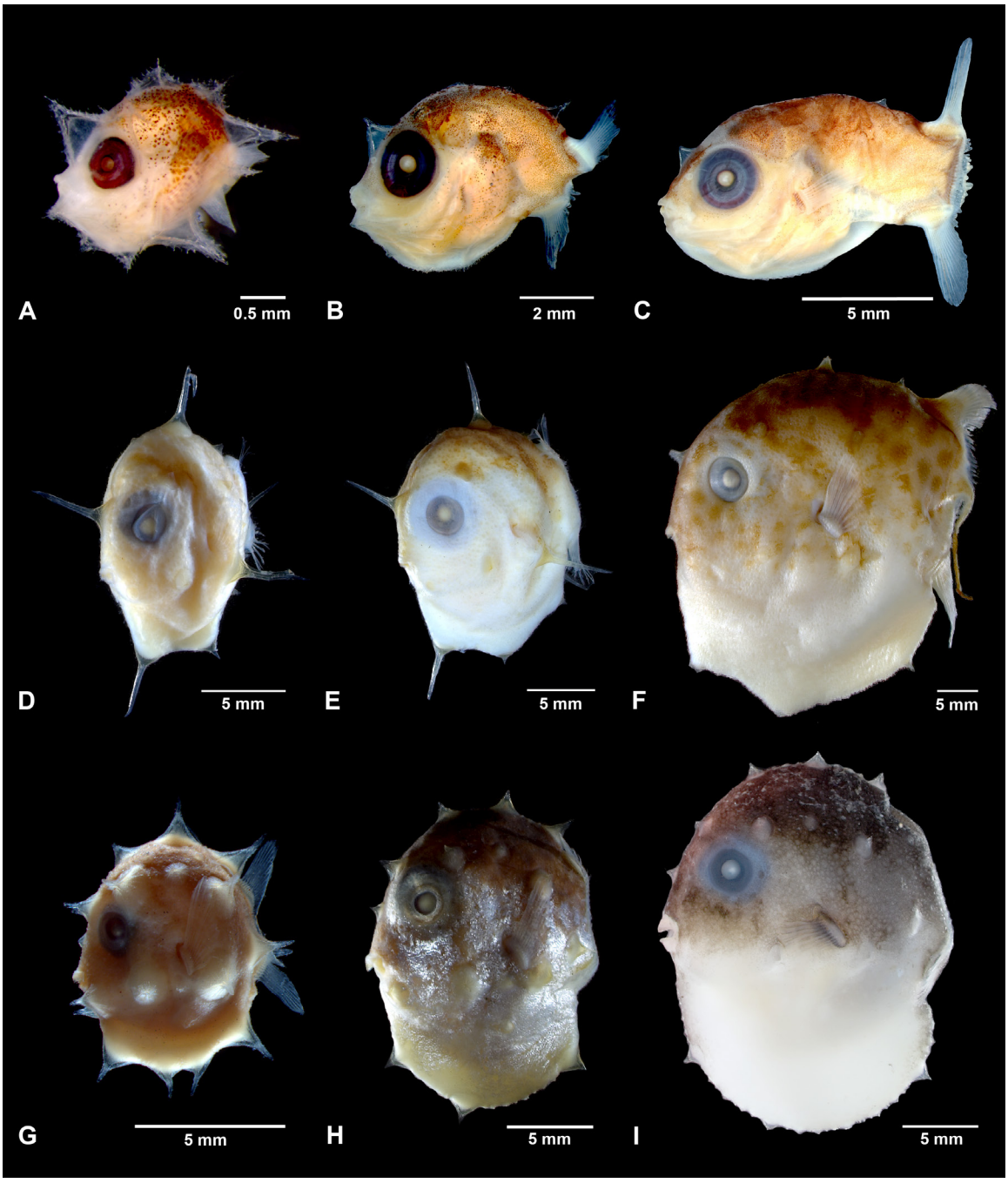

Chapter 3 Figure 4

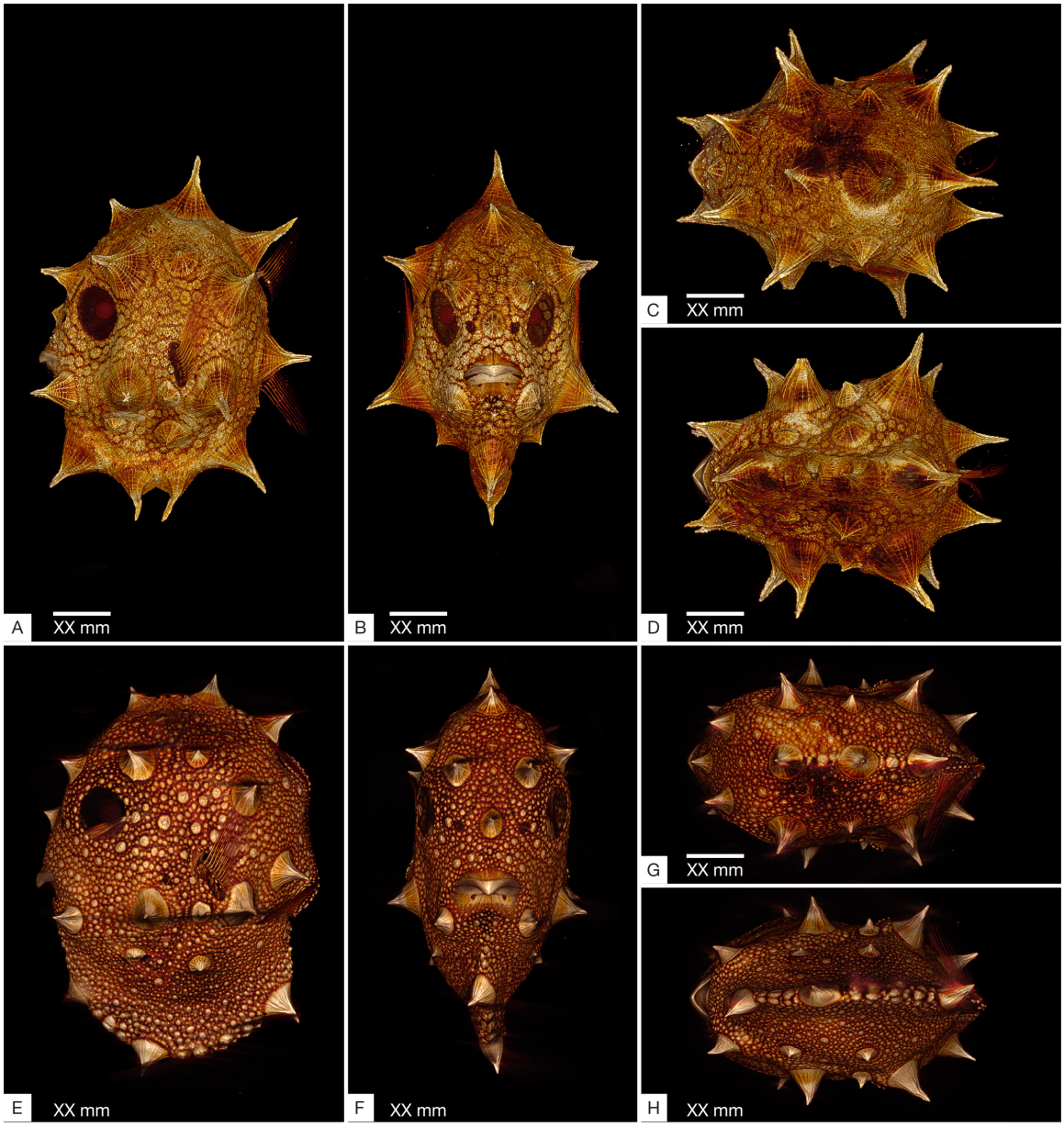

Chapter 3 Figure 5

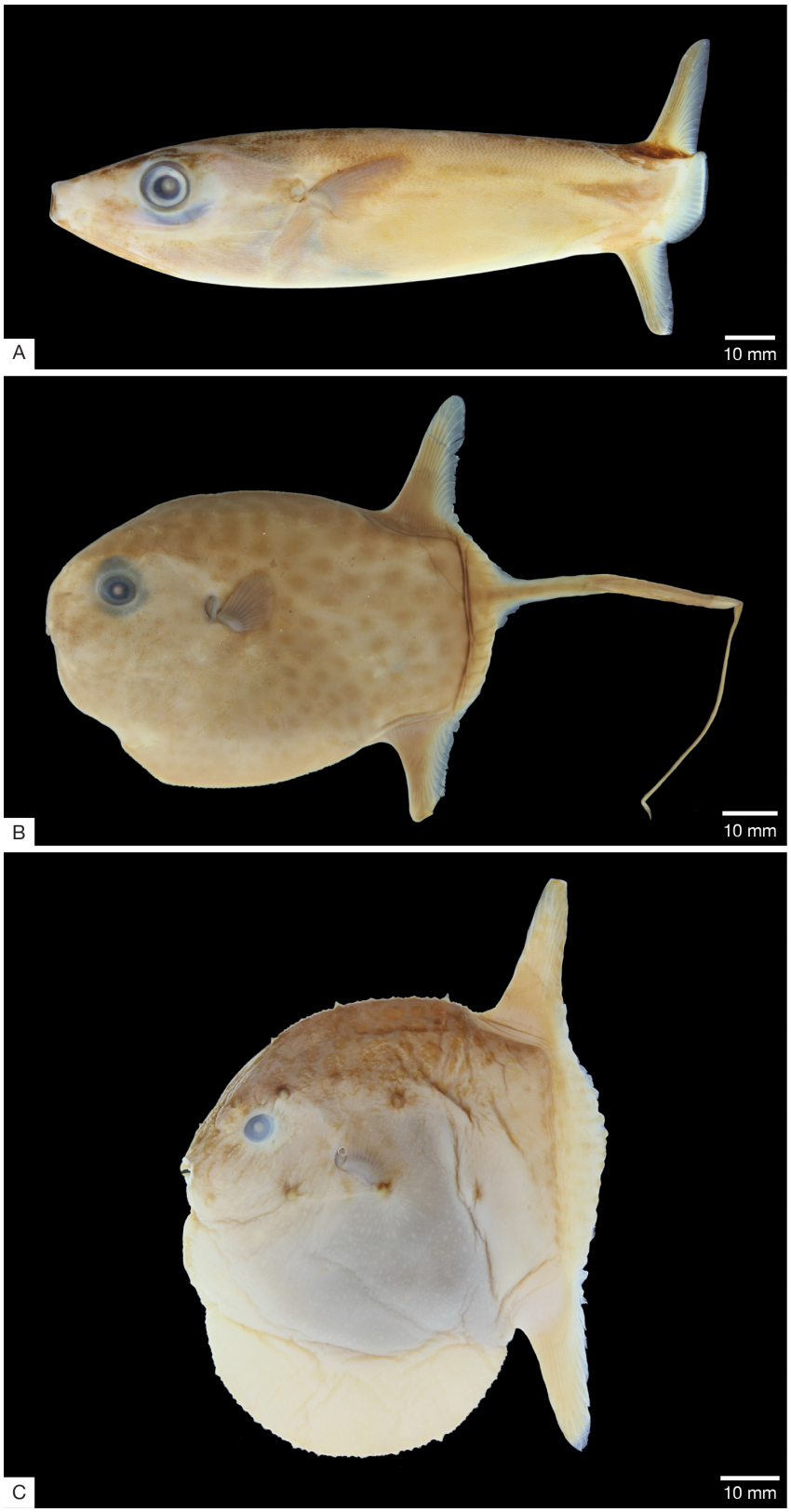

Chapter 3 Figure 6

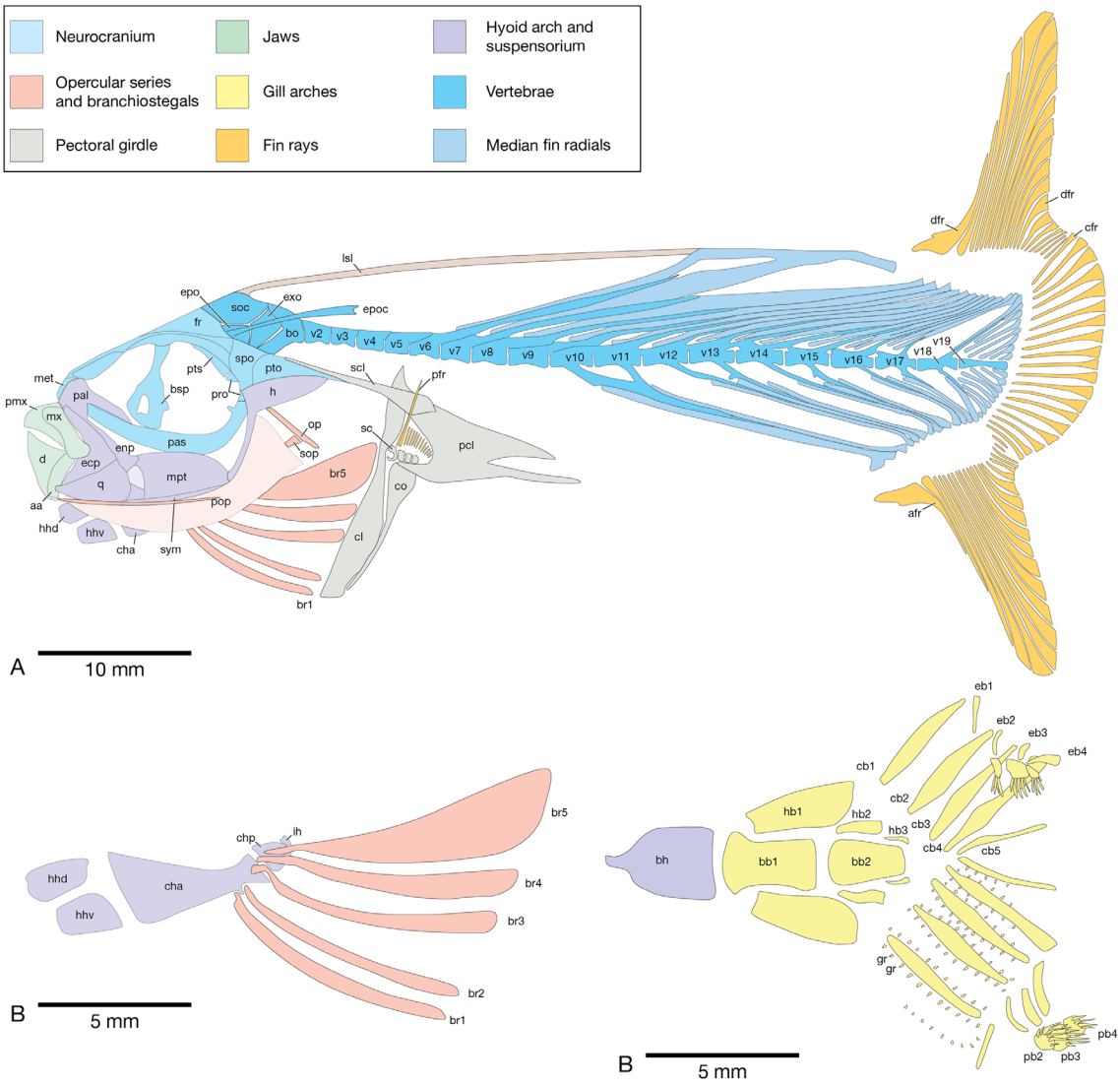

Chapter 3 Figure 7

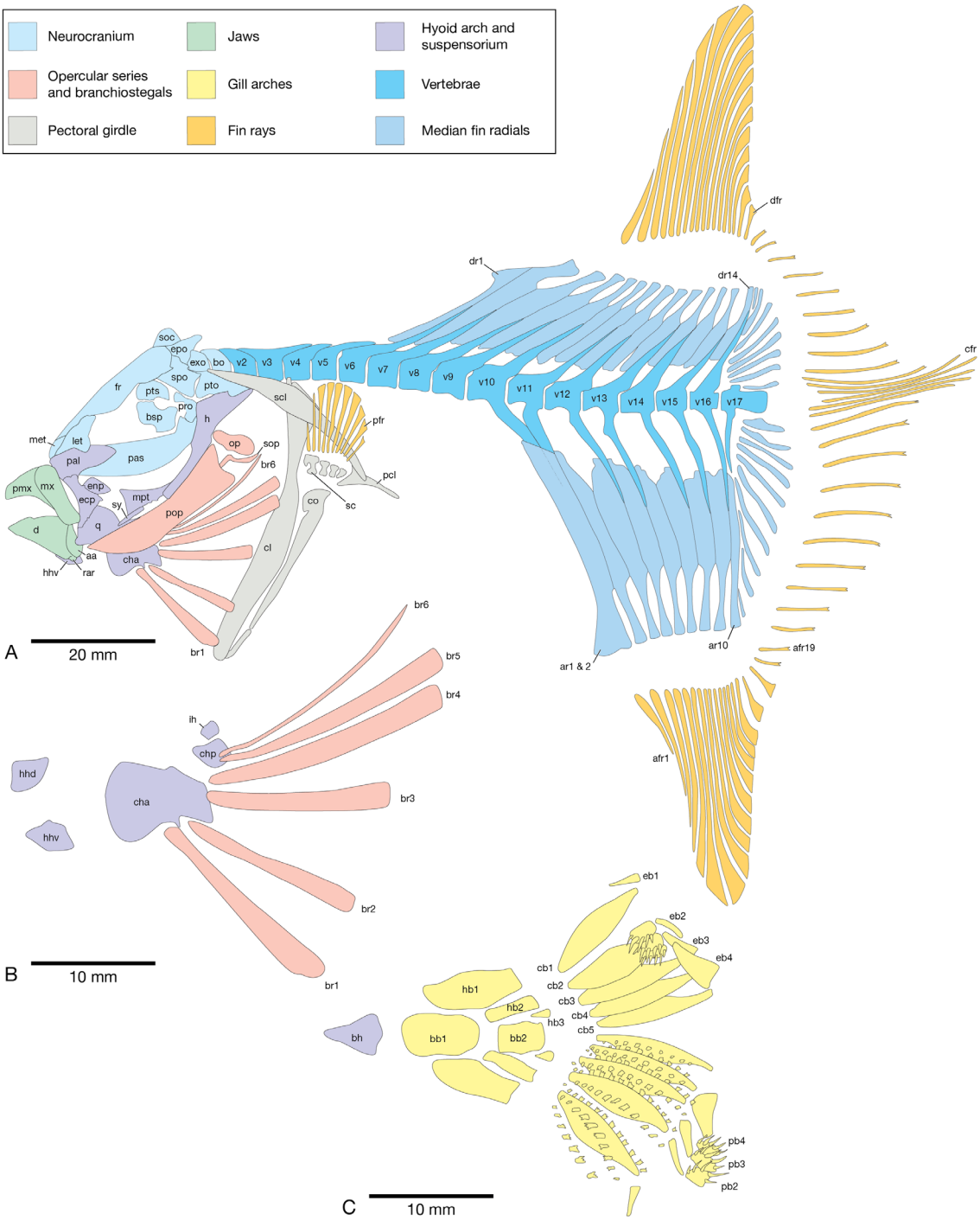

Chapter 3 Figure 8

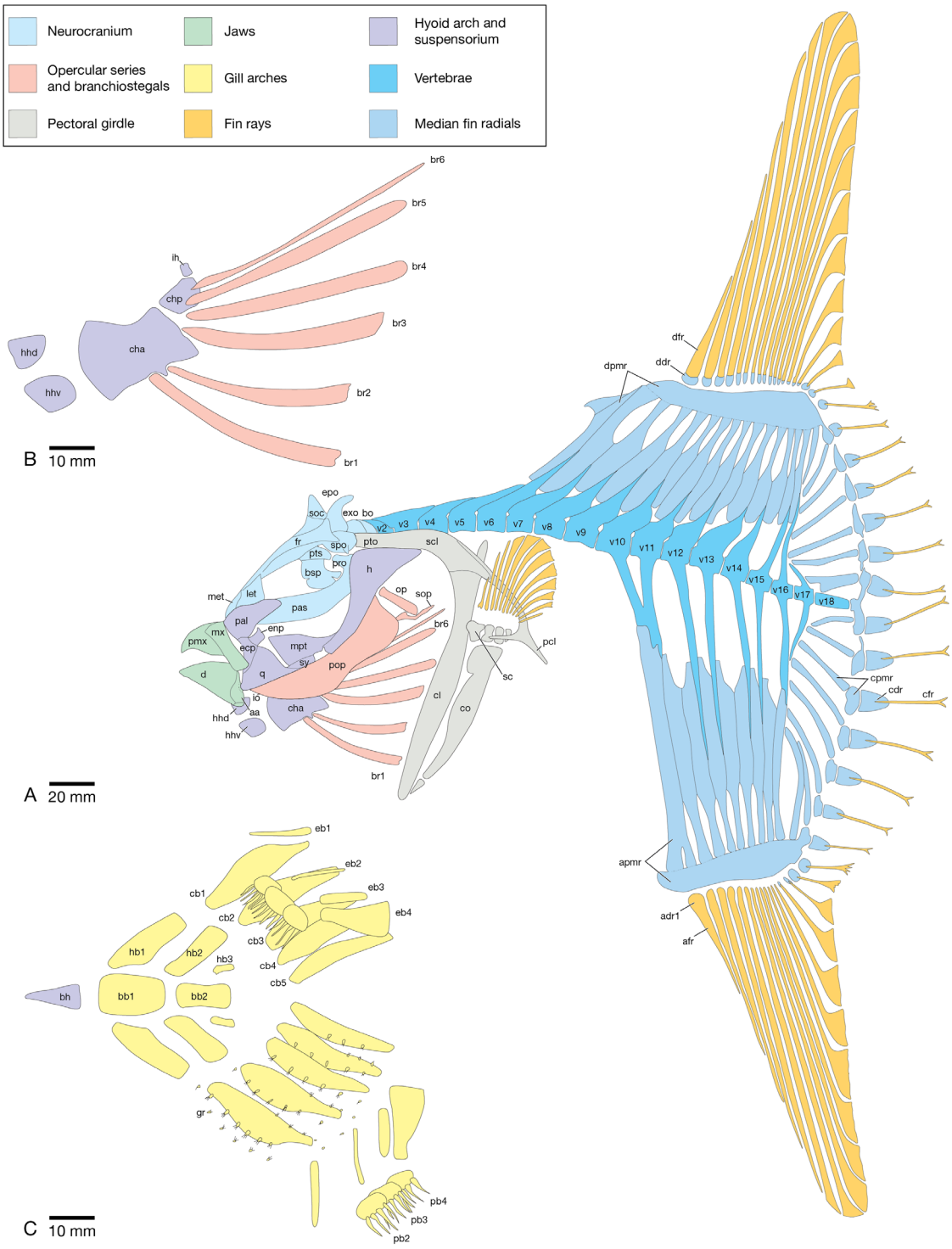

Chapter 3 Figure 9

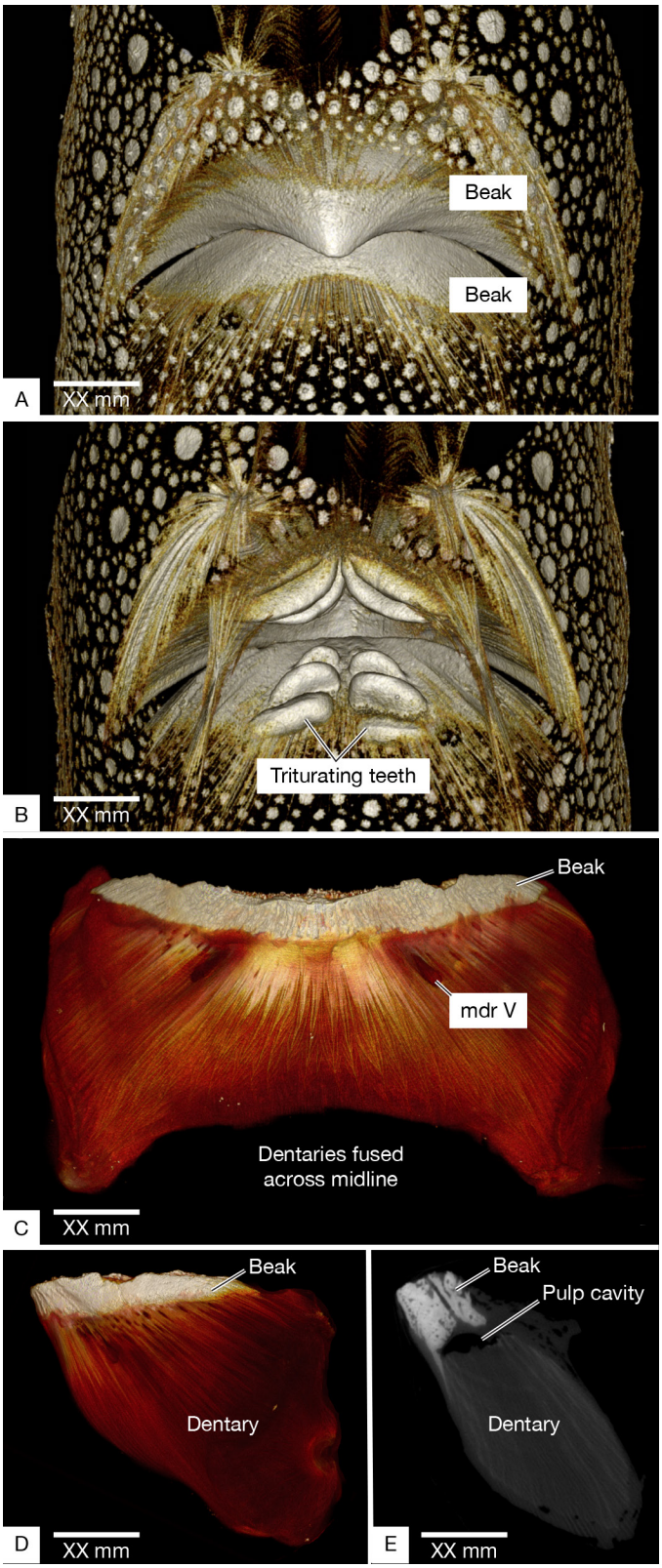

Chapter 3 Figure 10

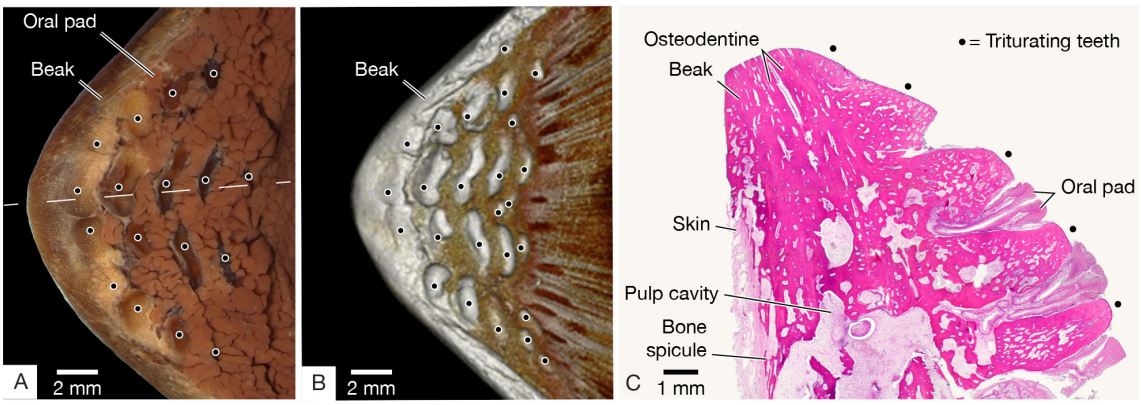

Chapter 3 Figure 11

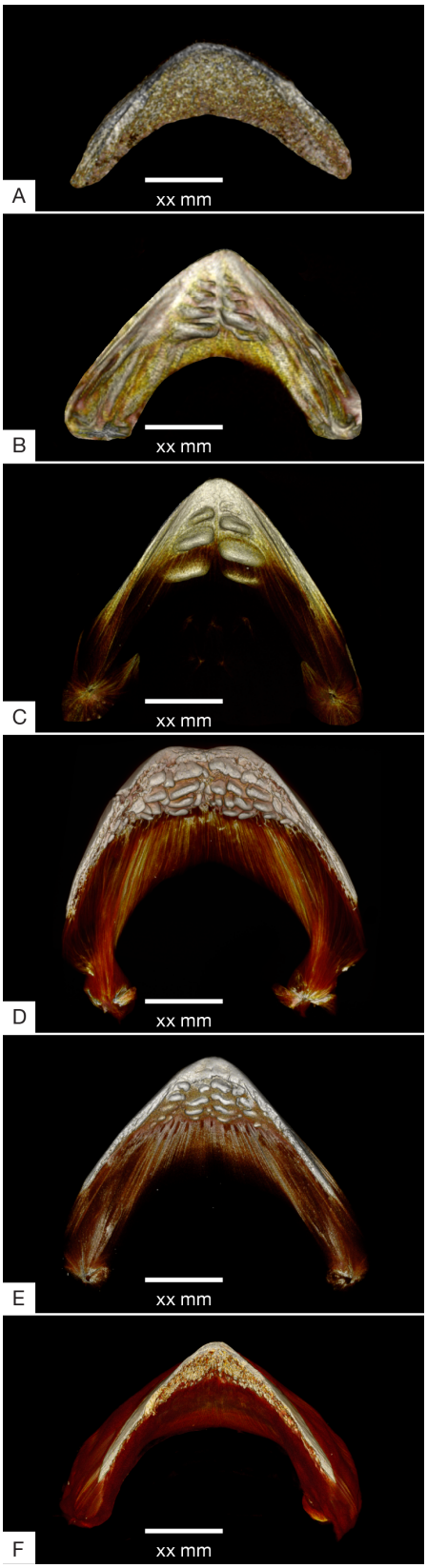

Chapter 3 Figure 12

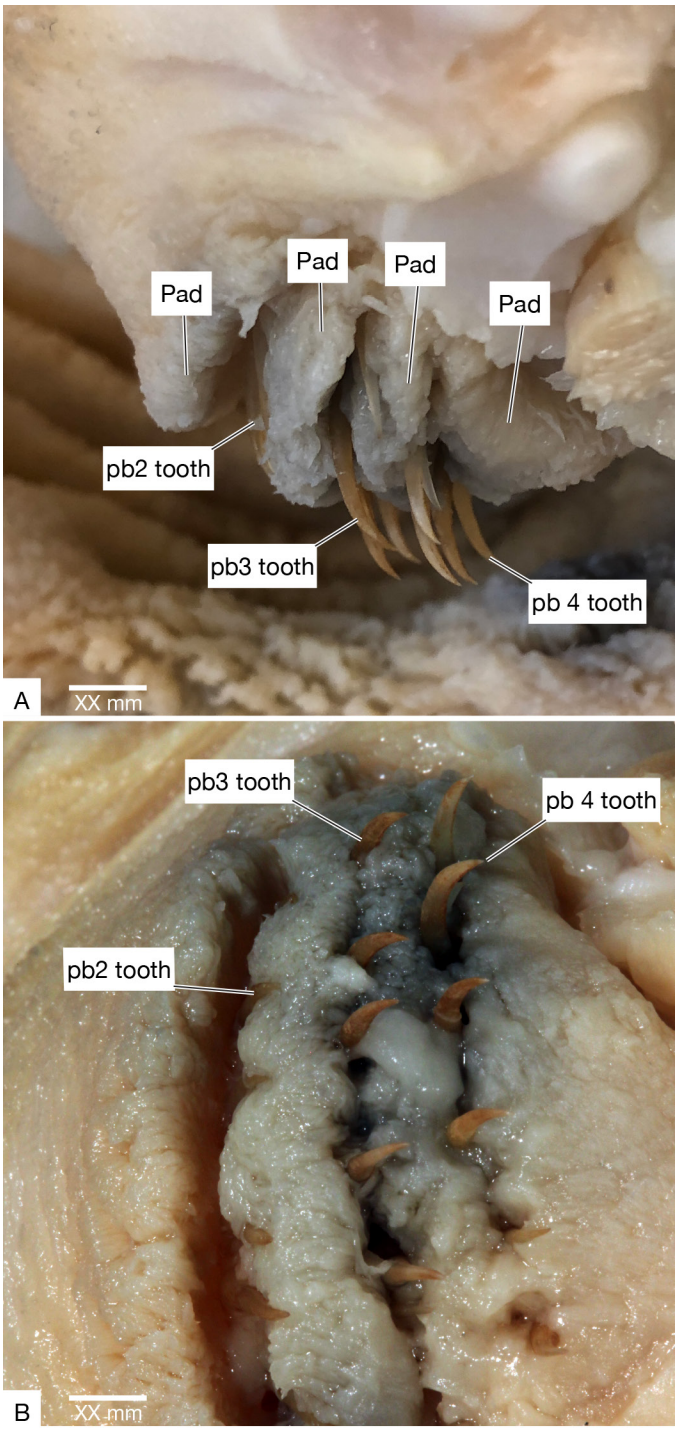

Chapter 3 Figure 13

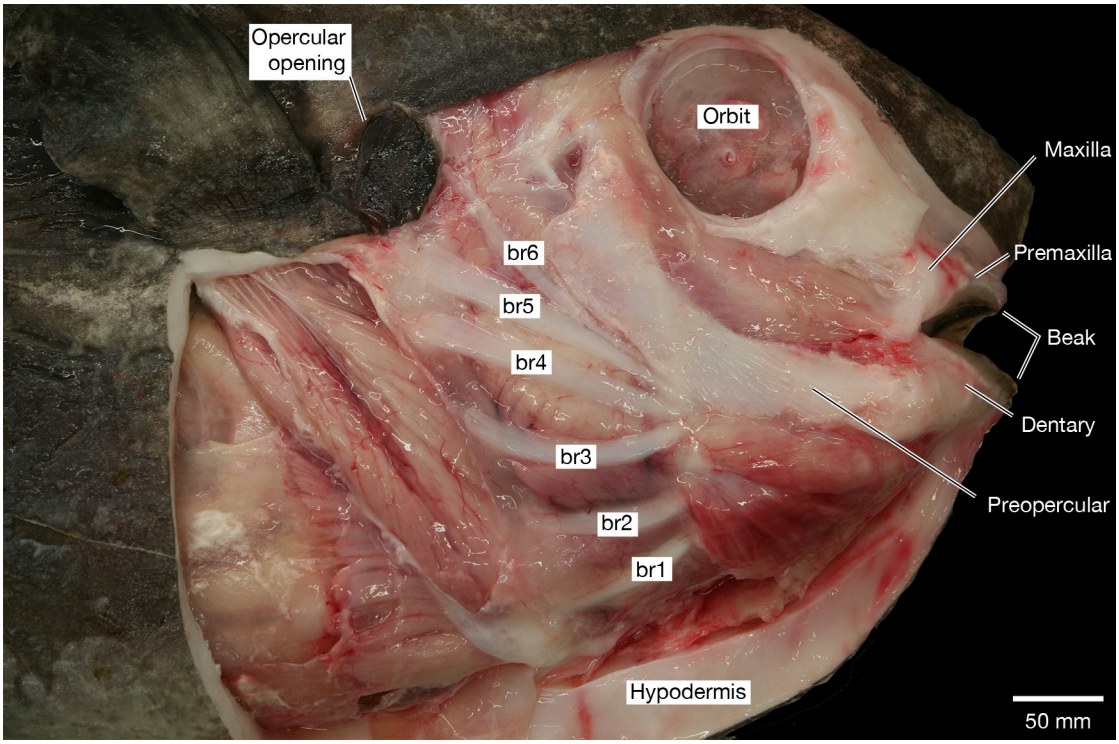

Chapter 3 Figure 14

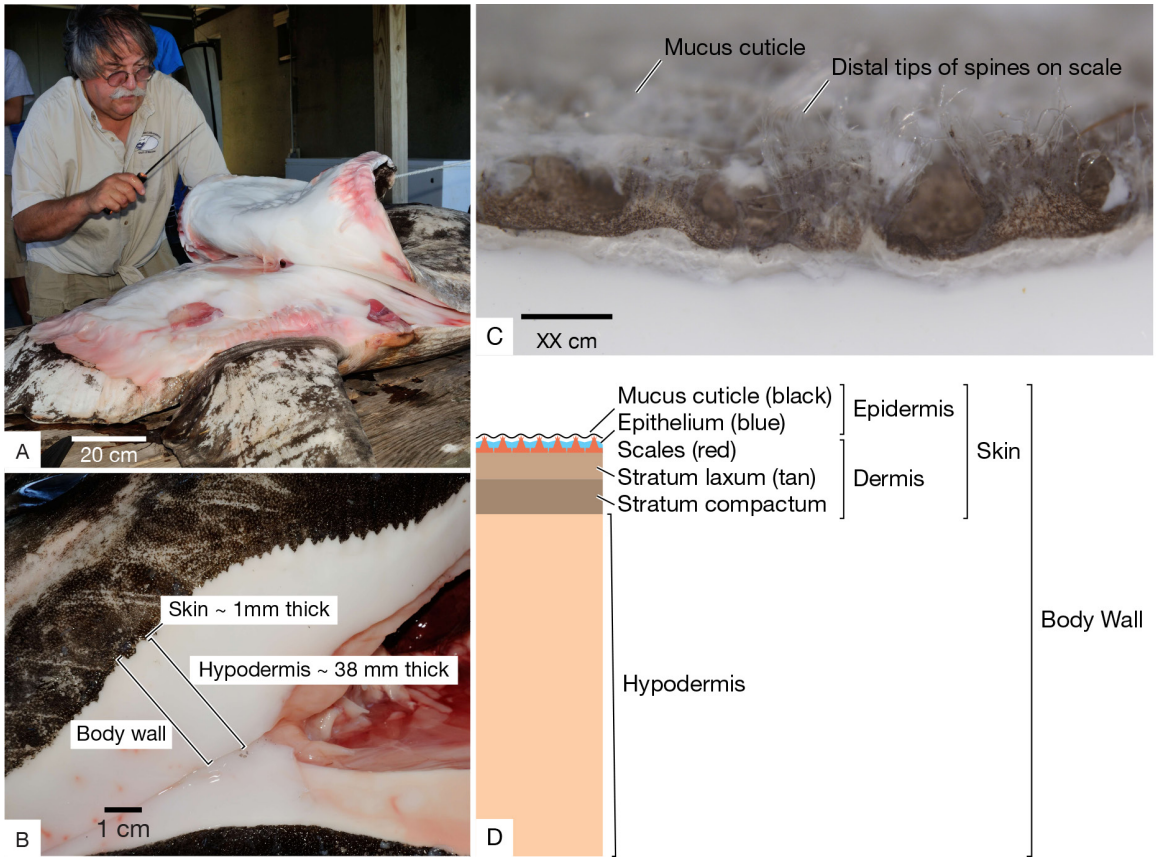

Chapter 3 Figure 15

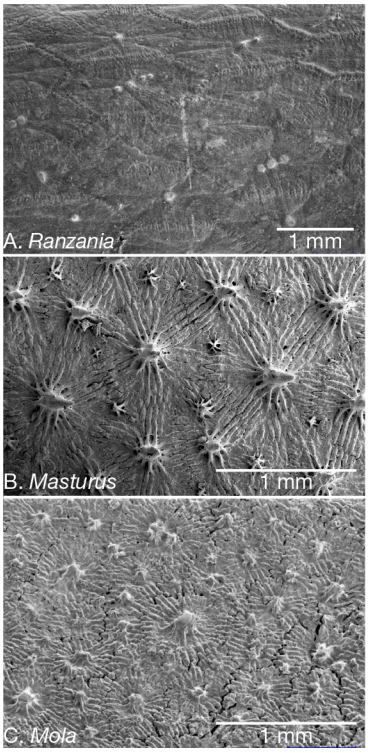

Chapter 3 Figure 16

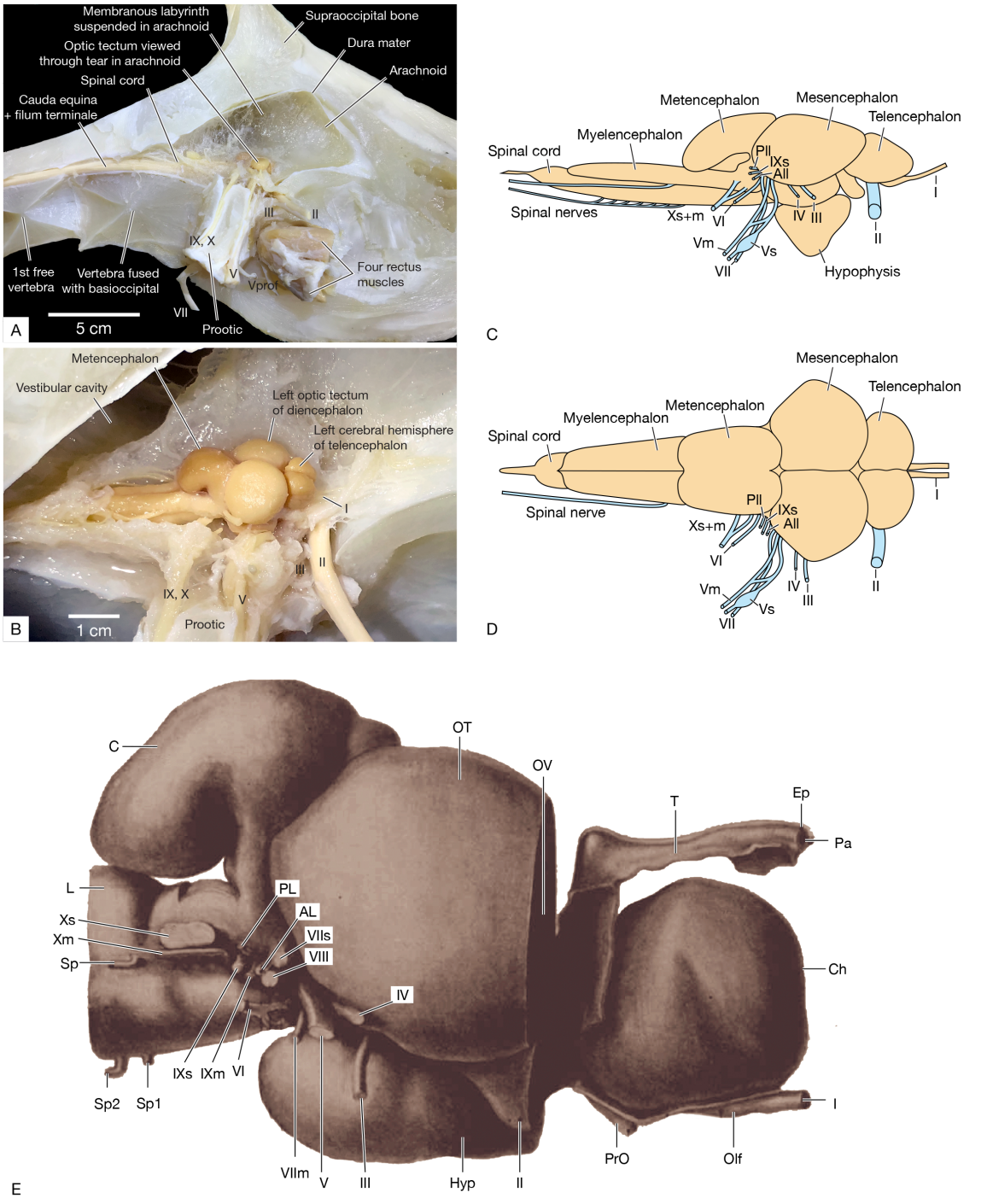

Chapter 3 Figure 17

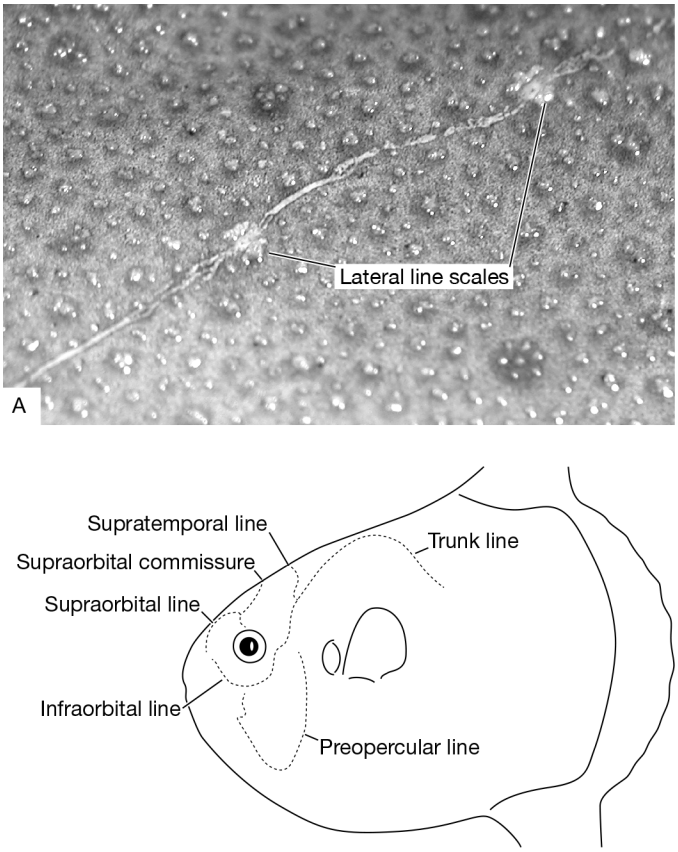

Chapter 3 Figure 18

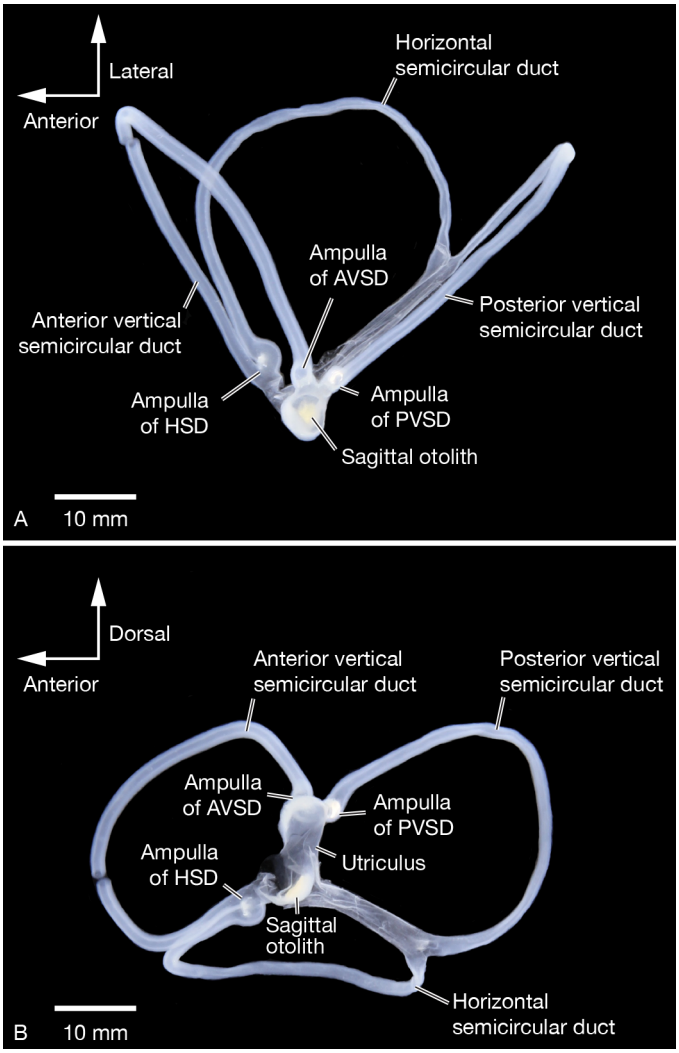

Chapter 3 Figure 19

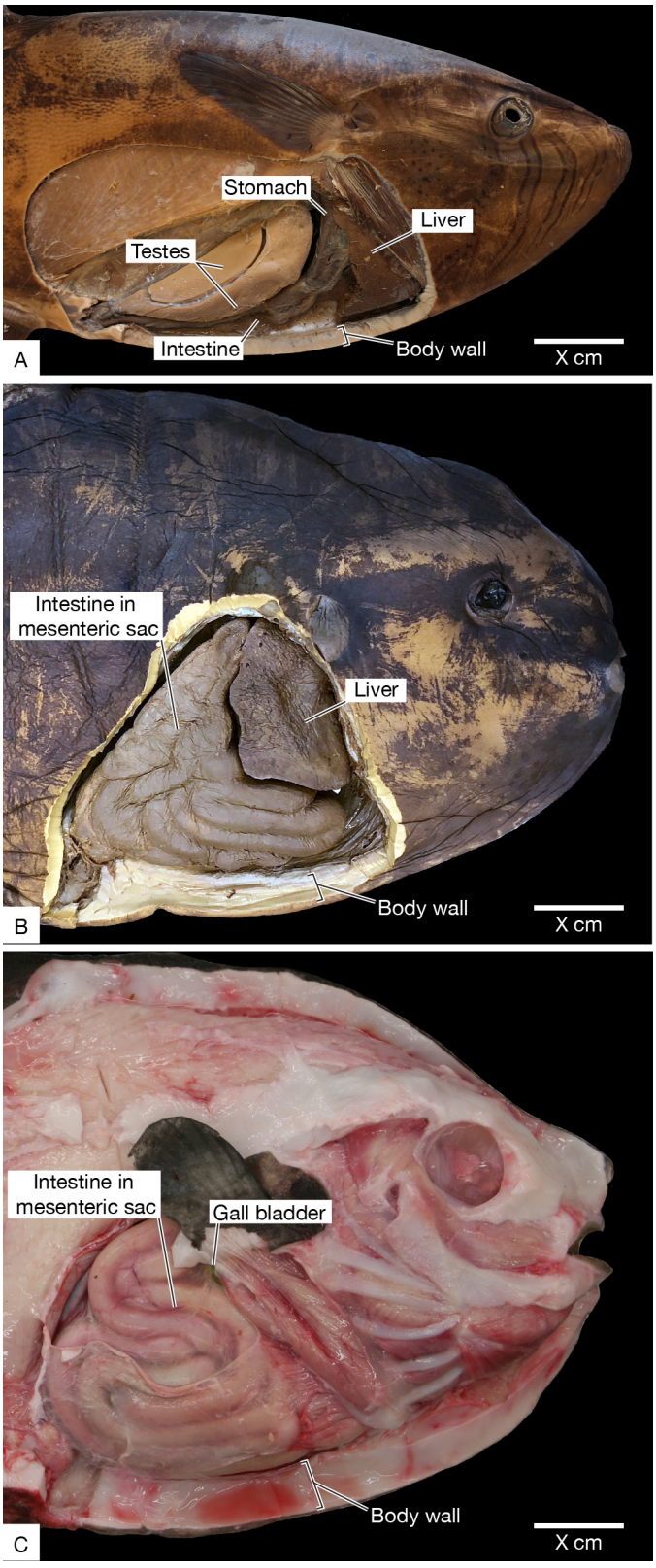

Chapter 3 Figure 20

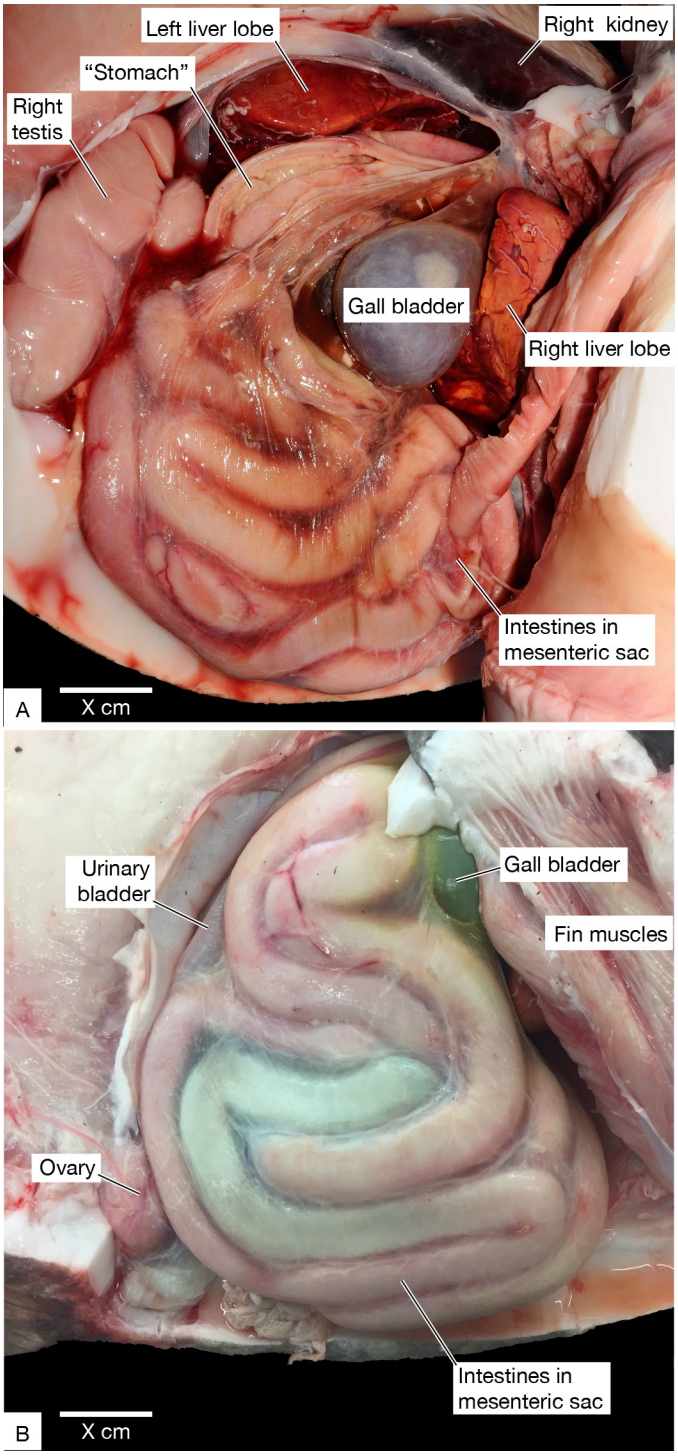

Chapter 3 Figure 21

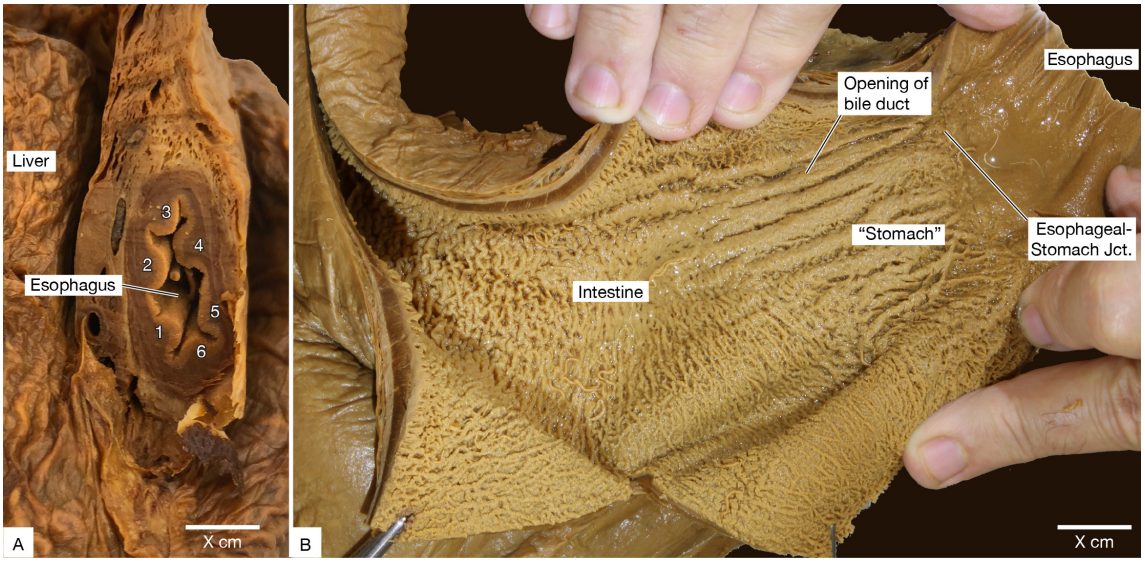

Chapter 3 Figure 22

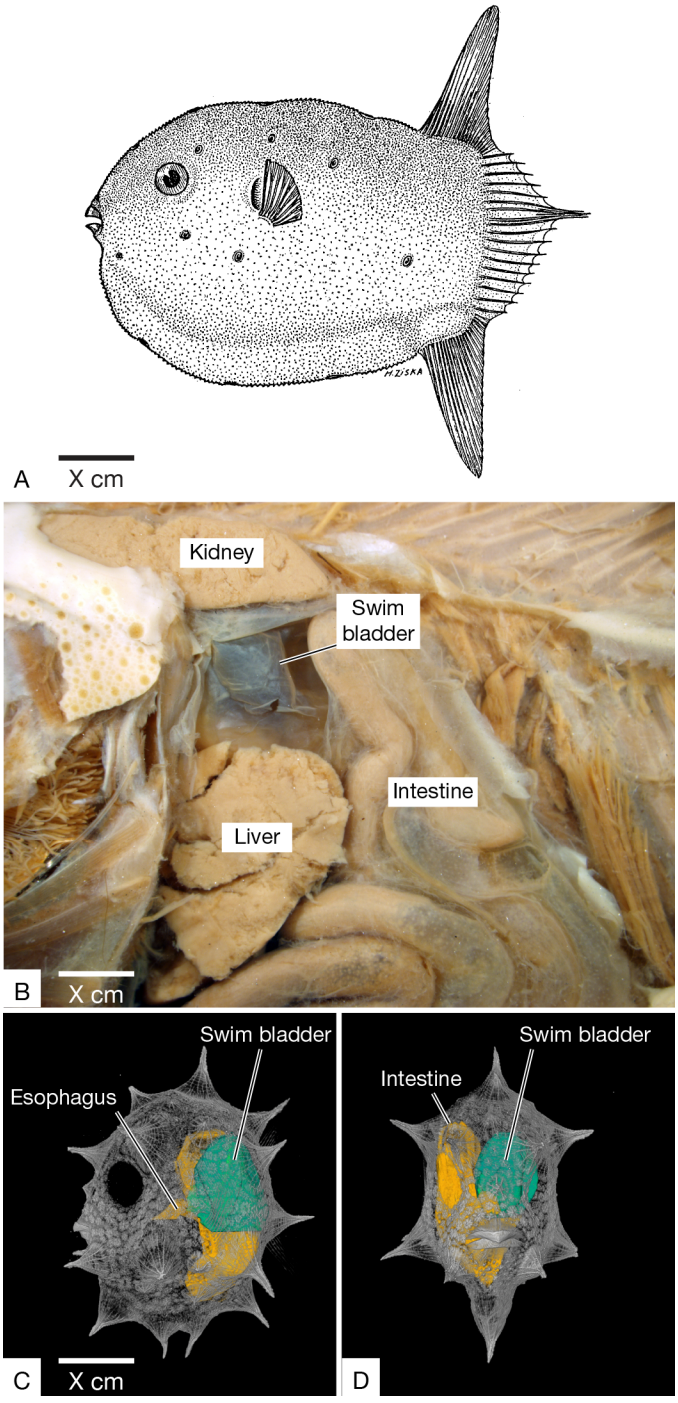

Chapter 3 Figure 23

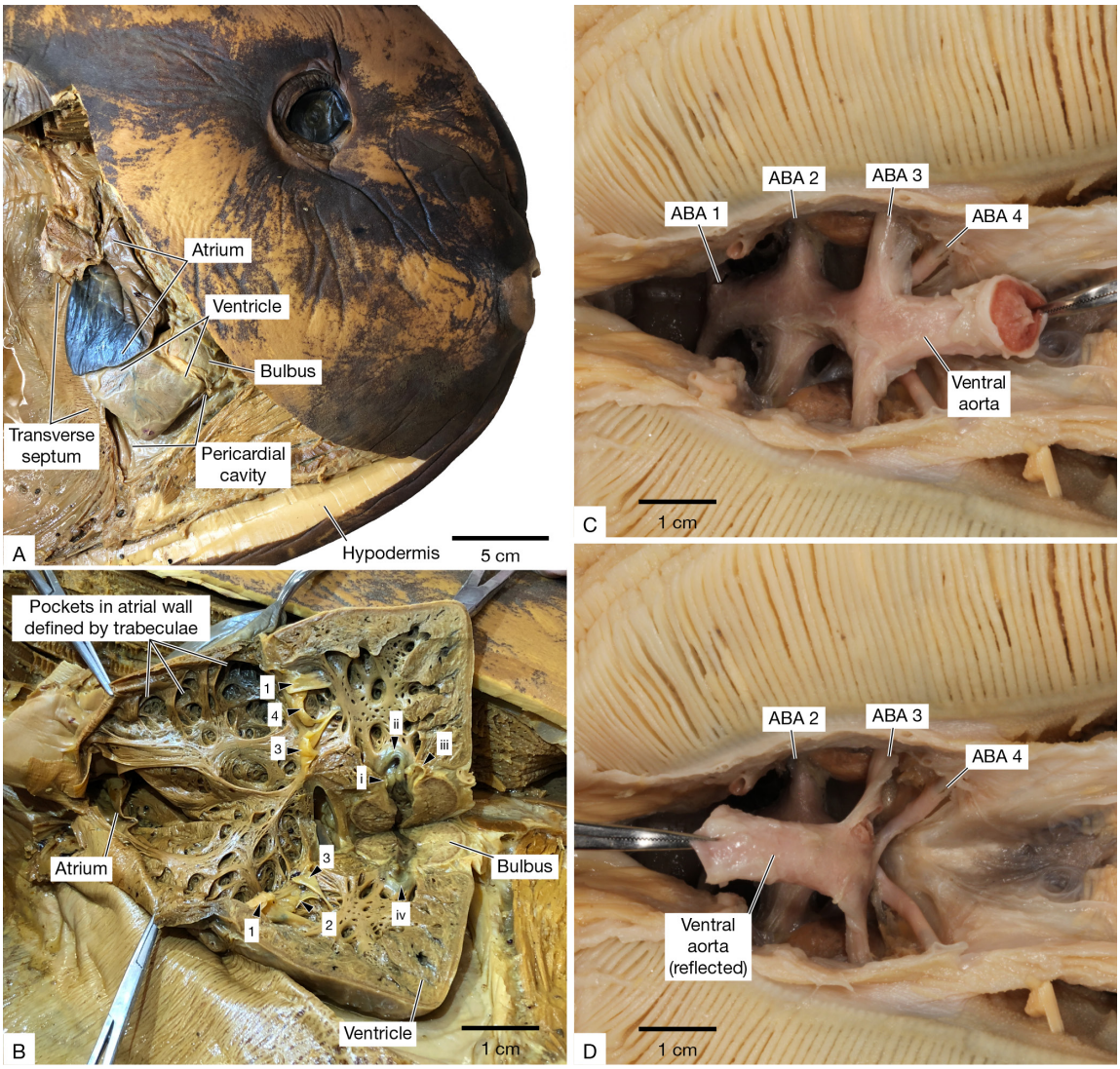

Chapter 3 Figure 24

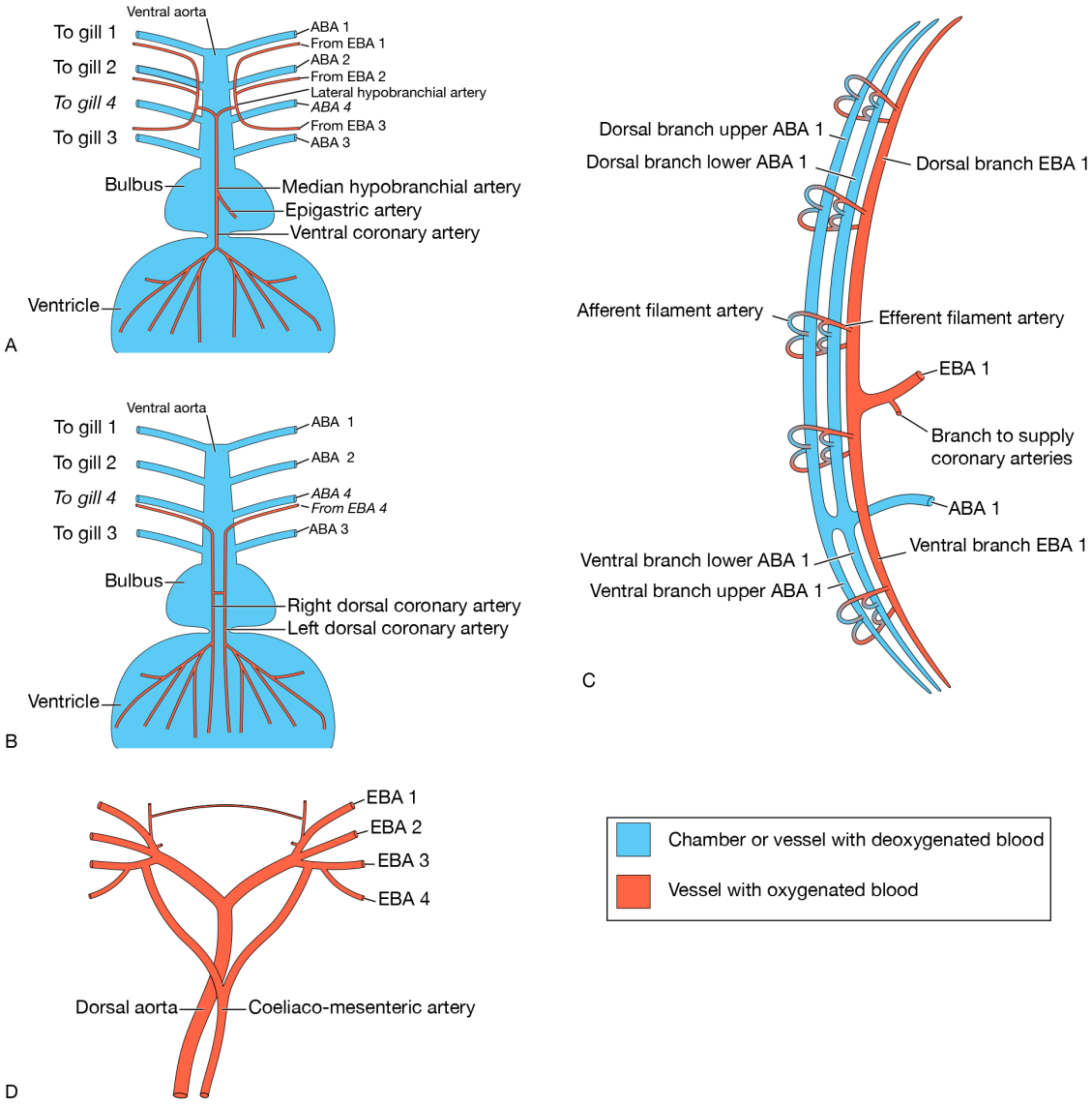

Chapter 3 Figure 25

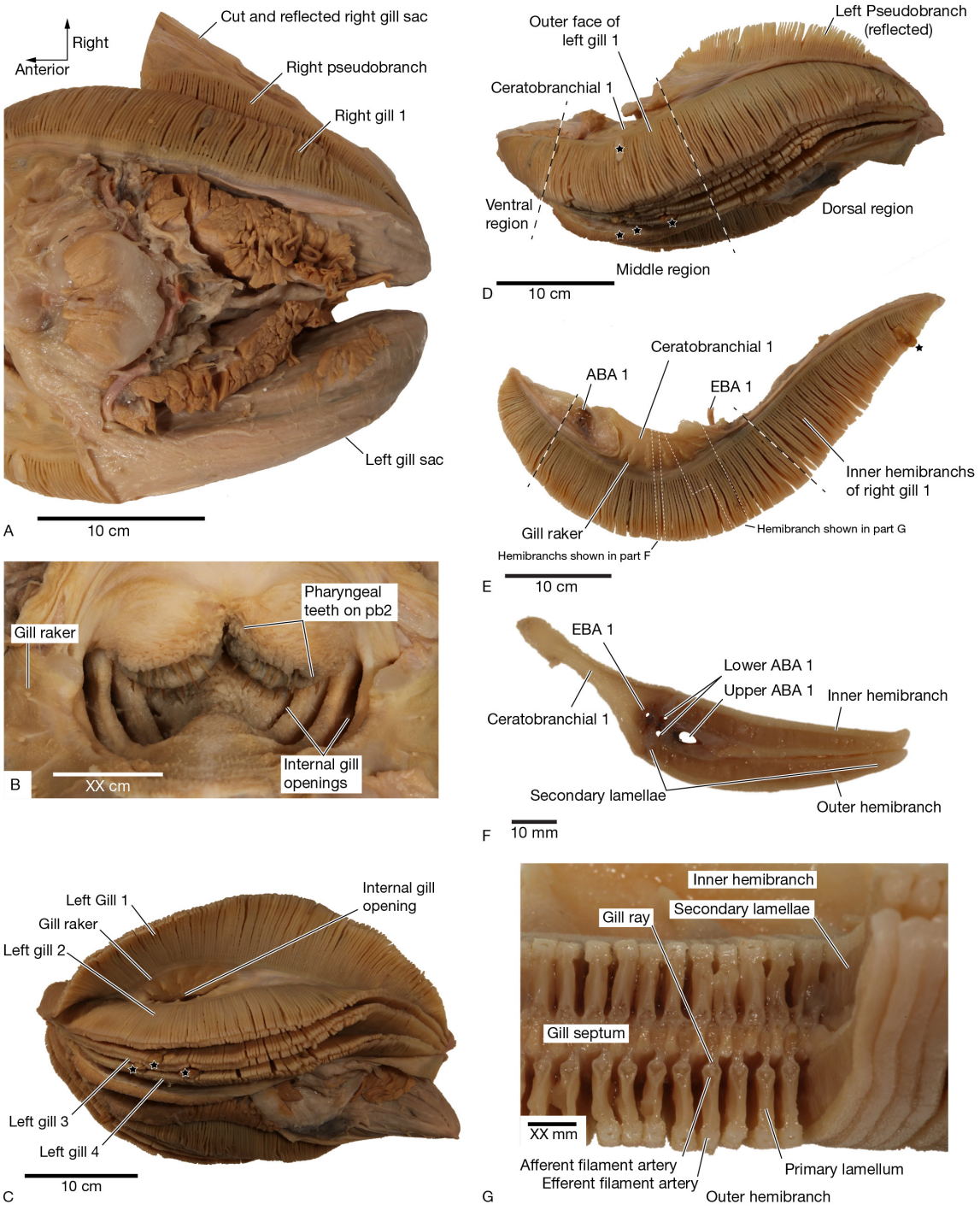

Chapter 3 Figure 26

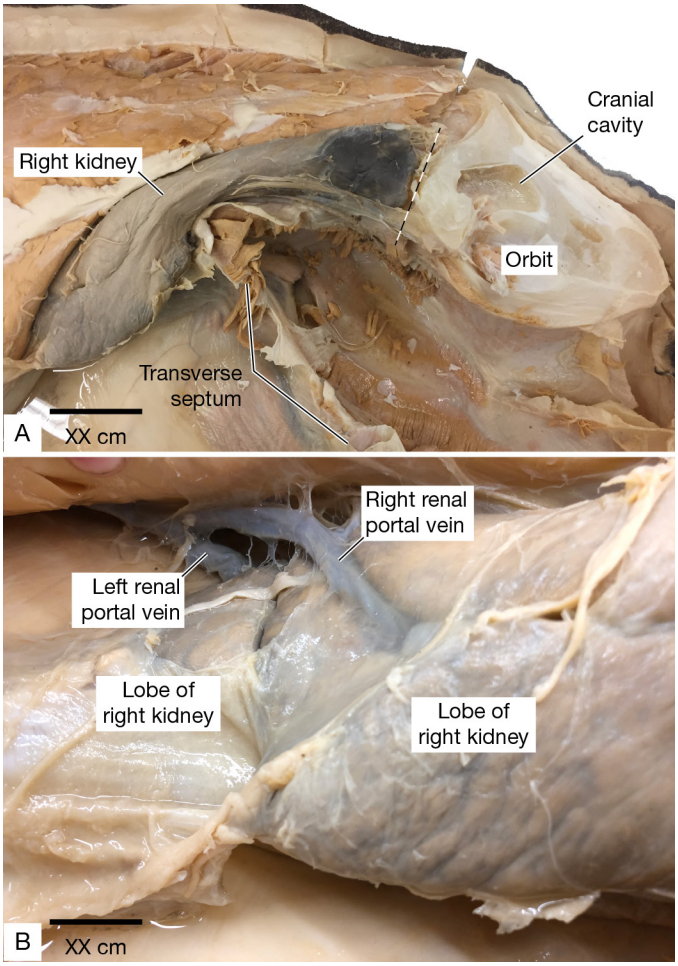

Chapter 3 Figure 27